THE UNIVERSITY OF QUEENSLAND

AUSTRALIA

Genetics of Functional Brain Networks

Benjamin James Sinclair

MSci, MRes

A thesis submitted for the degree of Doctor of Philosophy at

The University of Queensland in 2015

School of Psychology

Queensland Institute of Medical Research

Centre for Advanced Imaging

Abstract

In this thesis, the heritability of a number of features of brain functional connectivity and network behaviour was estimated, in order to assess their suitability as imaging endophenotypes. Phenotypes were chosen based on prior association with psychiatric disease in the literature, and current interest in the neuroimaging community. Heritability was estimated using a large MRI twin sample from the Queensland Twin Imaging Study.

The first study looks at intrinsic functional brain networks present at rest, in the absence of cognitive demand, and characterised them using graph theory, a mathematical formulation used to describe topological properties of complex networks. Such characteristics were found to be moderately to strongly heritable (h^2=20-60%). The heritability estimates varied substantially with methodological choices, in particular the removal or inclusion of global signal.

Connectivity of functional brain networks during working memory performance were also examined. Dynamic causal modelling was employed to determine task-related changes in functional coupling between frontal and parietal regions. Changes in connectivity with task demand were observed for both forward and backwards connections, but the changes had low test-retest reliability (ICC≤0.3), and subsequently, twin correlations and heritability were non-significant (r_{MZ}≤0.08, r_{DZ}≤-0.05).

Finally the functional connectivity profile of the dorsolateral prefrontal cortex during working memory was probed. Functional connectivity with ipsilateral parietal cortex (h^2=24%), contra-lateral dorsolateral prefrontal cortex (h^2=36%), posterior cingulate cortex (h^2=37%) and middle frontal cortex (h^2=26%) were found to be heritable. However, the connections during baseline condition were also heritable, suggesting the heritability did not pertain to WM-specific connectivity, and connectivity with left hippocampus was not found to be heritable.

Declaration by author

This thesis is composed of my original work, and contains no material previously published or written by another person except where due reference has been made in the text. I have clearly stated the contribution by others to jointly-authored works that I have included in my thesis.

I have clearly stated the contribution of others to my thesis as a whole, including statistical assistance, survey design, data analysis, significant technical procedures, professional editorial advice, and any other original research work used or reported in my thesis. The content of my thesis is the result of work I have carried out since the commencement of my research higher degree candidature and does not include a substantial part of work that has been submitted to qualify for the award of any other degree or diploma in any university or other tertiary institution. I have clearly stated which parts of my thesis, if any, have been submitted to qualify for another award.

I acknowledge that an electronic copy of my thesis must be lodged with the University Library and, subject to the policy and procedures of The University of Queensland, the thesis be made available for research and study in accordance with the Copyright Act 1968 unless a period of embargo has been approved by the Dean of the Graduate School.

I acknowledge that copyright of all material contained in my thesis resides with the copyright holder(s) of that material. Where appropriate I have obtained copyright permission from the copyright holder to reproduce material in this thesis.

Publications during candidature

Peer-Reviewed Papers

Sinclair, B. , Hansell, N.K., Blokland, G.A.M., Martin, N.G., Thompson, P.M., Breakspear, M., de Zubicaray, G.I., Wright, M.J., McMahon, K.L. (2015), Heritability of the Network Architecture of Intrinsic Brain Functional Connectivity, NeuroImage. *(in press).*

Sinclair, B., Martin, N.G., Thompson, P.M., Garrido, M., Breakspear, M., de Zubicaray, G.I., Wright, M.J., McMahon, K.L. (2015), Heritability of Effective Connectivity In Working Memory. Human Brain Mapping, *Submitted, under revision.*

Conference Abstracts

B. Sinclair, G. Blokland, M. Wright, G. de Zubicaray, K. McMahon. Genetic and Environmental Influences on Effective Connectivity in Working Memory Networks. OHBM, Seattle USA, June 16-20, 2013.

B Sinclair, K McMahon, G de Zubicaray, M Wright, N Martin, P Thompson, G Blokland, Heritability of Graph Theoretic Characteristics of Resting State fMRI Networks. OHBM, Beijing, China, June 10-14 2012.

Publications included in this thesis

Sinclair, B. , Hansell, N.K., Blokland, G.A.M., Martin, N.G., Thompson, P.M., Breakspear, M., de Zubicaray, G.I., Wright, M.J., McMahon, K.L. (2015), Heritability of the Network Architecture of Intrinsic Brain Functional Connectivity, NeuroImage. *(in press).*

Contributions by others to the thesis

All data analysed here have been collected as part of various larger research projects conducted at the Queensland Institute of Medical Research (QIMR), Australia. All imaging data were collected as part of the Queensland Twin Imaging Study (QTIMS). Margie Wright, Nick Martin, Paul Thompson, Greig de Zubicaray and Katie McMahon were responsible for the conception and design of the Queensland Twin Imaging Study. The initial imaging and genotype data collection, genotyping and cleaning process have been a substantial effort by many people. Marlene Grace, Ann Eldridge, Kerrie McAloney, and Natalie Garden were responsible for recruitment of twin pairs for the Imaging study. Radiographers Matthew Meredith, Peter Hobden, Kate Borg, Aiman Al Najjar, and Anita Burns, as well as Katie McMahon and Gabriella Blokland were responsible for MRI scanning. Kori Johnson, Natalie Garden, Aaron Quiggle, Angus Wallace, Lachlan Strike, Mitzy Kennis, Jan Hoffman, Chloe Najac, Sarah Gay, Felicity Martin, and Gabriella Blokland assisted with MRI scanning. All cognitive data were obtained from the Cognition Study, birth and demographic information from the Mole Study, and all genetic data used in association analyses were obtained as part of the Brisbane Adolescent Twin Study. Marlene Grace, Ann Eldridge, and Kathleen Moore were responsible for recruitment of twin pairs and data collection for the Cognition study. Nick Martin and Margie Wright were responsible for the design and administration of the questionnaire from which we obtained birth information and demographic information. Anjali Henders, Megan Campbell, and staff of the Molecular Epidemiology Laboratory were responsible for blood processing and DNA extraction. Greig de Zubicaray, Katie McMahon, Marta Garrido and Michael Breakspear helped to determine the best methods to prepare the imaging phenotypes. Margie Wright helped to determine the best strategies for the genetic analyses. Margie Wright, Greig de Zubicaray and Katie McMahon provided feedback on all drafts of all chapters in this thesis, contributing to the interpretation of the research data.

Statement of parts of the thesis submitted to qualify for the award of another degree

None

Acknowledgements

I acknowledge my parents and grandparents, and their parents and grandparents, all of whose genes pre-disposed me towards becoming a scientist, and my environment, which provided me with the opportunities and good fortune to express those genes. Particularly influential environmental factors were:

My primary supervisor, Katie McMahon, who struck a fine balance between allowing my wild goose chases, whilst keeping me focused and on track.

My brother, Joseph Clements, who found my lost degree certificate two hours before I needed to send it off for the PhD scholarship application, thereby ensuring (Royal Mail permitting) that I met the scholarship deadline, though given that we share 25% of our genetic polymorphisms (half-brother), it is unclear whether this factor was genetic, environmental, or gene by environment interaction.

Margie Wright and Greig de Zubicaray, my co-supervisors who provided much guidance and support.

Michael Breakspear, a sage who took me under his wing and taught me the wonders of graph theory and dynamic causal modelling.

Imperial College London, a thoroughly rainy place (figuratively and literally) to do an under-graduate physics degree, such that I was compelled to return to university and do it again properly.

Tamara Davis, an astrophysicist who brought me to Brisbane in the first place, thereby initiating an obsessive love affair with the city, which necessitated my return. And Captain James Cook, who discovered Australia, a few Dutch and Portuguese sailors and entire aboriginal civilization not-withstanding, which is a jolly nice place to live, once you have got to grips with the sharks, spiders and drop-bears.

Keywords

Neuroscience, working memory, resting state fMRI, dynamic causal modelling, graph theory, genetics, heritability

Australian and New Zealand Standard Research Classifications (ANZSRC)

ANZSRC code: 170205 Neurocognitive Patterns and Neural Networks; 60%
ANZSRC code: 060410 Neurogenetics; 40 %

Fields of Research (FoR) Classification

FoR code: 1109 Neurosciences; 40%
FoR code: 1702 Cognitive Sciences 20%
FoR code: 0604 Genetics; 40%

Table of Contents

1 List of Figures & Tables

environmental factors (E). The covariance in additive genetic factors is set to 1 for monozygotic (MZ) twins and ½ for dizygotic (DZ) twins.

Figure 4.2: Group wise activation (top panel), and connectivity profiles with dlPFC seed (bottom three panels). Positive activation/connections in red-yellow, negative activations/connections in blue-green. The t-statistics were thresholded at FWE $p<0.05$, corrected for multiple comparisons.

Figure S4.1: WFU Pick Atlas segmentation of the left hippocampus (red), overlaid on negative functional connectivity during 2B condition (blue-green). Segmentation does not overlap well with peak connectivity.

Figure S4.2: Using a Hanning filter to avoid interference between task conditions yields nearly identical correlation maps to Figure 2.

Figure S4.3: Group wise activation (top panel), and connectivity profiles with dlPFC seed (bottom three panels), with task related variance regressed out. With task related variance regressed out, the pattern of correlations during 0B and 2B remain very similar to those observed in Figure 2 (without task regression), demonstrating that condition specific correlations are not the result of common activation in response to task. The change in functional connectivity (bottom panel) has some differences to Figure 2. The connectivity with the posterior cingulate cortex goes from negative to less negative, and the connectivity with the right parietal cortex goes from positive to less positive. This pattern is unexpected and may be an introduced artefact by the task regression.

Table 2.1: Description of graph measures. For a full review see Rubinov & Sporns (2010).

Table 2.2a and Table 2.2b: Mean (SD) of the five graph measures (k=5-25%) across the 592 participants Twin correlations, Variance component estimates for A (additive genetic), C (common environment) and E (unique environment), and model fit for the five graph measures, k=5-25%. Computed without global signal regression. Table 2.2b: Computed with global signal regression.

2 List of Abbreviations used in the thesis

γ – clustering coefficient
ϕ – rich club coefficient
λ – global efficiency
σ – small world index
0B – zero back in working memory task
2B – two back in working memory task
ACC – anterior cingulate cortex
AD – Alzheimer's disease
AIC - Akaike Information Criterion
BD – bi-directional models
BMS – Bayesian model selection
BOLD – blood oxygen level dependent
BW – backward models
CI – confidence interval
COMT – Catechol-O-methyltransferase
CSF – cerebral spinal fluid
dACC – dorsal anterior cingulate cortex
dlPFC – dorsolateral prefrontal cortex
DCM – dynamic causal modelling
DMN – default mode network
DNA - Deoxyribonucleic Acid
DTI – diffusion tensor imaging
DZ – dizygotic
EEG - electroencephalogram
Ep – exceedance probability
EPI – echo planar imaging
FA – fractional anisotropy
FC – functional connectivity
fMRI – functional magnetic resonance imaging
FOV – field of view
FW – forward models
FWE – Family-wise error
GE-EPI - Gradient echo, echo planar imaging
GSR – global signal regression
GWAS - genome wide association
h^2 –heritability
HARDI – high angular resolution diffusion imaging
HF – hippocampal formation
HRF – haemodynamic response function
ICA - independent component analysis
ICC – intra-class coefficient
IFC – inferior frontal cortex
IFJ – inferior frontal junction
IPS – intraparietal sulcus
IQ – intelligence quotient
LMC – left somatomotor cortex
MEG – magnetoencephelogram
MFC – medial frontal cortex
MPRAGE - Magnetization Prepared RApid Gradient Echo
MRI - magnetic resonance imaging
MZ – monozygotic
NM – no task-dependent connectivity modulations
PC – parietal cortex
PFC – prefrontal cortex
pSMA – presupplementary motor area
Q – Modularity
QIMR – Queensland Institute of Medical Research

QTIMS – Queensland Twin Imaging Study
RMC – right somatomotor cortex
rs-fMRI – resting state functional magnetic resonance imaging
RSN – resting state networks
ROI – region of interest
SD – standard deviation
SEM – structural equation modelling
SLF – superior longitudinal fasciculus
SNP – single nucleotide polymorphism
SZ – schizophrenia
TE – echo time
TI – inversion time
TR – repetition time
vlPFC – ventrolateral prefrontal cortex
vmPFC – ventromedial prefrontal cortex
WM – working memory

1 Chapter 1: Introduction

1.1 Endophenotyping

In psychiatry, an endophenotype is a quantitative trait hypothesized to underlie disease syndromes (Gottesman and Gould, 2003, Bearden and Freimer, 2006). In general, an endophenotype measures a biological feature "upstream" from directly observable psychiatric symptoms, which is both associated with risk for a particular disorder, and associated with causes, rather than effects of the disorder, that is, they are on the causal pathway from genes to disease.

The search for psychiatric endophenotypes has three main motivations; (1) increased genetic penetrance, (2) elucidation and decomposition of psychological phenomena, and (3) increased specificity and objectivity for diagnosis.

Firstly, since genes code for biological processes, and not psychiatric diagnosis, it was initially assumed that genetic penetrance would be greater at the level of brain biochemistry and neuronal circuitry than at the level of the medical condition (Gottesman and Gould, 2003). This would give greater power for genetic association.

Secondly, endophenotyping will help decompose multi-genic, complex traits into distinct components. Most psychiatric disorders result from the interaction between multiple genes, and multiple environmental factors. Consequently, the contribution of any given gene or SNP to disease risk, as measured in candidate gene and genome-wide association studies are low (e.g. International Schizophrenia Consortium et al., 2009, Meyer-Lindenberg, 2010). One advantage of the endophenotyping approach is that by splitting a psychiatric disorder into its (multiple) underlying neuronal mechanisms, we can go some way to partitioning the genetic variance in the disorder and understand by which mechanism each genetic factor contributes to the disorder.

Finally, psychiatric diagnoses and phenotypes are inherently imprecise in that there is often disagreement over diagnostic criteria, there are generally multiple diagnostic criteria for a single condition, and disease groups can show large degrees of heterogeneity (e.g. major depressive disorder; Zimmermann et al., 2009, Schizophrenia (SZ); Tsuang and Faraone, 1995). As such, the endophenotype approach helps overcome this problem in psychiatric genetics by focusing on objective and quantitative intermediate biological mechanisms. It is well known that patients of the same diagnosis can respond differently to treatment. In the

cases where this is due to differing neural mechanisms of the same disease category, then understanding and diagnosing those mechanisms will lead to more appropriate treatment selection.

1.1.1 Uses, methodologies and current state of endophenotyping

Endophenotyping has generally been undertaken in one of two ways. The first and most common way is mechanism discovery. Given a known genome-wide significant variant, or polygenic risk profile score (RPS) associated with a psychiatric disease, this variant or RPS can be used in genetic association with possible disease mechanisms. A positive association between risk allele and neural mechanism suggests that the neural mechanism is on the causal pathway of the disease.

The second use of endophenotyping is gene discovery. Given a known pathological mechanism, one can then perform genome wide association (GWAS) on the mechanism to highlight genetic contributors. If for a particular disorder genes are more penetrant at the circuit level, using the mechanism rather than the diagnosis would give greater power for detecting genetic influences.

Recent GWAS of EEG (Iacono et al., 2014) and MRI structural phenotypes (Stein et al., 2012; Strike et al., 2015) have cast doubt on the assumption that genes will be more penetrant at the imaging endophenotype level, demonstrating that imaging endophenotypes are themselves highly polygenic, and effect sizes are not substantially larger than for clinical phenotypes.

The emphasis has thus shifted away from gene discovery and towards mechanism discovery. In this manner, endophenotyping can be used as a tool to interpret the results of GWAS on clinical phenotypes, by investigating the mechanism by which genetic variants confer disease risk (de Geus, 2014; Munafo and Flint, 2014). Similarly, mechanism discovery can help elucidate the imprecision inherent in DSM classifications of heritable diseases, whereby diseases with similar clinical presentations may be compared for underlying neurology (e.g. Autism spectrum disorder and Attention Deficiency Hyperactivity Disorder, Rommelse et al., 2011). Tellingly, Thomas Insel, the director of the National Institute for Mental Health, the world's largest funder of mental health research, greeted the publication of the most recent version of DSM with criticism that psychiatric disorders are still classified by sets of symptoms, announcing NIMH's intention to "transform diagnosis by incorporating

genetics, imaging, cognitive science, and other levels of information to lay the foundation for a new classification system". Endophenotyping is central to this broad aim of quantitative, biomarker based psychiatry.

Endophenotypes are often said to underlie a disorder, with the implicit assumption of linear causality, with clear pathways from gene to endophenotype to disease. This concept, though useful as a framework for hypothesis testing, is undoubtedly over-simplified. Psychiatric diseases are characterised by a cluster of symptoms and numerous neurological abnormalities/endophenotypes. In many cases symptoms are causally connected (Kim and Ahn, 2002), and the same is likely to be the case between endophenotypes. The consequence of this is that relationship between endophenotype and phenotype (psychiatric diagnosis) is unlikely to be linear and will depend on the state of other endophenotypes and unmeasured latent variables. Such systems may best be described using the apparatus of dynamic complex systems theory. As an example, Cramer et al. (2010) and Schmittmann et al. (2013) construct symptom networks, and argue that psychiatric disorders, rather than being causes of the symptoms, are best conceptualised as emergent properties of the network of symptoms, in this case, sub-networks of closely related and interacting symptoms. Along the same lines, disorders could be envisaged as attractor states in the state space of the dynamical system of symptoms (see Guastello et al., 2009 and Van Geert, 2009 for an overview of chaos theory and non-linear dynamical systems theory applied to psychology). Similar scenarios can easily be imagined with brain endophenotypes used en lieu of symptoms (Staniloiu and Markowitsch, 2010), with the added incentive that neurological substrates are more easily accepted as causes of a disease than are symptoms. Though this approach is not adopted in this thesis, it is important to have in mind throughout when we make the assertion that an endophenotype is underlying a disorder, that it is but one etiological factor in a complex dynamical system of inter-twined neural mechanisms.

1.1.2 Examples of Psychiatric Endophenotypes in the Literature

Although a recent field of study, endophenotyping has produced some encouraging early findings. Pezawas et al. (2005) investigate the role of connectivity between the anterior cingulate cortex (ACC) and amygdala in depression. In the healthy population, the subgenual anterior cingulate cortex is believed to inhibit processing of emotional adversity in the amygdala. In depressed patients, this circuit is compromised, leading to a lower control of

emotional state. Pezawas et al. (2005) investigated whether a risk factor of depression was implicated in this circuit. The risk factor was the short allele (small number of tandem repeats) in the promoter region (5-HTTLPR), of the serotonin transporter gene SLC6A4, which had been associated with depression in candidate gene studies and supported since in more recent GWAS (Haenisch et al., 2013). The short allele leads to reduced transcription of this gene, so it feasible that a reduction in the expression of this gene could cause a reduction in frontal-ACC connectivity. Pezawas et al. (2005) found this to be the case, with the short allele associated with reduced coupling between ACC and amygdala. Given that this coupling predicted ~30% of the variation in trait-anxiety in the cohort (Pezawas et al., 2005), this suggests that the genetic risk is mediated in part through this mechanism. This study controlled for population stratification by using only Caucasians of European descent and by genotyping 100 unlinked SNPs to rule out occult stratification between 5-HTTLPR groups.

Esslinger et al. (2009) looked at endophenotypes of SZ. SZ is highly heritable (Cardno and Gottesman, 2000), but multi-genic (International Schizophrenia Consortium et al., 2009; Schizophrenia Working Group of the Psychiatric Genomics Consortium, 2014), and the effect size of significant variants is typically small (Meyer-Lindenberg, 2010). Further SZ is believed to be caused by multiple deficiencies across the range of cognition, and not limited to a domain. Thus finding the constituent processes involved, and their genetic architecture is a promising way to shed light on this disease. The chosen characteristic was functional connectivity (FC) between dorsolateral prefrontal cortex (dlPFC) and hippocampal formation (HF) during an N-Back working memory (WM) task. During WM, SZ patients fail to uncouple these two regions (Meyer-Lindenberg et al., 2005), suggesting that SZ patients may be recruiting associative memory to assist them in (impaired) working memory. Esslinger et al. (2009) found a significant association between this hyper-connectivity and a genome-wide supported schizophrenia risk factor, SNP rs1344706 of gene ZNF804A. This risk factor was discovered in a sample of 479 SZ patients by O'Donovan et al., 2008, but not supported by the most recent and largest SZ GWAS (Schizophrenia Working Group of the Psychiatric Genomics Consortium, 2014). To control for population stratification, only subjects with parents and grandparent of European origin were used, and genotype group differences in gender, age, handedness, level of education, and task performance were measured and were not significant..

1.1.3 Requirements of an Endophenotype

Gottesman and Gould (2003) describe the consensual set of criteria required of an endophenoype.

1. Associated with illness in the population
2. Heritable
3. State independent, manifests in individual whether or not illness is active.
4. Co-segregates with illness in families
5. Found in non-affected family members at higher rate than in population.

In this thesis I chose phenotypes which have shown positive associations with psychiatric disease, thereby satisfying criteria (1), and go on to estimate their heritability, with significant heritability implying their validity as an imaging endophenotype. The exceptions are the functional connectivity phenotypes in Chapter 4, not all of which have been investigated in terms of psychiatric disease, but have shown interesting associations with features of cognition. One important assumption of the endophenotype concept is that intermediate phenotypes associated with psychiatric risk are present in the healthy population. Since genes confer susceptibility to disease via neuronal mechanisms, carriers of disease risk alleles who do not show clinical symptoms of the disease will show association with the intermediate brain phenotypes via similar genetic susceptibility mechanisms (Meyer-Lindenberg and Weinberger, 2006). This has been demonstrated by numerous neuroimaging studies of healthy relatives of schizophrenia patients (e.g. Seidman et al., 1999; Boos et al., 2007; Whitfield-Gabrieli et al., 2009; Callicott et al., 2014). An implication is that healthy subjects can be used for studies of genetic association with disease susceptibility mechanisms. This avoids the expense, difficulty and potential confounds of using patient groups.

1.1.4 Beyond Endophenotyping

The field of endophenotyping provides an over-riding framework and theme for the three papers of this thesis. However, the core concern of the three papers is the heritability of various functional systems. Heritability is of itself an informative measure, and is discussed further in section 1.3.4. For example, Chapter 2 measures the heritability of a number of network measures. A number of studies have demonstrated that the brain network displays certain features characteristic of optimal organisation under evolutionary pressure (see section 1.3.1.3). Thus, measuring the heritability of these features gives valuable information as to the etiology of individual differences in optimal brain organisation.

1.2 The Queensland Twin Imaging Study

The Queensland twin imaging study (QTIMS; de Zubicaray et al., 2008) ran from February 2007 to August 2012, during which time 1059 participants undertook a number of magnetic resonance imaging (MRI) scans on a 4 Tesla Bruker Medspec whole body scanner. 82 participants returned for rescanning at 3.6 months (SD 1.6) to test the reliability of the measures. The sample consisted of 389 identical (monozygotic; MZ), and 556 non-identical (dizygotic; DZ) twins, along with 113 siblings. These twins were recruited from the larger Brisbane Twin Cognition Study (Wright and Martin, 2004), through which a host of biological and psychological testing has been performed, including various measures of IQ, disease, height, weight, marriage statistics, etc. Each participant was scanned with a T1 weighted sequence, diffusion tensor imaging (DTI), high angular resolution diffusion imaging (HARDI), a 4 minute functional magnetic resonance imaging (fMRI) scan during an N-Back WM task, and a 5 minute resting state fMRI (rs-fMRI) scan.

To put into comparison with other large MRI twin studies, the Netherlands Twin Registry scanned 102/131 MZ/DZ pairs, while the ongoing Vietnam Era Twin Study of Aging has scanned 110/92 MZ/DZ pairs. Thus, this is to date the largest sample of twins scanned with MRI, giving the greatest available power for detecting genetic influences, aside from consortium initiatives such as ENIGMA, to which QTIMS contributes.

The Queensland twin imaging study has contributed to our understanding of the genetic influences on human brain structure and function. With the diffusion weighted scans, white matter integrity was been found to be under strong genetic influence (h^2=55-85%; Chiang et al., 2009), and numerous genetic polymorphisms affecting white matter structure have been discovered, (Chiang et al., 2011; Braskie et al., 2011). With the fMRI data, the heritability of functional activation during working memory was assessed. Heritability of the blood oxygen level dependency (BOLD) response ranged across regions between 0-65% with on average ~33% of variance in activation attributable to genetic factors (Blokland et al., 2011). Preliminary work has been done looking at the genetic influences on resting state functional connectivity, Castellanos et al. (2010) find a non-significant genetic influence on connectivity within the default mode network (DMN), in a subset of 108 participants.

1.3 Theoretical Background

1.3.1 Brain Connectivity

In this thesis, I investigate brain functional connectivity as a candidate endophenotype. In this section, the major conceptualisations and methodologies in brain connectivity are reviewed.

Functional activity in the brain adheres to two major organisational principles, segregation and integration. This has fuelled one of the major philosophical and scientific debates in the history of neuroscience, that of locationalism vs. holism. Locationalism stresses the specificity of neurons and brain regions, whereby a given function is performed (independently) by a localised brain region, whereas holism contends that function is achieved via the interaction of multiple brain regions, and that the patterns of interactions themselves are an integral part of the function. Evidence for specialisation of brain anatomy is widespread, from the early lesion work of Paul Broca, identifying cortical regions specialised for language processing, and the electrophysiological work of Wilder Penfield, revealing that sensory and motor cortices were organised into maps, through to modern-day functional neuroimaging, with given tasks and functions activating localised cortical regions. Whilst anatomical integration amongst cortical regions is evident from their dense interconnectedness via white matter fibres, functional integration between regions is more difficult to assess. The advent of neuroimaging and associated analytic techniques have shown distributed/widespread patterns of activation in response to a range of tasks, but particularly for tasks requiring higher cognitive function such as memory and attention. Methods of functional and effective connectivity (Section 1.3.1.1) have demonstrated that these distributed brain regions are far from acting independently, but exert measureable influences over each-other (Friston, 2002a, *"Beyond Phrenology"*). For low order operations such as sensory and motor processes, anatomic connections and functional interactions seem to form well ordered, largely feed-forward hierarchies of distinct functional units (e.g. visual processing: Hubel and Wiesel, 1962; Felleman and Van Essen, 1991; DiCarlo et al., 2012). For higher order cognitive processes, feedback loops are prevalent and processing occurs in a more interactive and integrated manner (e.g. attention, memory, language, emotion: Mesulam, 1990; McClelland and Rogers, 2003; Pessoa, 2008). In such cases the assignment of function to anatomy is less straightforward, with a given function distributed over disparate anatomy.

Functional integration is achieved via neuronal connectivity, a central concept in neuroscience. Individual neurons exert influence over each other via release of neurotransmitter molecules at the neuronal synapse. Computational networks of interacting units (neural networks) are capable of many of the functions we associate with cognition, e.g. learning, pattern recognition, and error detection (Hopfield, 1982). Likewise measurement of neuronal interactions from cellular recordings up to large scale cortical mass activity demonstrate that cognition in part relies on the interaction of distributed networks in the brain (Mountcastle and Edelman, 1979; Singer and Gray, 1995; McIntosh, 2000; Jirsa, 2004; Bressler and Menon, 2010). Thus, these interactions between neuronal networks could be a valuable marker for understanding normal and disease affected cognition.

1.3.1.1 Functional and Effective Connectivity

MRI lacks the spatial resolution to observe connections between individual neurons, with a typical imaging voxel between 2-3mm in each dimension (8-27mm^3). As such, when we measure connectivity using MRI, we are referring to the connectivity between large scale neuronal populations (Deco et al., 2008). Brain connectivity measured with MRI is broadly categorized into two fields, structural connectivity on the one hand, and functional and effective connectivity on the other (Friston, 2011). Structural connectivity has the limitation that it gives little information on the dynamic nature of brain connectivity, required for information processing.

Synaptic coupling between neurons varies rapidly depending on time and context, using a variety of molecular mechanisms (Abbott et al., 1997; Wolf et al., 2003; Saneyoshi et al., 2010). These changes in synaptic coupling feed forward to the dynamic functional integration of large scale cortical regions observed in neuroimaging (Friston, 1994; Friston, 2011), either directly or as an emergent synchrony by virtue of network dynamics (e.g. Breakspear et al., 2003). Functional and effective connectivity attempt to characterize this functional coupling and its context dependent variations.

Functional connectivity (FC) measures statistical dependencies between data. The most commonly used measure of functional connectivity is simply Pearson's correlation between the time series of two regions, where a significant correlation is taken as evidence of a dependence between the two regions. Pearson's correlation is the measure of connectivity used to construct networks for graph theoretical analysis, as described in section 1.3.1.3 and

Chapter 2, and to measure the connectivity profile of the dlPFC during WM in chapter 4. Though Pearson's correlation is overwhelmingly the most widely used measure of ROI to ROI functional connectivity, in principle any measure of statistical dependence can be used, including partial correlation/inverse covariance matrix (Marrelec et al., 2006), mutual information (Zhou et al., 2009), or coherence in the frequency domain (Chang and Glover, 2010). These various methods are reviewed, and their sensitivity and specificity evaluated on simulated data in (Smith et al., 2011). They found that partial correlation and inverse covariance matrix performed slightly better than full correlation, whereas coherence and mutual information performed substantially worse.

The aforementioned measures may be used to measure the FC between two regions, using the time series of two regions, or the FC between a seed region and all other voxels in the brain, giving a connectivity map. As such, they require the definition of a suitable seed region/regions. In contrast, hypothesis free, whole brain patterns of functional connectivity can be estimated using independent component analysis (ICA, Beckmann et al., 2005). ICA detects maximally independent sources and their linear combination which give rise to an observed set of measurements. When applied to spatio-temporal fMRI data, the output is a set of independent time series with a weight at each voxel. The weight maps for each independent component describe a spatial distribution of coherent voxels, and overlap with well established functional networks from activation studies (Smith et al., 2009).

Measures of functional connectivity make no inference on an underlying generative model, thus do not strictly imply the presence of a connection, only a dependency in the data. However, the ease of implementation and model independence make FC an attractive option in probing neuronal interactions. The validity of FC as a measure of interaction is enhanced if alternative causes of the interdependencies are controlled for, such as the influence of global signal, or common underlying causes such as task activation. In contrast, effective connectivity describes the causal influence of one neuronal population over another. It is derived from a generative model, in which observed data are modelled as arising from these influences, while an attempt is made to account for alternative contributions to the observed data by explicitly modelling them. The presence of effective connectivity is deduced by model inference, whereby a model with and without the hypothesized connection are compared.

The main methods used in fMRI to establish effective connectivity are structural equation modelling (SEM), dynamic causal modelling (DCM) and Granger causality. SEM specifies a set of linear relations between BOLD signals in different regions, with directed

interactions between regions present as path coefficients, and fits the observed covariance matrix to the model covariance matrix. DCM models neuronal activity in a region using differential equations with terms representing the influence regions on each-other and task-dependent modulations in these influences. DCM additionally models the subsequent BOLD signal using a separate set of differential equations, translating the neuronal model to an observation model. DCM is implemented in Chapter 3 of this thesis and its theoretical underpinnings are described in section 1.3.1.2. Finally, as opposed to SEM and DCM, which posits a set of causal structures and matches observation to model to determine the most likely causal structure, Granger causality uses temporal antecedence to determine causality. If the time series of one region can predict the time series of second, beyond that predicted by the second time series itself, the first time series is assumed to have been a cause of the second time series. All of these methodologies have their advantages and disadvantages. In this thesis I use DCM to determine effective connectivity during WM, because it is particularly suited to measure changes in connectivity in response to task manipulations.

1.3.1.2 Dynamic Causal Modelling

The goal of dynamic causal modelling (DCM; Friston et al., 2003) is to estimate how different brain regions interact (connections), the causal direction of those interactions, and how those interactions increase or decrease in strength in response to changing task demand (modulations).

This is achieved by solving computationally a set of coupled linear partial differential equations ultimately describing the signal detected from that brain region, such as the BOLD signal from the functional time series. The differential equations of DCM come in two levels. The first level describes the neuronal activity of each region (z), and the second level models how this neuronal activity gives rise to the BOLD signal, termed the haemodynamic model.

The change in neuronal activity of a region is assumed to have three causes. The first is the intrinsic connectivity with other regions, with the activity in region 2 causing a change in the activity in region 1, dependent on the strength of the directed connectivity from region 2 to region 1. This intrinsic connectivity is parameterized by the coefficient A, and appears in the first term of equation. The second influence is the change in those connections induced by some experimental manipulation. Changing task demand can alter the strength of connectivity from region 2 to region 1, and this is parameterised in the coefficient B. Finally, each region

may change its neuronal activity in response to some experimental input, such as a stimulus input, or a task demand. This final influence in parameterized in coefficient C.

$$\frac{d\boldsymbol{z}}{dt} = A\boldsymbol{z} + \sum_j u_j B^j \boldsymbol{z} + C\boldsymbol{u}$$

where j iterates over the experimental manipulations, **u**. This formula states that the rate of change in the neuronal activity, z_i, of a region is linearly proportional to the activity of all other regions, **z**, with weights given by A, to the additional weighting of a connection during a given experimental manipulation u_j, with weights given by B, and to experimental manipulations providing direct driving input to that region, with weights given by C.

This neuronal state is then mapped to a haemodynamic response. In DCM the haemodynamic model used is the Balloon/Windkessel model (Buxton et al., 1998; Mandeville et al., 1999). For each region this model consists of a set of biophysical parameters including, blood inflow, outflow, volume, and deoxyhaemoglobin content (see Equations 3, Friston et al., 2003). In contrast to conventional fMRI analysis in the general linear model framework, these biophysical parameters are allowed to vary from region to region. Finally, this haemodynamic response in mapped to an expected BOLD signal (see Equations 4; Friston et al., 2003). The resulting neuronal and haemodynamic states as specified by the forward model are then modelled simultaneously with model parameters estimated via an expectation maximisation scheme (Friston, 2002b), which utilises prior probabilities on neuronal and haemodynamic parameters, reflecting the dissipating/non-divergent nature of neuronal activity, and empirically determined haemodynamic behaviour.

An integral part of dynamic causal modelling is selection of the network configuration (combinations of connections, modulations and driving inputs) most likely to have caused the observed time series. We test a number of possible network configurations to see which configuration has the highest evidence. Given the large number of possible network configurations, we do not test all possible combinations, but rather restrict the model space to a computationally manageable size. Many configurations can be disregarded as physiologically unlikely, so typically we chose to model a subset of likely model configurations. For example, visual/auditory experimental input is typically constrained to enter the network via visual/auditory cortices, rather than testing all possible input locations for experimental inputs. We can further restrict the model space by generating specific hypothesis about the

physiological mechanisms, e.g. top-down vs. bottom-up processing, and testing only those hypothesis, and by using prior literature to inform our models.
Once a model space embodying our hypothesis has been defined, all models are fitted to the data (BOLD time series), and one can determine the best model, or the best family of models sharing a particular feature, using Bayesian model selection (BMS). Bayesian model selection differs from frequentist model selection in a number of important ways. Firstly BMS quantifies the relative probability that different models gave rise the observed data, and makes inferences based on the posterior probability (p(Model|Data)), in contrast to frequentist model selection, which is concerned with the relative likelihood of observing data, given a (known) model. Secondly, BMS accounts for our uncertainty in model parameters in making inferences, utilising the marginal likelihood function (the model "evidence"), which calculates the probability of the data given the model integrated over all possible model parameter values, in contrast to frequentist approaches, which generally use point estimates of parameter values (c.f. maximum likelihood estimation).

As described thus far, "deterministic" DCM requires an experimental driving input to initiate any activity. Further, deterministic DCM ignores the well documented spontaneous neuronal firing. To overcome these issues stochastic DCM (Daunizeau et al., 2009; Li et al., 2011) has been developed. Stochastic DCM simply adds a random noise component generated by a Weiner process at each node, which is introduced as a free parameter, and this spontaneous activity can propagate through existing connections. As such, stochastic DCM promises a more realistic modelling of task-based activity, and allows modelling of resting state time-series, where no experimental manipulation is present to provide a driving input. In this thesis I use deterministic, rather than stochastic DCM, since stochastic DCM is a very recent innovation and issues regarding inversion of stochastic non-linear systems, and with over-fitting are still being resolved (e.g. Daunizeau et al., 2012), stochastic DCM takes about 30 times as long as deterministic DCM, and though it would be nice to model neuronal noise, it is not necessary to test our hypotheses, since our design includes experimental input.

1.3.1.3 Graph Theory

Functional and effective connectivity are primarily used to investigate the interactions of a restricted set of regions of interest, usually sub-networks involved in a task. An alternative approach is to look at the set of all interactions between all regions, termed the connectome, and discern the topological characteristics of the whole network. Graph theory is an area of discrete mathematics concerned with the characterisation of networks. In graph theory a network, or graph, is treated as a set of nodes and a set of edges, which represent links/relationships between the nodes. Brain functional activity is ideally suited to being modelled as a graph, since it consists of functionally specialised regions which to some degree overlap with anatomically distinct regions, and these are treated as the nodes of the graph. These units communicate via white matter tracts in the brain, and the degree of coherence in the activity of different nodes is taken as the strength of the edge between nodes.

Once the graph has been constructed, there are a number of characteristics we can measure to elucidate the nature of the network. Figure 1.1 and the list below describe some common graph measures:

- Degree: The number of connections of a node (see red links, Figure 1.1).
- Clustering coefficient (mC): Describes the likelihood of two nodes that are connected to a common node being connected to each other. It is a measure of 'cliquishness' in a network. To calculate, the number of complete triangles (see blue triangle, Figure 1.1) around a node is divided by the number of possible triangles given the degree of a node:

$$C_i = \frac{2t_i}{k(k-1)}$$

  This is then averaged over all nodes to get the mean clustering coefficient of the network.
- Modularity (Q): The degree to which the network is partitioned into sub-graphs with a large number of connections within the sub-graphs, but relatively few connections between sub-graphs. An optimisation algorithm is used to assign modules (Newman, 2006), which maximises the number of within module connections, and minimises the number of between module connections. Once modules, u, have been assigned, the modularity is calculated as:

$$Q = \sum_{u \in M} [e_{uu} - \sum_{v \in M} e_{uv}]$$

where M is the set of modules, and e_{uv} is the proportion of links that connect nodes in module u with nodes in module v.

- Rich Club Coefficient (ϕ**)**: Quantifies the degree to which hubs (highly connected and/or central nodes) preferentially associate with each other:

$$\phi(k) = \frac{2E_{>k}}{N_{>k}(N_{>k} - 1)}$$

where $N_{>k}$ is the number of nodes with degree greater than k, and $E_{>k}$ is the number of links between those nodes.

- Efficiency (Eg): The inverse of path length, where path length is the number of connections traversed to get from one node to another (See green path, Figure 1.1).

$$Eg = \frac{1}{n}\sum_{i \in N} E_i = \frac{1}{n}\sum_{i \in N} \frac{\sum_{j \in N} d_{ij}^{-1}}{n-1}$$

where d_{ij} is the shortest path between nodes i and j. This is averaged over all node pairs to give global efficiency.

- Random network: The significance of graph measures must be assessed in comparison to null-hypothesis networks. The values of graph measures are strongly influenced by 'low' level network attributes such as the number of nodes, edges and the degree distribution, which say nothing of the network topology. To control for these factors, graph measures are typically normalized to those of an equivalent random network. The most common null-hypothesis network is a random network with the same number of nodes and edges, and the same binary degree distribution as the observed network. The graph measures can then be calculated for the random network, and normalized graph metrics calculated as:

$$\boldsymbol{\lambda} = \frac{\boldsymbol{E_g}}{\boldsymbol{E_g^{random}}} \quad , \boldsymbol{\gamma} = \frac{\boldsymbol{mC}}{\boldsymbol{mC^{random}}} \quad , \phi_{norm} = \frac{\phi}{\phi^{\boldsymbol{random}}}$$

- Small world index (σ): Describes how nodes in a network can be connected in relatively few steps, whilst maintaining local clustering. Complex networks generally have greater clustering than random networks, but comparable efficiency, giving them a greater small-worldness. Small world-ness is calculated as:

$$\boldsymbol{\sigma = \gamma\, \lambda}$$

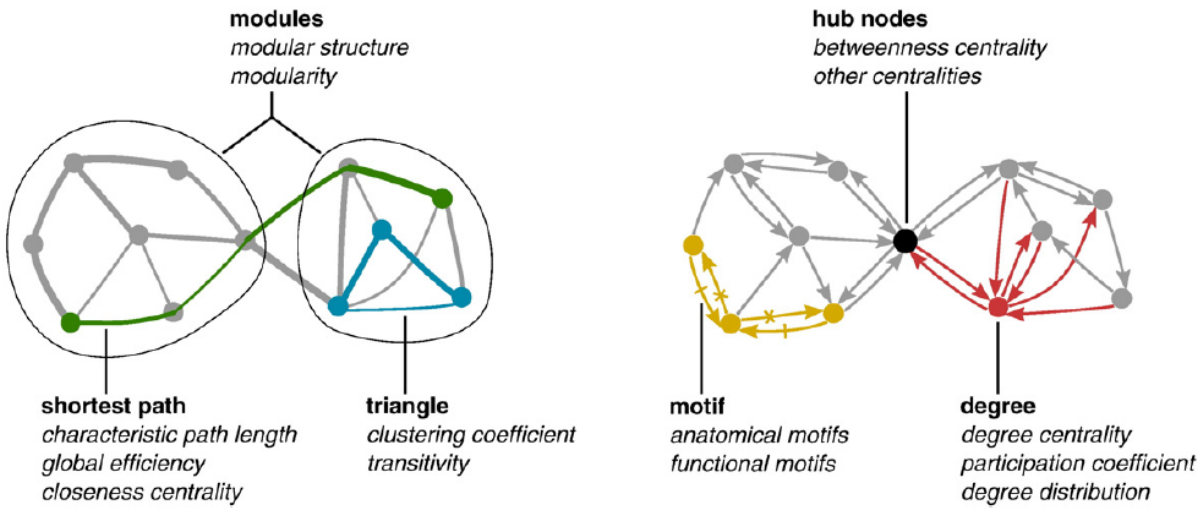

Figure 1.1: Depiction graph measures. Replicated from Rubinov and Sporns (2010)

The use of graph theory in the social and physical sciences underwent a massive expansion with the seminal paper of Watts and Strogatz (1998), which demonstrated that small-world networks with high clustering and short path lengths can be constructed with the random rewiring of just a few connections of a regular (highly clustered) network. The paper also demonstrated the ubiquity of the small-world organisation in man-made and natural systems, specifically, collaboration networks of Hollywood film actors, electricity power grid networks, and the neural network of the C.elegans nematode worm. The small-world property was quickly revealed in human brain networks with EEG (Stam, 2004), and fMRI (Achard et al., 2006). In the context of brain functional networks, the small world property allows effective specialised processing within modules, whilst maintaining effective integrated processing over the entire network. As the field has developed, emphasis has shifted towards the economy of networks, modular architecture and the behaviour of hub regions. Human brain networks are cost efficient (Achard and Bullmore, 2007), that is highly efficient whilst minimising wiring cost. Achard and Bullmore, 2007 also demonstrated that human functional brain networks follow an exponentially truncated power law degree distribution, shown to be resilient to targeted attack. The cost efficiency and resilience of brain networks reflects the notion that the brain evolved under evolutionary pressure, whereby efficient transfer of information, and robustness to damage conferred survival benefits, but must be achieved with scarce resources (Bullmore and Sporns, 2012). Functional brain networks are observed to be modular, sets of nodes segregate out into distinct groups with strong intra-group connections, and relatively few inter-group connections. The modules detected using graph modularity algorithms are qualitatively similar to the networks consistently observed by applying either

seed-based correlation or independent component analysis (ICA; Beckmann et al., 2005; Damoiseaux et al., 2006) to rs-fMRI data, and include somatosensory/motor and auditory, vision, attention, default mode, and limbic/paralimbic and subcortical networks (He et al., 2009; Fair et al., 2009; Meunier et al., 2009). These modules are depicted in Figure 2.1 of this thesis. The partitions displayed represent the optimal partition giving maximum modularity, however, it should be noted that graph theory modularity partitions are degenerate, in that many different partitions give similarly high modularity (Good et al., 2010; Rubinov and Sporns, 2011). Thus, observed partitions are influenced by pre-processing methodologies (and noise). Further, the degenerate nature of partitions may reflect the need for dynamic switching of nodes between modules, required for adapting to task context, or simply switching between systems in resting state (Bressler and McIntosh, 2007). Such considerations are reflected in the variable assignment of nodes in Figure 2.1. Recently, structural brain networks have demonstrated a "Rich-Club" property (van den Heuvel and Sporns, 2011), meaning that the highly connected nodes (hubs) are more highly connected with each other than would be expected based on their degree (number of connections) alone. This property is likewise known to give a network high efficiency of information transfer and resilience to targeted attack.

The role of network organisation as characterised by graph theory in cognitive function is a relatively unexplored area. van den Heuvel et al. (2009) find a negative correlation between normalised path length and IQ ($n=19$, $r=-0.54$, $p=0.01$). Working memory has also been investigated in a graph theory setting. Bassett et al. (2009) demonstrate that higher cost efficiency in MEG-derived functional brain networks is associated with higher performance in N-back working memory tasks ($n=57$, $p=0.02$). Stevens et al. (2012) measure strong positive correlations between inter-individual working memory performance and modularity ($n=22$, $r=0.56$, $p=0.009$) and small-worldness ($r=0.50$, $p=0.04$) of their resting functional brain networks. They also show a strong intra-individual correlation across sessions between modularity and WM performance ($r=0.54$, $p=0.013$). The authors estimated that modularity accounts for 25% of variability in the residual variance in WM capacity in the second session above and beyond that seen in the first session.

1.3.2 Experimental Domains

In this thesis, I explored the resting state brain networks and working memory brain networks. In the resting state experiment participants were instructed to remain at rest with their eyes closed, and to not think of anything in particular and not fall asleep, whilst a scanning sequence sensitive to BOLD contrast was run. In the working memory experiment, participants undertook a visuospatial version of the N-Back working memory task (Callicott et al., 1998). These two experimental domains are well studied, and were chosen for the Queensland Twin Imaging Study based on their relevance to contemporary systems neuroscience, and current interest in the neuroimaging community. The literature on these tasks, and the science relevant to my analysis is reviewed in following sections.

1.3.2.1 Resting State

At rest and in the absence of any externally driven cognitive demands, the brain is in a constant state of activity. Spontaneous fluctuations in neuronal activity, as represented by the BOLD fMRI signal, can be as large as those evoked in task paradigms (Fox and Raichle, 2007). Further, task-related metabolism increases account for only 5% of the brains total energy consumption, suggesting a large energy proportioned to intrinsic neuronal signalling (Raichle, 2006). Resting state fMRI (rs-fMRI), aims to characterise this intrinsic activity of the brain. Typically a subject is placed in the MRI scanner and told to lie still and refrain from falling asleep, with either eyes closed or focused on a tannenbaum, whilst a pulse sequence sensitive to the BOLD signal is executed.

In their landmark study (Biswal et al., 1995) were the first to note spatial correlation in the BOLD fMRI signal in the absence of any external driven task or cognitive demand. They demonstrated that the left and right regions of the primary motor cortex were coordinated in activity, despite the lack of any motor task.

This study sparked numerous others looking at the characteristics of the spontaneous fluctuations in the BOLD signal. A plethora of networks containing spatially distributed regions showing coherent activity have since been identified at rest and these networks largely constitute regions with overlapping function. Among the most consistently observed are the somatomotor network, the default mode network (DMN), the visual and auditory

networks and the dorsal and ventral attention networks. The default mode network is particularly noteworthy, in that its constituents (among them the posterior cingulate cortex, regions in medial prefrontal cortex and inferior parietal cortex) demonstrate greater activity at rest compared to task-performance (Shulman et al., 1997), and are intrinsically anti-correlated with other functional networks involved in attention and working memory (Fox et al., 2005). Temporal coherence of regions within resting state networks (RSNs) are similar during task-performance (Arfanakis et al., 2000). In fact, there is growing evidence that resting state activity influences task response, and/or explains much of the variability in task-evoked activity. For example, (Arieli et al., 1996) showed with optical imaging and electrophysiological recordings that the much of the variability in response of neurons in the visual cortex to visual stimulation was accounted for by the ongoing activity of those neurons at time of stimulus presentation. In humans (Fox et al., 2006) show that much of the trial-to-trial variability in the left somatomotor cortex (LMC) during right handed finger tapping task was accounted for by variability in the right somatomotor cortex (RMC) which was not involved in the task. They suggest that rest activity and task-evoked activity are linearly superimposed in this task paradigm.

Resting state networks (RSNs) display a number of characteristics which supports their interpretation as intrinsic neural activity, rather than poorly constrained behaviour/self-determined-task activity, or conscious mentation. The following list of considerations supporting the intrinsic connectivity nature of resting state fluctuations is replicated directly from a review on resting state fMRI (Fox and Raichle, 2007):

- Similar patterns of BOLD fluctuations to those of traditional resting conditions are observed in sleep and under anaesthesia.
- Coherent activity between brain regions at rest occur within systems associated with behaviour, even in the absence of that behaviour.
- Resting state activity persists during task-evoked responses, where brain activity is a superposition of resting activity and task-evoked activity.
- Resting state coherence patterns differ from those expected of conscious mentation. For example, Nir et al. (2006) show that the patterns of activation in visual regions during mental imagery are different to those observed in visual regions in resting state.

- Resting state networks encompass a wide range of neuroanatomical systems. It is unlikely that unconstrained conscious mental activity engages all these systems simultaneously.

Under these considerations, a number of interpretations of spontaneous BOLD fluctuations have been suggested. One possibility is that spontaneous activity is a record of which regions have interacted in the past, an interpretation based on Hebbian theory, whereby a presynaptic neuron's repeated stimulation of the post-synaptic neuron results in an increase of synaptic strength between those two cells.

A related interpretation is that spontaneous activity `prepares the system' for future use, by keeping in close contact those regions which are likely to need to interact in response to external stimulation.

1.3.2.2 Working Memory

1.3.2.2.1 Historical Overview

Working Memory is a conceptual framework designed to characterize the short-term maintenance and concurrent manipulation of information. Its cognitive psychology manifestation was proposed by Baddeley and Hitch (1974), which expanded prevailing unitary models of short term memory (e.g. Atkinson and Shiffrin, 1968) into a multi-component model, which emphasized the interplay between storage and processing required for execution of complex cognitive and behavioural tasks. Working memory was proposed to consist of multiple subsystems, the visuospatial sketchpad, the phonological loop and the central executive. As suggested by their names, the visuospatial sketchpad stores visual information as a visual representation. The phonological loop corresponds to sub-vocalisation as a store of information. It is sub-dived into a phonological short term store, and an articulatory sub-vocal rehearsal process. These systems are controlled by the central executive which in addition to regulating these storage buffers, performs a number of high-level operations, among them directing attention and integrating information.
More recently Baddeley (2000) added a fourth component to the model, the episodic buffer, in order to describe the integration between the different subsystems and interface with long term memory. In the multi-component WM model, these four subcomponents are suggested to interact as depicted in Figure 1.2.

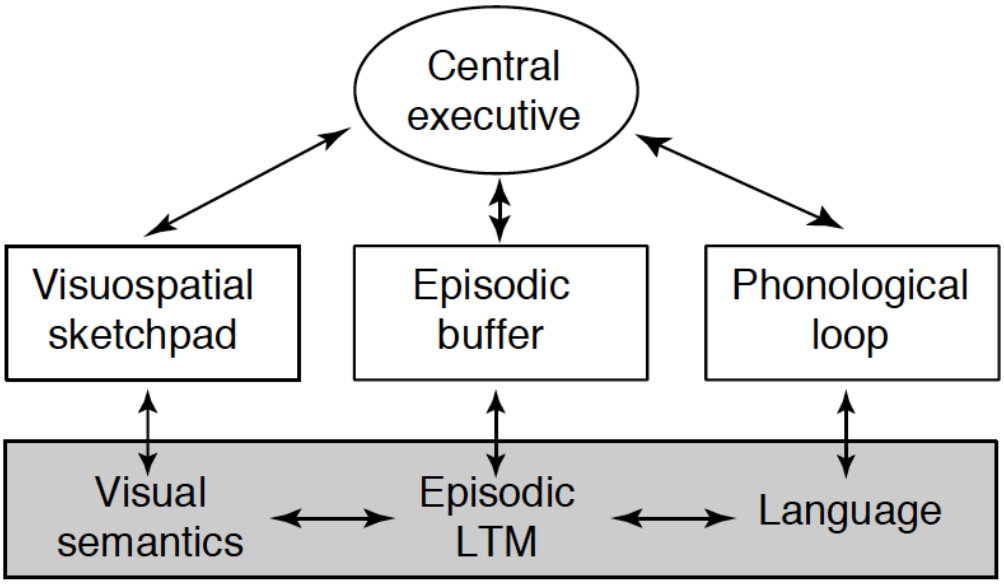

Figure 1.2: The multi-component model of WM. Unshaded elements represent fluid systems, unchanged by learning, whereas shaded elements are stable, 'crystallized' systems. Replicated from Figure 1; Baddeley (2000).

The neuroscience of working memory has long been guided by the early electrophysiological work in monkeys demonstrating sustained activity (firing rates) in the prefrontal cortex (PFC) during the delay period of working memory (Fuster and Alexander, 1971; Kubota and Niki, 1971). This PFC activity was suggested to represent the storage of information during the delay period. Later work demonstrated dissociations in PFC activity, which was interpreted as representing separate storage buffers. Most notably, the sustained activity in more ventral PFC regions was associated with WM for objects, and dorsal PFC activity with WM for spatial locations (Wilson et al., 1993). This matched nicely with the established ventral "what" and dorsal "where" visual processing streams, suggesting a preservation of processing streams all the way through to executive processing and memory storage. The combination of the cognitive and neuroscientific theories, with the storage buffers of the cognitive model assumed to reside in the pre-frontal cortex, has been the dominant paradigm of WM research since the 1980's.

Although this standard model of WM is still hugely influential, a number of alternative interpretations of data, and direct refutations of the model exist. In general, these alternative models describe prefrontal activity, along with parietal activity, as carrying out executive processes such as attention and manipulation of information, with storage capabilities located elsewhere. In a review of evidence opposed to the standard model, Postle (2006) describes

WM as an emergent property of sensory-motor and attentional systems, with existing sensory systems holding memory traces, and PFC acting as a coordinator to determine which memory traces are maintained. The primary motivation behind this view are the multiple observed neural dissociations for different types of WM, with different brain regions involved in "storage" of stimuli of different nature. The extent of the dissociations requires the un-parsimonious hypothesis of a large number of independent specialised memory systems, rather than a multipurpose system capable of handling different types of information. Consequently, alternative interpretations of the sustained prefrontal activity have been suggested. Curtis and D'Esposito (2003) interpret the sustained activity of the PFC as facilitating response selection, rehearsal and motor planning, rather than storage, with representations held in posterior sensory areas and PFC activity "working on" the held information. Additionally, many authors note the strong overlap between the neural correlates of WM and those of attention (Awh et al., 2006; Chun, 2011), with some going so far as to label WM as working attention. For example Gazzaley and Nobre (2012) review evidence that the top down control of sensory cortices by prefrontal and parietal regions is a shared feature of both WM and attention.

Whilst sustained activity (spiking) of neurons in the PFC remain a key neurological correlate of WM (Fuster and Alexander, 1971; Funahashi et al., 1989; Goldman-Rakic, 1995; Curtis and D'Esposito, 2003) recent efforts have been made to reframe WM neurophysiology in terms of neural networks. Computational neural networks can store information via the pattern of connections between neurons (Hopfield, 1982; Haykin, 1998). Mongillo et al. (2008) propose a mechanism by which biological neural networks may achieve the same outcome. In their model, a WM memory is maintained by short term facilitation between populations of neurons, mediated via increased calcium residue at the presynaptic terminals between the neuronal population (presynaptic calcium influx is the mechanism triggering neurotransmitter release). This population of connected neurons form an 'offline'/metabolically inexpensive memory state which can be activated by a global excitatory input to the system. Likewise, network models on the macroscopic systems level are being developed, e.g. Edin et al., 2009 describe a computational model whereby storage of information in the PC is boosted by top-down excitation from the dlPFC. Similarly, network models describing fMRI BOLD activity of large macro-anatomical regions during WM, such as structural equation modelling and dynamic causal modelling, are on the increase (Honey et al.,

2002; Schlosser et al., 2006; Ma et al., 2012). It is these systems-level, macro-anatomical network descriptions which are utilised in Chapters 3 and 4.

1.3.2.2.2 Neuroimaging of Working Memory

WM has been extensively studied with neuroimaging, with many regions other than prefrontal cortex identified as important, which highlights the distributed nature of working memory processing. Although the regions involved in working memory are now well established, there is no consensus on the subdivision of their function.

In their meta-analysis and literature survey on the N-Back WM task (verbal, object and spatial), Owen et al. (2005) identify the dorsolateral prefrontal cortex (dlPFC), ventrolateral prefrontal cortex (vlPFC), frontal pole, medial premotor cortex and posterior parietal cortex as regions commonly activated across tasks.

The view of prefrontal cortex delay-period activity prevalent in the 1970's-1990's, that this activity represents storage, and that representations of different material type (verbal, object, spatial) are stored in different PFC subregions (Section 1.3.2.2.2.), has been eroded in the last two decades, largely as a consequence of neuroimaging data. Studies designed to separate the various components of working memory attribute the persistent activity to selection processes (Rowe et al., 2000; Schumacher et al., 2003), storage and use of task rules and variables (Wallis et al., 2001; Warden and Miller, 2010; Riggall and Postle, 2012), directing of attention to internal representations (Gazzaley and Nobre, 2012) and motor planning (Pochon et al., 2001; Romo et al., 1999), rather than storage of memoranda. The evidence for these multiple roles primarily consists of differential dlPFC BOLD response to experimenter manipulations to each of the aforementioned task components independently (Curtis and D'Esposito, 2003), for example, some studies report that the dlPFC is active when a location being maintained is selected for response, but not during the delay period (Rowe et al., 2000), and dlPFC activity varies with demands of response selection, even in the absence of retention of information over a delay period. More recently, multivariate pattern analysis applied to working memory has supported these roles of the dlPFC by revealing task-relevant information held via population coding in the dlPFC (Sreenivasan et al., 2014). Of particular note is that the lateral prefrontal cortex is able to encode multiple task variables (rules, categories, temporal ordering etc.) within a single population of neurons, and each task

variable can be extracted independently from the population code (Barak et al., 2010; Jun et al., 2010; Machens et al., 2010). Similarly, multivariate patterns of activity during the delay period in the visual cortex contain information about visual features held in working memory (Harrison and Tong, 2009; Xing et al., 2013), despite the lack of persistent heightened activity during the delay period (Offen et al., 2009).

Regarding the specialisation of dorso-lateral verses ventro-lateral regions within the pre-frontal cortex, a popular contemporary view is that prefrontal cortex function can be subdivided by executive process type. Owen et al. (2005) suggest that the primary role of the dorsolateral prefrontal cortex to be strategic reorganisation and control of working memory contents. Working memory capacity is greatly enhanced when remembered material is organized into higher level chunks (Ericcson et al., 1980). The dlPFC is more strongly activated during tasks requiring such reorganization (Bor et al., 2003) and in some studies (Owen et al., 1996; Petrides and Milner, 1982) patients with frontal lobe damage are seen to have deficits in working memory tasks where organizational strategy is required, but normal performance in tasks where no obvious strategy to facilitate performance exists. D'Esposito et al. (1998) come to a similar conclusion in their review, noting that in 16 out of 18 studies requiring complex executive management of memory, the dlPFC is activated, compared to 6 out of 24 where the manipulations are more basic. In this view, the ventrolateral prefrontal cortex is more involved in tasks involving simpler maintenance (Hartley and Speer, 2000), and implementation of intended plans (Owen et al., 2005), which is related to the regions role in behavioural inhibition, such as in Go-no go tasks (Garavan et al., 1999). However, other accounts of process-dependent PFC sub-division do not allocate the same roles to dlPFC and vlPFC. In their meta-analysis of 60 WM tasks, Wager and Smith (2003) find that the dlPFC is preferentially activated for the operations of continuous updating and temporal order memory, operations fundamental to the N-Back WM task, whereas the vlPFC is preferentially activated for operations which transform the identity or characteristics of remembered material, operations which they suggest may involve inhibition and attention switching. A third interpretation of PFC function, is that it is not critical to WM at all. The review of Muller and Knight (2006) describe the literature on lesion studies including their own work, and claim that whilst some studies of frontal-lobe patients do show impairment in WM (Baldo and Shimamura, 2002), others do not (D'Esposito and Postle, 1999). In their own work, (Muller et al., 2002), they find that neither patients with ventromedial PFC (vmPFC) nor dorsolateral PFC lesions had lower WM performance than controls on either 1-back or 2-Back tasks, and

only patients with damage to both dlPFC and vmPFC were impaired, predominantly on the 2-Back task. Their conclusion was that the crucial portion of WM seems not to rely solely on PFC, that the PFC sustains non-mnemonic functions, and that executive sub-processes are not specialised to dlPFC or vmPFC, but rather are distributed, and that PFC neurons adapt their behaviour to current task demands (e.g. Miller, 2000).

As with the PFC, the parietal cortex has been attributed a large number of functions in working memory. One widely accepted finding is that the storage of memory for visuo-spatial material is organised along the same lines as the perceptual processing of that material. WM for objects recruits the occipito-temporal "ventral" processing stream, and WM for spatial locations recruits the occipito-superior parietal "dorsal" processing stream. This interpretation is supported by meta-analysis of neuroimaging activation studies (Wager and Smith, 2003) and patient lesion studies (Muller and Knight, 2006). In addition to storage and rehearsal functions, the parietal cortex is known to be involved in attentional shifts and other executive roles (Corbetta et al., 1995; Cabeza and Nyberg, 2000). Wager and Smith (2003) find the superior parietal cortex (BA7) to be the only region showing significant effects for all types of storage material and all executive processes, and they suggest that this region may act as a mediator of basic control over the focus of attention.

Finally, there is a proposed neuroanatomical dissociation in WM between verbal and spatial working memory, with verbal working memory more strongly activating the left hemisphere, and spatial working memory the right (D'Esposito et al., 1998), though the verbal lateralisation is more apparent at low executive demands, and the spatial lateralisation at high executive demands (Wager and Smith, 2003).

In summary, neuroimaging has revealed the participation of numerous neuroanatomical regions in WM. These regions have been ascribed functions related to the multiple sub-processes of working memory, though there exists controversy over the allocation of structure to function particularly for the dlPFC. The distributed anatomy, in conjunction with the cognitive hypothesis of a multi-model WM, motivates the investigation of interactions between these regions and processes, rather than considering them in isolation. This is the subject of the next subsection.

1.3.2.2.3 Brain Functional Connectivity and Working Memory

This thesis contains one study measuring the functional connectivity pattern of the dlPFC during WM, and one study investigating the directed connectivity between dlPFC and parietal (PC). These phenotypes were chosen as there has been prior work implicating dlPFC connectivity as a core mechanism subserving working memory.

The literature on connectivity during working memory supports the notion of top down modulation of perceptual regions (visual cortex, fusiform face area etc.) by control regions (PFC, PC), manifesting in increased functional connectivity between these regions (Curtis and D'Esposito, 2003, Zanto et al., 2011). In their review Gazzaley and Nobre (2012) point out that this top down modulation is a mechanism shared with selective attention, which recruits the same brain regions as those involved in encoding, maintenance and retrieval during WM, and propose that the top-down modulation is a feature of the influence of attention on early perceptual processing and not a process specific for WM.

Fronto-parietal connectivity has been consistently associated with WM tasks. Electrophysiology in monkeys demonstrate synchronised activity between prefrontal and parietal neurons (Chafee and Goldman-Rakic, 1998), which has been proposed to integrate perception with action (Quintana and Fuster, 1999). Likewise human neuroimaging has been used to measure the interaction between these regions during WM. Honey et al., 2002 found increased inferior fronto-parietal connectivity with increasing memory load (verbal N-Back task). Woodward et al. (2006) looked at functional connectivity networks during a Sternberg item recognition test, and found separate networks involved in encoding and maintenance, with a network including dlPFC, superior parietal and visual cortices increasing their functional connectivity during the encoding stage.

Despite its traditional interpretation as the task-negative network, functional connectivity in the DMN both at rest and during WM tasks has been shown to correlated with WM performance. Hampson et al. (2006) found that accuracy in a verbal N-Back working memory task was correlated with the strength of connectivity (Pearson's correlation) between the medial frontal cortex and the posterior cingulate cortex at rest ($p=0.01$, $N=9$) and during WM ($p=0.04$). In a follow up study, Hampson et al. (2010) demonstrated that interaction between task positive and task-negative regions can mediate performance, with the (negative) connection between left dlPFC and medial frontal cortex (MFC) at rest

correlating with task accuracy (r=-0.73, p=0.03, N=9). A possible mechanistic role for the antagonistic relationship between task-positive and task-negative regions has been suggested elsewhere by Kelly et al. (2008) , who show that the negative correlation is related to response time variability in the Eriksen flanker task (a response inhibition task), suggesting that the anti-correlation may suppress default mode activity during task performance. Enhanced DMN activity during task performance has been implicated with attentional lapses (Weissman et al., 2006), and mind wandering (Mason et al., 2007), so increased anti-correlation may contribute to lower response time variability via the suppression of mind wandering and attentional lapses.

More recently, dynamic causal modelling has been applied to working memory tasks, with the focus being on fronto-parietal interactions. Deserno et al. (2012) used DCM to characterise the interaction between the dlPFC, PC and visual cortex, in SZ patients and healthy controls, using a numeric working memory task. The best fitting models were those in which the connectivity from dlPFC to PC was increased during the two-back (2B) condition. However, it was found that the SZ patients did not exhibit this load-dependent increase in connectivity, suggesting a possible pathological mechanism. This finding motivated the study in Chapter 3 of this thesis, where we use DCM with a modified version of the Deserno et al. (2012) models to estimate the heritability of this disease related task-dependent connectivity modulation.

Other studies have used DCM to characterise fronto-parietal interactions during WM, but the results have not been consistent, perhaps due to differing task paradigms and region of interest selection. Ma et al. (2012), use a numeric delayed match to sample task, and model the activity of bilateral posterior parietal cortex (PPC), inferior frontal cortex (IFC) and middle frontal gyrus (MFG), and anterior cingulate cortex. They find load-enhanced connectivity from Right PPC to right middle frontal gyrus, right IFC, left ACC, left MFG and left PCC. The modulation of the forward connection contrasts with the modulation of the backward connection seen by Deserno et al. (2012). Dima et al. (2014) similarly see increased connectivity from PC to dlPFC, using a verbal N-Back WM task, and using DCM to model the activity of bilateral PC, dlPFC and ACC.

In contrast to these previous three studies, Harding et al. (2014) do not observe any task-dependent increase in fronto-parietal connectivity. Using a verbal N-Back WM task, they

find load reduced connectivity from Intra-parietal sulcus (IPS) to presupplementary motor area/dorsal anterior cingulate cortex (pSMA/dACC), and dlPFC to pSMA/dACC, and load-increase connectivity from inferior frontal junction (IFJ) to pSMA/dACC. The differences between these 4 studies demonstrate that the conclusions drawn from DCM are sensitive to task design and DCM model space, and further that the issue of effective connectivity during working memory is not settled, and a large sample size study will be a valuable contribution.

The choice of endophenotypes in chapters 3 and 4 of this thesis are based on the literature reviewed in this section. The central role of the dlPFC in WM makes it the focus of Chapter 4, whilst the connectivity between prefrontal and parietal cortices is the focus of Chapter 3.

1.3.3 Psychiatric Disease

One of the requirements of an endophenotype (section 1.1 and Gottesman and Gould, 2003) is that it be associated with disease. In this thesis, the features of neural connectivity investigated were chosen on the basis of prior association with disease, or prior association with cognitive performance. In this section I review the literature investigating the relationship between resting state fMRI and working memory with psychiatric disease.

1.3.3.1 Resting State fMRI and Psychiatric Disease

Abnormalities in spontaneous fluctuations in neuronal activity have been linked to a wide range of neuropsychiatric disorders. Before detailing the literature on rs-fMRI in pathology, I note the opinion expressed in Greicius (2008) that rs-fMRI has the advantage over task fMRI in a clinical setting as sick patients may be too impaired to properly perform a task, whereas a resting scan can be easily performed. Further, longitudinal cataloguing of disease progression may be confounded in task fMRI by habituation or practice effects which is not an issue in rs-fMRI.

Alzheimer's disease (AD) shows consistent reductions in resting state functional connectivity, and has been the most extensively examined using rs-fMRI. The first study to examine resting state alterations in AD showed that connectivity between right and left hippocampus reduced in AD (Li et al., 2002). Later studies showed reduction in connectivity between the hippocampus and regions within the DMN; Sorg et al. (2007) and Greicius et al. (2004) investigated AD using an Independent Component Analysis (ICA) approach, in which all RSNs were extracted and analysed. They found reduced overall functional connectivity in the DMN, but no abnormalities in any other network (other than the dorsal attention network in Sorg et al., 2007), suggesting a key role of the DMN in Alzheimer's disease. This finding is particularly pertinent in that the DMN has been implicated in episodic memory, the deterioration of which is the hallmark of Alzheimer's disease.

RSNs are also seen to be abnormal in depression, with some studies showing potentially clinically significant results. Greicius et al. (2007) observed increased connectivity in the subgenual ACC, precuneus and medial thalamus within the DMN in depressed patients. Furthermore the connectivity strength in the subgenual ACC correlated with duration of

depressive episode. Anand et al. (2005) considered a different set of regions, the dorsal ACC, amygdala and subcortical regions including medial thalamus. They found reduced connectivity between dorsal ACC and the other regions, which was partially restored after 6 weeks of sertraline treatment.

Schizophrenia has also been widely studied with rs-fMRI. Schizophrenia is considered by many in the neuroimaging community to be a disconnection syndrome, with multiple brain-wide connectivity abnormalities contributing to the numerous symptoms of the disease (Friston and Frith, 1995). Although both reductions (Bluhm et al., 2007; Ongur et al., 2010) and increases (Zhou et al., 2007; Whitfield-Gabrieli et al., 2009) in connectivity within the DMN during resting state have been reported, systematic reviews of resting state fMRI of schizophrenia, indicate that the majority of studies support specific and system wide reductions in connectivity across all stages of the disease (Pettersson-Yeo et al., 2011).

1.3.3.2 Graph Theory and Psychiatric Disease

There is a considerable literature on pathological departures from the idealised network configuration described in section 1.3.1.2.

In AD, Supekar et al. (2008) demonstrate that AD patients have lower normalised[1] clustering coefficient than controls, and that this graph measure detects AD with sensitivity 72% and specificity 78%. Buckner et al. (2009) took a nodal approach to investigating Alzheimer's and attempted to identify network hubs and ascertain whether these hubs were preferentially targeted in the disease. They found a correlation of 0.68 between the pattern of cortical hubs and the amyloid beta deposition distribution in AD patients (linked to disease severity), suggesting that AD does indeed affect the most critical nodes of functional brain networks. Functional brain networks in AD have also been explored with EEG and MEG. Networks constructed using EEG demonstrate longer path lengths in AD patients (Stam et al., 2007).

Like AD, functional brain networks extracted with rs-fMRI in Schizophrenia also display lower clustering coefficients, but are also associated with a wide range of other network abnormalities (Fornito et al., 2012), including higher path lengths, and abnormal

[1] normalised to the value of clustering coefficient in a random graph with the same degree distribution and overall functional connectivity.

nodal characteristics (Liu et al., 2008). Lynall et al., 2010 produced similar results, lower clustering coefficients and reduced small worldness, but further reported lower overall functional connectivity, and a lower probability of high degree hubs, giving rise to a more diversified and resilient network in Schizophrenia patients. This paper also reported higher global efficiency in SZ patients compared to controls which contrasts with the longer path length seen in Liu et al. (2008), but is in agreement with Alexander-Bloch et al. (2010). With EEG, lower clustering coefficients are also seen, with path lengths hardly changed (Micheloyannis et al., 2006). Such changes can be summarised as a tendency towards random networks in schizophrenia.

In summary, these neuropsychiatric graph theory studies tend to show some change in a graph measure away from the economical small world model, and the graph measures have moderate discriminatory power in detecting disease within the clinical group. However, there is currently little work on whether graph measures have the sensitivity to distinguish between different neuropsychiatric diseases.

1.3.3.3 Working Memory and Psychiatric Disorder

Working memory deficits are a core feature of Schizophrenia. Numerous studies demonstrate a reduction in WM performance for both medicated and unmedicated SZ patients (e.g. Carter et al., 1996; Park and Holzman, 1992; Wexler et al., 1998), and that the deficit is present across a range of WM tasks and modalities (Lee and Park, 2005). A large number of clinical studies implicate reduced prefrontal activation in the WM deficits in SZ (Barch et al., 2001; Carter et al., 1998) , though this finding is not invariable (Manoach, 2003). Glahn et al. (2005) stress that WM deficits in SZ are not restricted to prefrontal hypo-frontality, and increased activation in anterior cingulate cortex and left frontal pole is a consistent feature of N-Back WM task in SZ patients. Other researchers place the emphasis on dis-connectivity in SZ (Friston and Frith, 1995), since numerous aspects of brain connectivity are disrupted in SZ (see sections 1.3.3.1 and 1.3.3.2), including during WM (Meyer-Lindenberg et al., 2001).

1.3.4 Genetics

The primary concern of this thesis is measuring the heritability of a number of features of brain connectivity. Heritability is defined as the proportion of the total variance in a trait that is due to the genetic differences in the population.

Any phenotype can be considered as arising from genetic and environmental effects:

$$P = G + E$$

And so the variance of a trait is given by:

$$Var(P) = Var(G) + Var(E) + 2cov(G, E)$$

The heritability of a trait is thus defined as:

$$h^2 = \frac{Var(G)}{Var(P)}$$

It is important to note that heritability does not equal the contribution of genes to a trait, but rather the contribution of genetic variance to variance in the trait, and is dependent on the genetic and environmental variation within the population. Equivalently, heritability measures the genetic contribution to inter-individual differences in a trait.

To measure heritability, we use the classical twin design and structural equation modelling (Neale and Cardon, 1992). The basic premise of twin studies is that genetic and environmental influences can be deduced from comparing the similarity between MZ twins as compared to DZ twins. Since MZ twins share all genetic polymorphisms, and DZ twins share on average 50% of their polymorphisms, a greater similarity in a trait between MZ twins than DZ twins is indicative of a genetic contribution to that trait. The most straightforward measure one can take is the correlation between twin 1 and twin 2 in a trait, where a MZ twin correlation greater than a DZ twin correlation indicates a genetic contribution, whereas similar twin correlations indicates environmental contributions. If both twin correlations are high, this suggests a common environmental contribution to the covariance, whereas if both twin correlations are low, this indicates that environmental influences unique to each twin account for much of the variance.

Alternatively, we can estimate a more precise contribution of genetic and environmental factors to a trait by explicitly modelling these effects. Structural equation modelling (SEM) specifies a set of linear equations relating observed dependent variables to their hidden causes, and relationships between these causes. For genetic modelling, the

dependent variables are the phenotypes, and the latent causes are the genetic and environmental factors. The covariance between dependent variables predicted by the equations is then matched to the observed covariance between dependent variables, and the parameters linking causes to their effects are optimised via maximum likelihood fitting.

For the classical twin design, a phenotype is modelled as having contributions from additive genetic factors, A, common environmental factors, C, and unique environmental factors, E, which includes measurement error.

$$P_i = aA_i + cC_i + eE_i$$

where a,c,e are path coefficients, and A_i,C_i,E_i are latent factors for the ith twin. The equations predicting the covariance structure are given as:

$$Var(P) = a^2 + c^2 + e^2$$

$$Cov(MZ) = a^2 + c^2$$

$$Cov(DZ) = 0.5a^2 + c^2$$

where the covariance between additive genetic factors has been set to 0.5 for DZ twins and 1.0 for DZ twins. The covariance between common environmental factors has been set to 1.0 for both MZ and DZ twins. These equations can be presented alternatively as mathematically complete path diagrams (Figure 1.2). Once the path coefficients a, c and e have been estimated, the heritability can be simply calculated as:

$$h^2 = \frac{a^2}{Var(P)}$$

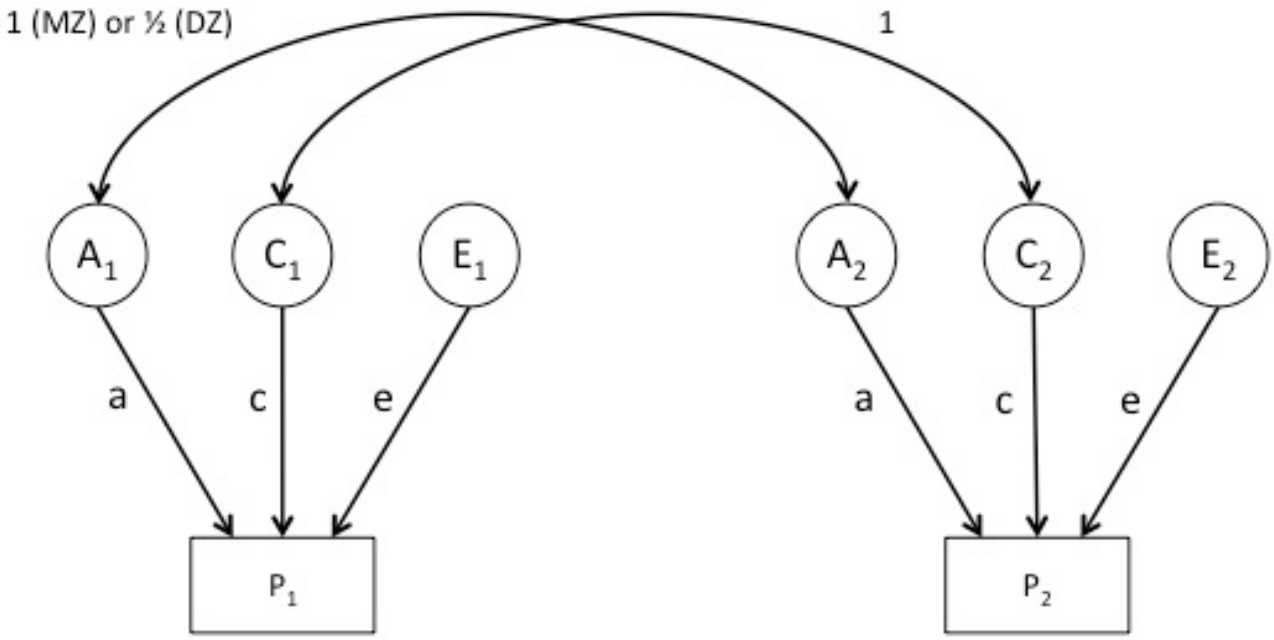

Figure 1.2: Path diagram for twin design ACE model.

The classical twin study makes a number of assumptions (Evans et al., 2002; Verweij et al., 2012). Firstly, genetic effects are assumed to be additive, where allelic effects within a gene add linearly. The model can be modified to estimate dominant genetic effects. Dominant genetic effects predict a MZ twin correlation of 1.0, and a DZ twin correlation of 0.25, since on average DZ twins share 25% of their pairwise allelic combinations. Dominant genetic variance, D, and common environmental variance can not be estimated in the same model using MZ and DZ twins only, since the effect of C is to increase the DZ correlation relative to the MZ correlation, whereas the effect of D is to decrease the DZ correlation relative to MZ correlation. Other assumptions of the classical twin model are that trait-related environments are similar for MZ and DZ twins, mating is assumed to be not assortative (where individuals with similar characteristics preferentially mate), and gene-environment interactions and correlations are ignored. Some of these assumptions may be relaxed when other relatives such as parents and non-twin siblings are added to the design.

1.3.4.1 Genetics of Resting State fMRI

Glahn et al. (2010) showed that functional connectivity within the DMN is heritable (heritability, h^2=0.42±0.17). This study focused specifically on the ICA corresponding to the DMN. The heritability estimate reported refers to the overall coherence of time series within the DMN.

In a preliminary and unpublished study using a small sample of 108 twins from the Queensland Twin Imaging Study, Castellanos et al. (2010) took a seed based approach[2] rather than an ICA approach. They chose components of the DMN as the seed time series, namely the anterior cingulate cortex and precuneus, so their findings refer to connectivity of these a priori chosen regions, contrasting with the results of (Glahn et al., 2010) which refer to overall levels of coherence within the DMN. They find that the connectivity of some regions of the DMN to the ACC and precuneus have significant Falconers heritability. However, structural equation modelling (SEM) does not produce significant estimates of additive genetic contribution, though it should be noted that this study was underpowered.

[2] where the time series of a region of interest is extracted, and the correlation of voxel time series with the ROI time series is calculated for all voxels in the brain

Some genetic association studies have been conducted on rs-fMRI. Filippini et al. (2009) find that healthy carriers of the AD risk factor ApoE ε4 allele have greater DMN coactivation. This is unexpected in light of Greicius et al. (2004) and Sorg et al. (2007), where functional connectivity in the DMN is shown to decrease in AD. The authors note the discrepancy and attribute the contrast to differences in clinical group, that is, AD patients compared to healthy carriers of the risk-allele. The short-allele of the serotonin transporter linked polymorphic region 5-HTTLPR, a risk-factor for depression, is associated with reduced resting state functional connectivity between superior medial frontal cortex and posterior hub (Wiggins et al., 2012).

1.3.4.2 Genetics and Graph Theory

Only 4 studies have been published regarding the genetic regulation of graph theoretic characteristics of functional brain networks.

The first by Smit et al. (2008) used EEG and focused on clustering, path length and the composite small-worldness. They found that clustering (h^2=46-89%) and path length (h^2=37-62%) were strongly heritable. However, small-worldness, the ratio of these two graph measures, was not significantly heritable (heritability estimates ranged from 0-51% and had wide confidence intervals (CIs)) and the authors attribute the null result to insufficient power (760 subjects). This paper also reported no significant correlation between any graph measure and IQ. This study was followed up by a longitudinal design and multivariate genetic modelling in Smit et al. (2010), which reported that genetic stability was high for clustering path length and synchronisation likelihood between ages 16-25, and that path length and synchronisation likelihood shared common genetic influences.

Using resting state fMRI, Fornito et al. (2011) took a small sample of twins (N=60) and calculated a host of network attributes of resting state functional networks. The most significant result was that the cost efficiency of the networks was under strong genetic control (h^2=60%). This finding is consistent with the hypothesis that cost efficiency of functional brain networks is a competitive selection criteria[3] . Also using resting state fMRI, van den Heuvel et al. (2013) estimate significant heritability of global efficiency (h^2=42%) but no genetic influence to mean clustering coefficient in a sample of 86 twins.

[3] Though a heritable feature is not necessarily evolutionary selected, e.g. genetic disease

1.3.4.3 Genetics of working memory

Working memory capacity is a moderately heritable trait. Ando et al. (2001) estimate storage and executive components of spatial and visual WM to have similar heritability between 43-49%. Likewise Chen et al. (2009) (h^2=53%) and Toulopoulou et al. (2007) (h^2=65%) estimate moderate-high heritability for WM performance. However the biological mechanisms by which genetic variation in WM performance are conferred are not known. In their review, Karlsgodt et al. (2011), identify four neural substrates which may independently contribute to genetic variation in WM; dopaminergic function, glutamatergic function, white matter integrity and grey matter integrity.

Dopamine

Dopamine is a modulatory neurotransmitter, involved in reward-motivated behaviour, motor control and higher cognitive functioning. In their seminal paper, Brozoski et al. (1979) demonstrate that depleting dopamine levels in the prefrontal cortex has as substantial an effect on spatial working memory performance as removing the area itself. More recently is has been shown that, WM performance follows an inverted U pattern with respect to stimulation of the dopamine receptor D1, with both low levels and high levels of D1 stimulation associated with impaired performance, suggesting an intermediate level of D1 stimulation giving rise to optimal performance (Goldman-Rakic et al., 2000).

A number of genes are involved in the regulation of dopamine levels in the brain. The most widely studied are COMT(Catechol-O-methyltransferase), a gene involved in the catabolisation of dopamine in the prefrontal cortex, and DRD2, the gene encoding the dopamine receptor D2. The Val158Met polymorphism of the COMT gene (Lachman et al., 1996), is a common SNP in which the met form gives lower activity of the gene. This polymorphism is associated with lower prefrontal activity, but its relationship to WM performance has been inconsistent. Karlsgodt et al. (2011) suggest that the mixed findings may be due to its interaction with other alleles on the COMT gene, and with other dopamine regulating genes such as DRD2. DRD2 (the gene encoding the D2 dopamine receptor) agonists and antagonists have been shown to effect WM performance, (Stelzel et al., 2009), and a number of SNPs on the DRD2 gene are associated with WM performance (Markett et al., 2010). Notably, DRD2 was recently confirmed as a SZ risk factor in a GWAS of 36,989 patients

(Schizophrenia Working Group of the Psychiatric Genomics Consortium, 2014), though COMT was not.

Glutamate and GABA

Glutamate is the major excitatory neurotransmitter in the central nervous system, whilst GABA is the primary inhibitory neurotransmitter. The prefrontal "memory-fields" proposed by Goldman-Rakic and colleagues are suggested to arise from interactions between excitatory pyramidal neurons and inhibitory interneurons (Goldman-Rakic, 1995; Compte et al., 2000) in much the same way as excitatory/inhibitory interactions establish visual-fields in the visual cortex (Sillito and Murphy, 1988). Thus any genetic variance in glutamatergic or GABAergic systems would be expected to affect WM performance. For example, dysbindin is a gene involved in glutamate signalling, and has been linked to WM performance in mutant mice (Jentsch et al., 2009) and schizophrenic patients (Donohoe et al., 2007).

White Matter Integrity

Total white matter volume is significantly correlated with WM performance (r=0.28), and is genetically correlated (r_g=0.33), meaning that the two share common genetic influences (Posthuma et al., 2003). White matter integrity as indexed by fractional anisotropy is a genetically influenced trait, (h^2=55-85%; Chiang et al., 2009). Of particular relevance to chapter 3 of this thesis, which estimates the heritability of fronto-parietal effective connectivity, Karlsgodt et al. (2010), found that the integrity or fractional anisotropy (FA) of the primary fibre tract linking the dlPFC to the PC, the superior longitudinal fasciculus (SLF), is heritable (h^2 (FA)=59%), and is genetically correlated specifically with spatial working memory performance (r_g=0.59).

1.4 Thesis Aims

The aim of this thesis is to identify promising neural endophenotypes, using the relatively unexplored resting state fMRI and working memory fMRI data sets of the Queensland Twin Imaging Study, which is the largest sample of twins scanned with MRI in the world. I have primarily chosen phenotypes which have been associated with psychiatric disease. Features of brain connectivity found to be highly heritable and associated with psychiatric disease are

potential endophenotype and may be useful in unravelling the genetic contributions to disease.

Based on current areas of interest in the neuroimaging community, the literature review in section 1.3 reveals a number of potential phenotypes.

Given the large amount of literature linking disrupted brain network behaviour, as quantified with graph theory, to psychiatric disease, understanding the genetic architecture of these network features will shed light on potential disease mechanisms. Thus, Chapter 2 of this thesis aims to measure the genetic influences on graph theoretic measures of brain networks. As discussed in section 1.3.4.2, there have been two prior studies on the heritability of graph measures using rs-fMRI (Fornito et al., 2011; van den Heuvel et al., 2013). Both of these found significant heritability of network integration, but neither study reported a genetic influence on network community structure. Given the small sample sizes of these studies (60 and 86), it is likely that they were underpowered (See Chapter 2 for our power calculations).

In Chapter 3 I measure the heritability of the proposed SZ disease mechanism from Deserno et al. (2012), fronto-parietal effective connectivity during WM. No study has measured the heritability of effective connectivity during WM or the heritability of DCM-derived connectivity parameters in any cognitive field. Additionally, this study is the largest yet to apply DCM to WM, and given that previous studies of WM using DCM have yielded variable results, the use of a large data set will provide a valuable contribution.

In Chapter 4 I look at the functional connectivity profile of the dlPFC during WM. Although alterations in seed based functional connectivity (Pearson's correlation) during working memory have not been widely investigated in psychiatric disease, I chose them as phenotypes of interest as functional connectivity of right dlPFC with left hippocampus and left dlPFC have shown association with schizophrenia risk alleles (Esslinger et al., 2009), and dlPFC functional connectivity is associated with task performance (Hampson et al., 2010).

In each of Chapters 2, 3 and 4, the formal hypothesis is that the phenotype is heritable. This is tested using the classical twin design.

2 Chapter 2: Heritability of the Network Architecture of Intrinsic Brain Functional Connectivity

This paper has been accepted by Neuroimage in July 2015. The paper and supplementary material have been replicated here. The contents have been altered only slightly to reflect formatting changes.

Heritability of the Network Architecture of Intrinsic Brain Functional Connectivity

Benjamin Sinclair[a,b,c], Narelle K. Hansell[c], Gabriëlla A.M. Blokland[c], Nicholas G. Martin[c], Paul M. Thompson[d], Michael Breakspear[c], Greig I. de Zubicaray[b], Margaret J. Wright[c], Katie L. McMahon[a]

a Centre for Advanced Imaging, University of Queensland, Brisbane, QLD 4072, Australia
b School of Psychology, University of Queensland, Brisbane, QLD 4072, Australia
c QIMR Berghofer Medical Research Institute, Brisbane, QLD 4029, Australia
d Imaging Genetics Center, Dept. of Neurology, Keck School of Medicine, University of Southern California, Los Angeles, CA 90095, USA

Benjamin Sinclair: b.sinclair@uq.edu.au
Narelle K Hansell: Narelle.Hansell@qimrberghofer.edu.au
Gabriella AM Blokland: gabriellablokland@gmail.com
Nicholas G Martin: Nick.Martin@qimrberghofer.edu.au
Paul M Thompson: pthomp@usc.edu
Michael Breakspear: mjbreaks@gmail.com
Greig I de Zubicaray: Greig.dezubicaray@uq.edu.au
Margaret J Wright: Margie.Wright@qimrberghofer.edu.au
Katie L McMahon: Katie.McMahon@uq.edu.au

Please address correspondence to:
Ben Sinclair,
Centre for Advanced Imaging,
University of Queensland, Brisbane,
QLD 4072, Australia
+61 415314218
b.sinclair@uq.edu.au

Abstract

The brain's functional network exhibits many features facilitating functional specialization, integration and robustness to attack. Using graph theory to characterize brain networks, studies demonstrate their small-world, modular, and "rich-club" properties, with deviations reported in many common neuropathological conditions. Here we estimate the heritability of five widely used graph theoretical measures (Mean Clustering Coefficient (γ), Modularity (Q), Rich Club Coefficient (ϕ_{norm}), Global Efficiency (λ), Small Worldness (σ)) over a range of connection densities (k=5-25%) in a large cohort of twins (N=592, 84 MZ and 89 DZ twin pairs, 246 single twins, age 23±2.5). We also considered the effects of global signal regression (GSR). We found the graph measures were moderately influenced by genetic factors h^2(γ=47-59%, Q=38-59%, ϕ_{norm}=0-29%, λ =52-64%, σ=51-59%) at lower connection densities (≤15%), and when global signal regression was implemented heritability estimates decreased substantially h^2(γ=0-26%, Q=0-28%, ϕ_{norm}=0%, λ =23-30%, σ=0-27%). Distinct network features were phenotypically correlated (|r|=0.15-0.81) and γ, Q and λ were found to be influenced by overlapping genetic factors. Our findings suggest that these graph measures may be potential endophenotypes for psychiatric disease and suitable for genetic association studies, but that genetic effects must be interpreted with respect to methodological choices.
Keywords: resting state, graph theory, genetics, heritability, functional connectivity

Introduction

There is growing evidence that the functional architecture of human brain networks has a profound influence on cognition and disease. The efficiency of information propagation in brain networks, or how far signals must travel to reach disparate parts of the network, has been shown to correlate significantly with intelligence (Li et al., 2009; van den Heuvel et al., 2009). The modularity of an individual's functional brain network, or the degree to which the network is partitioned into sub networks (e.g., visual, sensory-motor, and default mode networks), can also predict performance on working memory tasks (Stevens et al., 2012). Further, almost all psychiatric diseases studied with neuroimaging have been characterized by departures from the established network architecture seen in healthy individuals (see Wang et al., 2010).

Even in the absence of a specific task or stimulus, fluctuations in the blood-oxygenation level dependent (BOLD) signal are correlated across the brain, revealing spatially distributed networks of coherent activity (Fox and Raichle, 2007), which overlap with task-related functional networks (Smith et al., 2009) and underlying structural networks (Damoiseaux and Greicius, 2009; Honey et al., 2009). Graph theory- a mathematical approach to study networks - has been applied to such resting state data (rs-fMRI) to measure higher order features of the functional connectome network, such as efficiency and modularity (for a brief description of graph theory measures see Table 2.1, and Rubinov and Sporns, 2010 for a review). These features provide measures of the topological organization of brain networks, which have direct biological significance. For example, modularity is widely thought to reflect the brain's division of cognitive processes to cooperating subunits, and network efficiency the need for rapid transfer of information between separate cognitive processes (e.g. Sporns, 2014). Here we consider three measures of network segregation and community structure (γ, Q, ϕ_{norm}), a measure of network integration (**λ**), and a composite measure describing the trade-off between integration and segregation (σ).

Features showing strong heritability may be promising endophenotypes for neuropsychiatric disorders. More significantly, they may serve as targets for subsequent searches to identify particular sets of influential genes, to better understand molecular mechanisms affecting intra-brain communication. Prior twin studies of the functional connectome network suggest that cost efficiency (Fornito et al., 2011) and global efficiency

(van den Heuvel et al., 2013) are moderately to strongly heritable (heritability, h^2 =60% and 42% respectively). However, both of these studies had small samples, examined different age groups (n=58 and 86; ages 40 and 12; for Fornito et al. (2011) and van den Heuvel et al. (2013), respectively) and did not correct for nuisance covariates of global signal, white matter and CSF. Heritability of graph measures of brain networks have also been observed with diffusion weighted MRI (Dennis et al., 2011) and EEG (Smit et al., 2008).

We hypothesized that the common graph measures of the functional connectome network (γ, Q, ϕ_{norm}, $\boldsymbol{\lambda}$ and σ) calculated using a standard processing pipeline, would be moderately heritable and we examined the association between graph measures and to what extent any association is due to a common genetic factor. As a network may vary according to the number of links, we estimated the heritability of each graph measure over a range of connection densities (k=5-25%), as well as considering the effect of binarising graphs. In addition, given the ongoing debate as to the inclusion of global signal regression (Murphy et al., 2009; Fox et al., 2009), we conducted our analysis both with and without GSR. We tested these predictions in a large cohort (N=592) at approximately full brain maturation (mean age 23.5; e.g. Lebel et al., 2008).

Materials and Methods

Participants. Adult twins were recruited as part of the Queensland Twin IMaging (QTIM) study (de Zubicaray et al., 2008), under approval of the Human Research Ethics Committees of the QIMR Berghofer Medical Research Institute, University of Queensland, and Uniting Health Care, Wesley Hospital. Written informed consent was obtained for each participant. Twins were scanned in the same session or within a week of each other. Participants were excluded if they reported any history of psychiatric disease, brain injury, substance abuse or MR incompatibility.

Of the 619 participants with rs-fMRI data, 27 participants (including one twin pair) were rejected due to excessive head motion (translation>3mm, rotation>2°), image artifacts or observable neurological abnormalities (on visual inspection of images). The final sample consisted of 346 paired twins (84 monozygotic (MZ) pairs (61 female, 23 male) and 89 dizygotic (DZ) pairs (34 female, 13 male, 42 opposite sex)), and 246 unpaired twins, mean age 23.5 (±2.5), range 18-30. Zygosity was established using 9 independent polymorphic DNA markers, cross checked with blood group and phenotypic data to give a greater than 99.99%

probability of correct zygosity assignment (Wright and Martin, 2004). Zygosity was later confirmed by genome-wide single nucleotide polymorphism genotyping (Illumina 610K chip).

Table 2.1: Description of graph measures. For a full review see Rubinov & Sporns (2010).

Graph measure	**Description**	**Mathematical Definition**
Mean Clustering Coefficient, $\boldsymbol{\gamma = \frac{mC}{mC^{random}}}$	The clustering coefficient describes the likelihood of two nodes that are connected to a common node being connected to each other. It is a measure of 'cliquishness' in a network. To normalize, this probability is divided by the corresponding probability one would observe for a null hypothesis random network.	$mC = \frac{1}{n}\sum_{i \in N} C_i$ $C_i = \frac{2t_i}{k(k-1)}$ where t_i is the number of complete triangles around node i.
Modularity, Q	Modularity is the degree to which the network is partitioned into sub-graphs with a large number of connections within the sub-graphs, but relatively few connections between sub-graphs.	$Q = \sum_{u \in M}[e_{uu} - \sum_{v \in M} e_{uv}]$ where M is the set of modules, and e_{uv} is the proportion of links that connect nodes in module u with nodes in module v.
Rich Club Coefficient, ϕ	ϕ quantifies the degree to which hubs (highly connected and/or central nodes) preferentially associate with each other. To normalize, this proportion is divided by the proportion that would be observed in a random network.	$\phi(k) = \frac{2E_{>k}}{N_{>k}(N_{>k}-1)}$ where $N_{>k}$ is the number of nodes with degree greater than k, and $E_{>k}$ is the number of links between those nodes.
Global Efficiency, $\boldsymbol{\lambda = \frac{E_g}{E_g^{random}}}$	Efficiency is the inverse of path length, where path length is the number of connections traversed to get from one node to another. This is averaged over all node pairs to give global efficiency. To normalize, the efficiency is divided by the efficiency one would observe in a random network.	$Eg = \frac{1}{n}\sum_{i \in N} E_i = \frac{1}{n}\sum_{i \in N} \frac{\sum_{j \in N} d_{ij}^{-1}}{n-1}$ where d_{ij} is the shortest path between nodes i and j.
Small World Index, $\boldsymbol{\sigma = \gamma\,\lambda}$	Small world index describes how nodes in a network can be connected in relatively few steps, whilst maintaining local clustering. Complex networks generally have greater clustering than random networks, but comparable efficiency, giving them a greater small-worldness.	$\boldsymbol{\sigma = \gamma\,\lambda}$ $\boldsymbol{\lambda} = \frac{1}{\Lambda}$ where Λ is the harmonic mean of path length, i.e. the shortest number of links between two nodes.

Image Acquisition. Imaging was conducted on a 4 Tesla Bruker Medspec whole body scanner (Bruker). Participants were instructed to remain at rest with their eyes closed, and to not think of anything in particular and not fall asleep. The imaging sequence was a T2*-weighted gradient echo, echo planar imaging (GE-EPI) sequence (repetition time TR = 2100 ms; echo time TE = 30 ms; flip angle = 90°; field of view FOV = 230 mm x 230 mm, pixel size 3.6x3.6mm, 36 coronal 3.0mm slices with 0.6mm gap, 150 volumes, total scan time 315s). Prior to the rs-fMRI scan a T1-weighted 3D structural image was acquired (MPRAGE, TR = 1500 ms; TE = 3.35 ms; inversion time TI=700ms; flip angle = 8°; FOV = 230 mm^3, pixel size 0.9x0.9x0.9mm).

Image Processing. Images were preprocessed using FSL (www.fmrib.ox.ac.uk) and AFNI (http://afni.nimh.nih.gov/afni) as implemented in the 1000 Functional Connectomes Project scripts (https://www.nitrc.org/projects/fcon_1000/). The first 5 EPI volumes were removed to allow for steady state tissue magnetization. EPI volumes were realigned to a mean image to correct for between-scan head movement, spatially normalized to the standard template of the Montreal Neurological Institute (MNI), smoothed and detrended. Signal from white matter and CSF was regressed from voxel time-series to remove non-neuronal BOLD fluctuations. We conducted our analysis both with and without GSR, where global signal is a calculated at each time point as the mean signal BOLD signal within a whole-brain mask. The set of 6 motion parameters from the realignment was also regressed out, and a mean motion summary measure retained for inclusion as a nuisance covariate in group level analysis (average across all volumes of $\sqrt{x^2 + y^2 + z^2}$; Van Dijk et al., 2012). Finally, the normalized volumes were temporally filtered (0.01-0.1Hz).

Graph Construction. The AAL template (Tzourio-Mazoyer et al., 2002) comprising 116 macro-anatomical regions, which is the most widely used atlas in the graph theory literature, was used to establish ROIs. The time series were extracted from each ROI by taking the mean signal in all voxels. FC was calculated as the pairwise correlation between all ROI time series, which resulted in a 116x116 connectivity matrix for each participant. Negative weights were set to zero and matrices were thresholded at connection densities of k=5-25% (k; proportion of total connections retained). Sub-threshold connections were retained if removing them would fragment the network. We analysed both weighted and binary graphs. For the binary graphs, suprathreshold connections were then set to 1, resulting in graphs where 1 signified a connection and 0 no connection. Thresholding is important in binary graphs to exclude weak connections, which are assigned the same weight (1) as stronger connections. In weighted

graphs, thresholding is still important as the sheer number of low weight connections can dominate the value of graph measures, and graph measures tend to those of random graphs as the connection density tends to 100%. Network features are known to vary with different numbers of links considered (Stam and Reijneveld, 2007; van Wijk et al., 2010), and so a range of connection densities (typically between 5-35%) is typically used. High thresholds (lower connection densities, i.e., 5-10%) correspond to networks comprising the strongest and presumably most important routes in a network, with functional units clearly separated into distinct modules, but higher connection densities also consider weaker links in the network, with greater cross-talk between modules.

Graph measures. Non-normalised mean clustering coefficient (mC), global efficiency (Eg), modularity (Q) and rich-club coefficient **(**ϕ) were first calculated using the brain connectivity toolbox (Rubinov and Sporns, 2010). mC, Eg and ϕ were then normalized to remove the effect of overall functional connectivity and basic network features such as degree distribution. Doing so more specifically elucidates the network structure, while removing contributions from lower level connectivity attributes. Normalisation was achieved by dividing the values of mC, Eg and ϕ by those obtained from a random network with the same number of nodes, links and degree distribution (null networks). To obtain null networks, each link in the thresholded, binarised connectivity matrix was randomly reconnected an average of three times using the Maslov-Sneppen algorithm (Maslov and Sneppen, 2002), and mC, Eg and ϕ calculated on the resulting random graph. This process was repeated 20 times, and the average of randomized mC, Eg and ϕ calculated. γ, λ and ϕ_{norm} are then defined as mC/mC_{rand}, Eg/Eg_{rand} and ϕ / ϕ_{rand} respectively. Correlation matrices have an inherent clustering by virtue of the transitive nature of the correlation coefficient. It has been demonstrated that randomly rewiring the topological (thresholded/binarised) networks derived from correlation matrices does not preserve this transitive clustering, and subsequently the normalized clustering coefficient may over-estimate the degree of topological clustering (Zalesky et al., 2012). This over-estimation may be avoided by either randomizing the correlation matrix prior to thresholding, or randomizing the time series themselves. Here we have chosen to implement the standard Maslov-Sneppen randomization, with the acknowledgement that the nominal values of normalized clustering will be artificially inflated by our measure of functional connectivity. We assume that the degree of inflation is constant across subjects, and thus will not affect heritability estimates. To calculate small-worldness (σ), γ and λ were multiplied, $\sigma = \gamma \times \lambda$, or equivalently $\sigma = \gamma \div \Lambda$, where Λ is the harmonic mean

of path length[1]. Graph measures were all normally distributed and did not require further transformation prior to genetic analysis. To reduce the influence of outliers, data was winsorised, with the maximum distance from the mean for all graph measures set to three standard deviations.

Genetic Modeling. MZ and DZ twin correlations were calculated for each graph measure via maximum likelihood estimation implemented in Mx (Neale et al., 2002). An MZ correlation higher than DZ correlation is indicative of a genetic contribution. We then used structural equation models (SEM) to estimate to what extent the variance in each graph measure was attributable to additive genetic, A, common environment, C, and unique environment/residual modeling error, E (Neale et al., 2002). Initially, variance models including all components A, C and E were fitted, including age, sex and mean head motion as covariates. We tested additive genetic models (ACE) rather than genetic dominance models (ADE), even though in some cases the MZ correlations were more than double the DZ correlations (Tables 2.2a,b), since preliminary testing of ADE models (data not shown) indicated low power (i.e. wide confidence intervals) to discriminate A and D factors. Parameters were successively dropped from the model and reduced models were tested for goodness of fit. The model with greatest model parsimony as quantified by the lowest Akaike Information Criterion (AIC) was retained for heritability estimation.

Phenotypic Relationships. Pairwise Pearson correlations between 3 of the graph measures were calculated. σ was not included in either the correlational or multivariate genetic analysis, as it is a composite of two of the other graph measures. Correlated graph measures were tested in a multivariate ACE model using Cholesky decomposition (Neale et al., 2002) to see if the relationship could be attributed to common genetic factors, or common environmental factors influencing all phenotypes (Figure 2.5).

Test-Retest Reliability: To determine whether observed differences in heritability between measures and methodologies were in part explained by differences in the stability of the measures, test-retest reliabilities were calculated for a subsample of 53 twins who returned for rescanning an average of 3.6(±1.6) months after the first.

[1] Path length between two nodes is the smallest number of links required to connect the two nodes.

Results

Network Visualisation

To visualize networks obtained over the range of connection densities, the mean over participants of each pairwise connection was taken, resulting in a groupwise graph, which was then thresholded (k=5-35%) and binarised. This graph was decomposed into modules using the modularity algorithm of (Newman, 2006), and illustrated using BrainNet Viewer (http://www.nitrc.org/projects/bnv/; Figure 2.1). Note, partitioning the mean connectivity matrix over all subjects (c.f. He et al., 2009), ignores variability of node module membership. Alternative methods decompose each subject separately and can quantify a consensus network (c.f. Lancichinetti and Fortunato, 2012) or detect the most representative subject (c.f. Meunier et al., 2009). Between k=5-25%, a familiar pattern of resting state networks appears. The default mode network (DMN; blue), dorsal attention/task positive network (red), visual network (pink), subcortical (yellow), sensorimotor (cyan), cerebellar (green), and hippocampus/amygdala/temporal (black) are apparent at various connection densities. As the connection density is increased, different modules lose their distinction and merge, leading to fewer and larger modules. After k = 25%, the modular network architecture is lost. The main difference between global signal regression being implemented and not implemented, is that networks with GSR implemented are more modular, with more distinct modules observable, in particular, the default mode network is observable only with GSR implemented.

Average Graph Measures

Means of our five graph measures are given in Tables 2.2a and 2.2b. The mean values of the graph measures are typical of those seen in the literature (e.g. Achard et al., 2006; Lord et al., 2012), and indicate small world, modular, rich-club topology, irrespective of methodological choices. However, the means of the graph measures do differ depending on methodological choices, indicating that the nature of the networks obtained varies. The choice of threshold has a strong effect on the graph measure means and variances, with γ, λ and σ tending to 1 as k increases, indicating a loss of small world properties as the addition of weaker connections causes a shift towards random

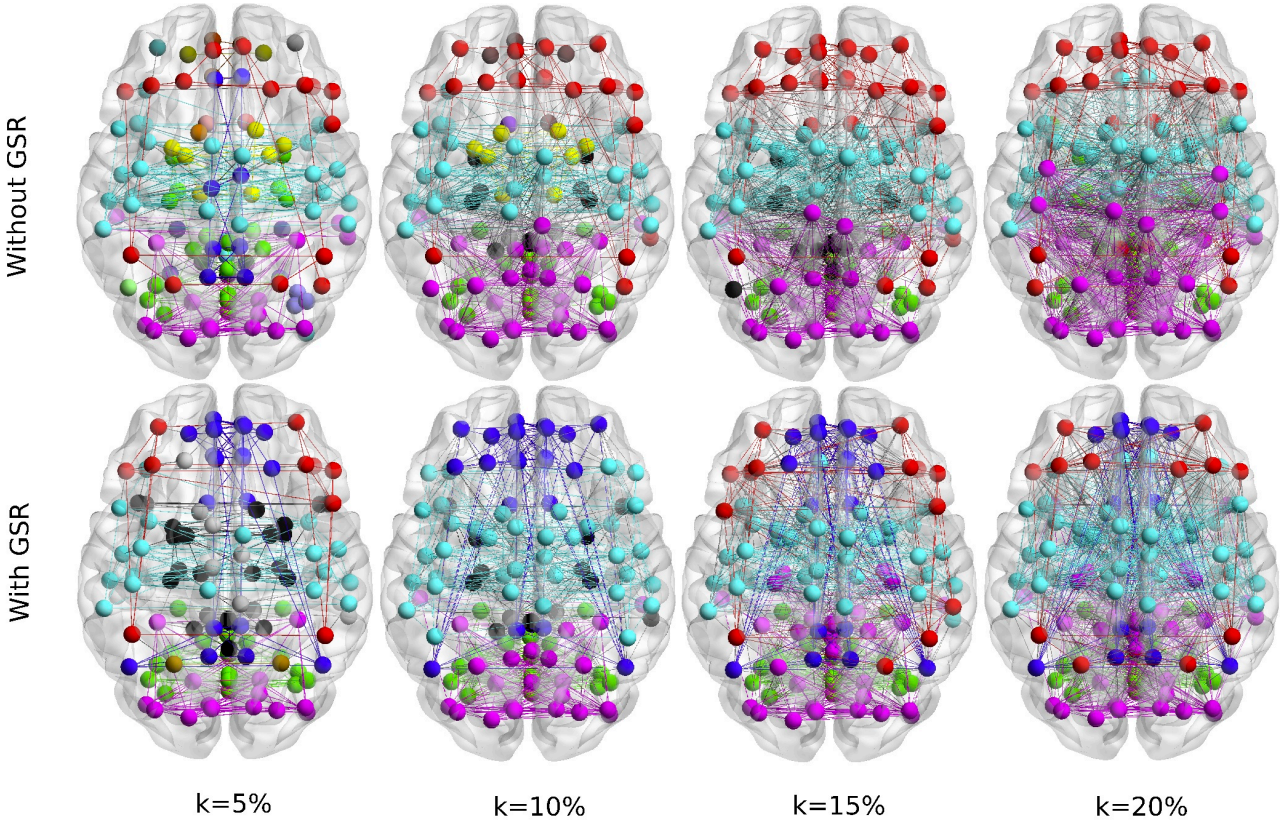

Figure 2.1: Modular decomposition of groupwise mean network over a range of connection densities (i.e. k=5-35%), without and with global signal regression (GSR). Yellow lines indicate a supra-threshold connection and node colors indicate module membership (DMN (blue), dorsal attention network (red), visual network (pink), subcortical (yellow), sensorimotor (cyan), hippocampus/amygdala/temporal (black). As the connection density increases, different modules lose their distinction and merge, leading to fewer and larger modules. After k = 25%, the modular network architecture is lost.

graphs. Likewise, Q reduces as k increases, indicating a loss of modular architecture, as depicted in Figure 2.1. We thus henceforth primarily discuss results at k=10%, which we believe to represent an optimal balance between removing spurious weak connections on the one hand and avoiding graph fragmentation on the other (observed to occur extensively at a threshold of 5%). The behavior of ϕ_{norm} with k was less straightforward and depended on GSR and binarising (Tables 2.2a,b and Supplementary tables 2.1a,b). γ, Q, ϕ_{norm} and σ are greatly increased if GSR is employed (% change(p-value) = 101%($p<10^{-15}$),43%($p<10^{-15}$),7%($p<10^{-15}$),93%($p<10^{-15}$) respectively at k=10%), whilst λ is relatively unchanged (-2%($p<10^{-4}$) at k=10%). Finally, binarising seems to have little effect on graph measure mean values of γ, Q, λ , σ (-1%(p=0.33), -5%($p<10^{-4}$), 2%($p<10^{-4}$), 1%(p=0.32) respectively at k=10%), but a large effect on ϕ_{norm} (38%($p<10^{-15}$) at k=10%).

Heritability

Heritability estimates were seen to vary substantially depending on threshold and implementation of global signal regression, and weakly affected by binarising. Generally, heritability estimates were higher at lower connection densities, without global signal regression and without binarising. Without GSR, all graph measures had a higher MZ correlation than DZ correlation over the whole range of connection densities, both for weighted (Table 2.2a) and binary graphs (Supplementary Table 2.1a), indicating a genetic contribution. MZ correlations ranged from 0.22-0.42 across graph measures and connection densities and were significant at all k, whereas DZ correlations ranged from 0.10-0.20 and were not all significant. SEM revealed that all graph measures had significant estimates of genetic variance (a^2) over a certain range of connection densities (Table 2.2a, Figure 2.2). Dropping the C parameter gave improved model parsimony for all graph measures over connection densities 5-15%. At k=20% and above, the best fitting model was CE for some graph measures. However, notably the fit of the AE and CE models were often very similar. The heritability estimates (i.e., A (=a^2)) for the best fitting model are given in Table 2.2a. γ, Q, λ and σ were all strongly heritable, (51, 46, 54, 54% respectively, k=10%) with similar estimates for binary networks. ϕ_{norm} was moderately heritable (29%, k=10%) for weighted graphs, but not for binary networks. As k increased from 10% to 25%, progressively more variance is attributed to unique environmental variance and/or modeling/experimental error for all graph measures. The heritability estimates varied little between weighted and binary graphs with the exception of ϕ_{norm} which for binary networks has best fitting model without genetic component. The heritability of Q was lower for binary compared to weighted graphs at k=5-10%, and at k=15% and above the best fitting model did not have a genetic component.

Regressing out global signal substantially reduced the heritability estimates (Table 2.2b, Figure 2.3). At k=10%, Q, λ and σ were moderately heritable (28%, 23% and 27%), whereas γ and ϕ_{norm} had a best fitting model without a genetic component, although AE and CE models had similar fit. As with the no global signal regression case, binarising had little effect on heritability estimates (Supplementary Table 2.1), although γ_{binary} had a best fitting model with genetic component and corresponding a^2 of 26(8,42), and Q had best fitting model without genetic component, and as k increased beyond 10%, variance attributable to unique environmental/modeling error increased (See Supplementary Tables 2.1a-b).

Tables 2.2a and 2.2b: Mean (SD) of the five graph measures (k=5-25%) across the 592 participants Twin correlations, Variance component estimates for A (additive genetic), C (common environment) and E (unique environment), and model fit for the 5 graph measures, k=5-25%. Computed without (Table 2.2a) and with (Table 2.2b) global signal regression.

Phenotype		Twin Correlations (95% CI)			Model fit (AIC)[a]				Variance estimates (%) from best fitting model (95% CI)		
k		Mean(SD)	MZ (N= 84 pairs)	DZ (N= 89 pairs)	ACE	AE	CE	E	A	C	E
5	**ϒ**	3.14(1.64)	0.45 (0.31,0.58)	0.12 (-0.02,0.25)	388.16	**386.16**	398.77	420.21	58(42,69)	-	42(31,58)
	Q	0.54(0.08)	0.43 (0.28,0.55)	0.23 (0.09,0.36)	366.25	**365.82**	366.62	409.62	59(45,69)	-	41(31,55)
	ϕ_{norm}	1.02(0.01)	0.21 (0.05,0.37)	0.03 (-0.11,0.17)	384.65	**382.65**	383.82	385.17	19(1,35)	-	81(65,99)
	λ	0.66(0.08)	0.43 (0.28,0.55)	0.15 (0.01,0.29)	399.17	**397.17**	403.68	431.43	54(40,66)	-	46(34,60)
	σ	2.18(1.28)	0.47 (0.32,0.59)	0.11 (-0.03,0.25)	387.81	**385.81**	399.38	420.52	58(43,70)	-	42(30,57)
10	**ϒ**	2.02(0.80)	0.40 (0.25,0.54)	0.13 (-0.01,0.26)	386.18	**384.18**	390.68	412.63	51(35,63)	-	49(37,65)
	Q	0.40(0.08)	0.36 (0.20,0.50)	0.13 (-0.01,0.27)	378.64	**376.79**	378.71	401.39	46(31,59)	-	54(41,69)
	ϕ_{norm}	1.02(0.02)	0.29 (0.13,0.44)	0.09 (-0.05,0.23)	387.85	**385.85**	387.29	394.53	29(12,44)	-	71(56,88)
	λ	0.77(0.07)	0.37 (0.21,0.50)	0.16 (0.02,0.30)	395.80	**393.82**	398.41	423.95	54(39,66)	-	46(34,61)
	σ	1.59(0.71)	0.42 (0.28,0.55)	0.13 (-0.01,0.27)	384.32	**382.32**	390.46	414.06	54(39,66)	-	46(34,61)
15	**ϒ**	1.67(0.52)	0.37 (0.21,0.51)	0.14 (0.00,0.28)	387.34	**385.37**	388.38	410.87	48(32,60)	-	52(40,68)
	Q	0.33(0.08)	0.29 (0.13,0.44)	0.13 (-0.01,0.26)	379.95	**378.35**	378.67	395.24	40(23,54)	-	60(46,77)
	ϕ_{norm}	1.03(0.02)	0.29 (0.12,0.43)	0.08 (-0.06,0.22)	380.32	**378.32**	380.33	387.67	29(13,44)	-	71(56,87)
	λ	0.82(0.05)	0.35 (0.20,0.49)	0.15 (0.02,0.29)	395.92	**393.94**	397.78	420.68	52(35,64)	-	48(36,65)
	σ	1.39(0.48)	0.39 (0.24,0.52)	0.16 (0.02,0.29)	383.53	**381.56**	385.44	411.11	51(36,63)	-	49(37,64)
20	**ϒ**	1.48(0.37)	0.34 (0.18,0.48)	0.15 (0.01,0.28)	384.61	**382.96**	383.99	405.37	44(28,57)	-	56(43,72)
	Q	0.29(0.07)	0.23 (0.07,0.38)	0.13 (-0.01,0.27)	382.67	382.06	**380.67**	392.77	-	29(14,42)	71(58,86)
	ϕ_{norm}	1.03(0.03)	0.21 (0.05,0.37)	0.10 (-0.04,0.23)	366.51	**364.57**	364.96	370.25	24(7,39)	-	76(61,93)
	λ	0.86(0.04)	0.31 (0.15,0.46)	0.16 (0.02,0.29)	395.77	**393.89**	395.91	414.61	45(28,59)	-	55(41,72)
	σ	1.28(0.35)	0.36 (0.20,0.49)	0.16 (0.02,0.30)	380.51	**378.85**	380.45	405.02	48(32,60)	-	52(40,68)
25	**ϒ**	1.36(0.28)	0.30 (0.14,0.44)	0.14 (0.00,0.28)	387.70	386.32	**386.19**	403.59	-	33(19,45)	67(55,81)
	Q	0.26(0.07)	0.21 (0.05,0.37)	0.11 (-0.03,0.25)	390.68	389.54	**388.68**	397.72	-	26(11,39)	74(61,89)
	ϕ_{norm}	1.04(0.03)	0.22 (0.05,0.37)	0.15 (0.01,0.28)	370.88	370.01	**368.88**	377.25	-	22(9,34)	78(66,91)
	λ	0.88(0.04)	0.27 (0.11,0.42)	0.18 (0.04,0.31)	392.15	**390.63**	390.97	406.83	40(23,54)	-	60(46,77)
	σ	1.20(0.27)	0.32 (0.16,0.46)	0.17 (0.03,0.30)	382.35	**381.10**	381.14	402.53	44(28,57)	-	56(43,72)

Table 2.2a

Phenotype		Twin Correlations (95% CI)			Model fit (AIC)				Variance estimates (%) from best fitting model (95% CI)		
k		Mean(SD)	MZ (N= 84 pairs)	DZ (N= 89 pairs)	ACE	AE	CE	E	A	C	E
5	**ϒ**	6.46(1.44)	0.19 (0.03,0.35)	0.17 (0.03,0.30)	410.62	409.12	**408.78**	416.62	-	22(8,35)	78(65,92)
	Q	0.68(0.04)	0.17 (0.01,0.33)	0.17 (0.03,0.30)	399.07	398.49	**397.07**	405.38	-	24(9,37)	76(63,91)
	ϕ_{norm}	1.07(0.03)	0.07 (-0.09,0.24)	-0.03 (-0.17,0.11)	445.81	443.81	444.02	**442.06**	-	-	100(100,100)
	λ	0.63(0.06)	0.32 (0.16,0.46)	0.01 (-0.13,0.15)	420.86	**418.86**	423.07	426.44	30(11,46)	-	70(54,89)
	σ	4.14(1.11)	0.19 (0.03,0.35)	0.11 (-0.03,0.25)	425.64	**423.64**	424.41	428.36	24(6,40)	-	76(60,94)
10	**ϒ**	4.06(0.55)	0.19 (0.02,0.34)	0.12 (-0.02,0.26)	400.51	398.77	**398.74**	404.73	-	21(7,34)	79(66,93)
	Q	0.57(0.04)	0.22 (0.05,0.37)	0.04 (-0.10,0.17)	419.05	**417.05**	419.68	421.61	28(7,46)	-	72(54,93)
	ϕ_{norm}	1.10(0.04)	-0.01 (-0.17,0.16)	-0.04 (-0.18,0.10)	432.73	430.73	430.73	**428.73**	-	-	100(100,100)
	λ	0.75(0.04)	0.26 (0.09,0.41)	-0.01 (-0.15,0.13)	426.71	**424.71**	427.35	428.94	23(5,40)	-	77(60,95)
	σ	3.06(0.47)	0.20 (0.03,0.36)	0.12 (-0.02,0.26)	407.75	**405.98**	405.99	412.11	27(9,42)	-	73(58,91)
15	**ϒ**	3.09(0.28)	0.10 (-0.07,0.26)	0.04 (-0.10,0.18)	397.58	**395.60**	395.69	395.65	13(0,30)	-	87(70,100)
	Q	0.51(0.03)	0.20 (0.04,0.36)	0.01 (-0.13,0.15)	421.95	**419.95**	422.24	422.70	24(2,43)	-	76(57,98)
	ϕ_{norm}	1.13(0.05)	0.08 (-0.09,0.24)	0.14 (0.00,0.28)	435.06	434.25	**433.06**	435.54	-	16(1,29)	84(71,99)
	λ	0.79(0.03)	0.31 (0.15,0.45)	-0.03 (-0.16,0.11)	414.39	**412.39**	416.43	419.19	28(10,44)	-	72(56,90)
	σ	2.43(0.24)	0.12 (-0.05,0.28)	0.05 (-0.09,0.19)	396.23	**394.25**	394.35	395.03	15(0,31)	-	85(69,100)
20	**ϒ**	2.56(0.17)	0.09 (-0.08,0.25)	-0.02 (-0.16,0.12)	390.79	388.79	389.20	**387.48**	-	-	100(100,100)
	Q	0.46(0.03)	0.19 (0.02,0.35)	0.00 (-0.14,0.14)	421.04	**419.04**	420.88	420.77	21(0,39)	-	79(61,100)
	ϕ_{norm}	1.16(0.07)	0.02 (-0.15,0.19)	0.05 (-0.09,0.19)	433.36	431.57	431.36	**429.94**	-	-	100(100,100)
	λ	0.79(0.02)	0.30 (0.14,0.44)	-0.00 (-0.14,0.14)	421.06	**419.06**	422.63	425.97	28(10,44)	-	72(56,90)
	σ	2.03(0.13)	0.05 (-0.11,0.22)	0.01 (-0.13,0.15)	370.28	368.28	368.35	**366.76**	-	-	100(100,100)
25	**ϒ**	2.21(0.13)	0.11 (-0.06,0.27)	-0.07 (-0.20,0.07)	404.25	402.25	402.81	**400.87**	-	-	100(100,100)
	Q	0.42(0.03)	0.14 (-0.03,0.30)	0.00 (-0.14,0.14)	415.69	413.69	414.53	**413.45**	-	-	100(100,100)
	ϕ_{norm}	1.18(0.08)	0.06 (-0.11,0.22)	-0.01 (-0.15,0.13)	454.45	452.45	452.56	**450.64**	-	-	100(100,100)
	λ	0.80(0.02)	0.31 (0.15,0.46)	-0.00 (-0.14,0.14)	421.25	**419.25**	423.53	427.16	30(12,47)	-	70(53,88)
	σ	1.76(0.08)	0.01 (-0.15,0.18)	-0.05 (-0.19,0.09)	369.29	367.29	367.29	**365.29**	-	-	100(100,100)

Table 2.2b [a] Where an AE model has only a slightly worse fit than a CE model, and vice-versa, both models are worthy of consideration. In addition, confidence intervals for ACE estimates were wide indicating low power to discriminate between A and C.

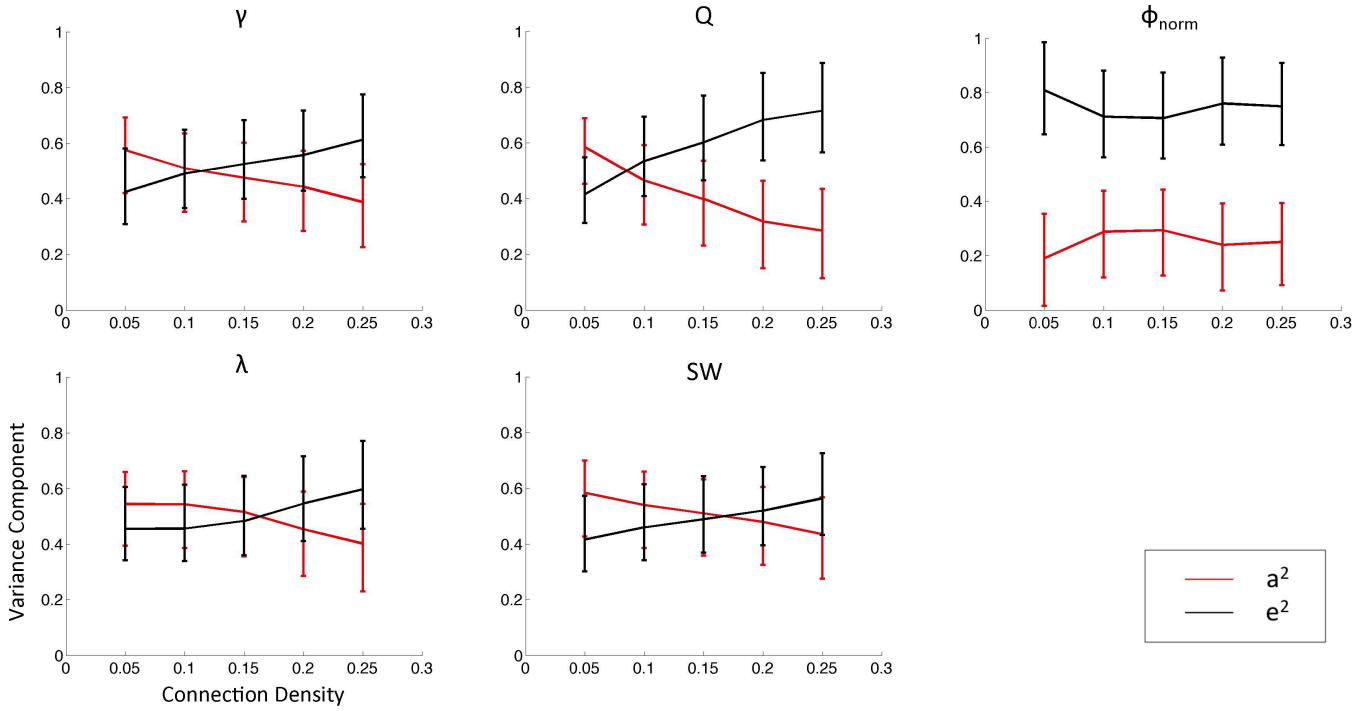

Figure 2.2: Additive genetic (a^2) and unique environmental (e^2) variance components across graph measures and thresholds, GSR not implemented.

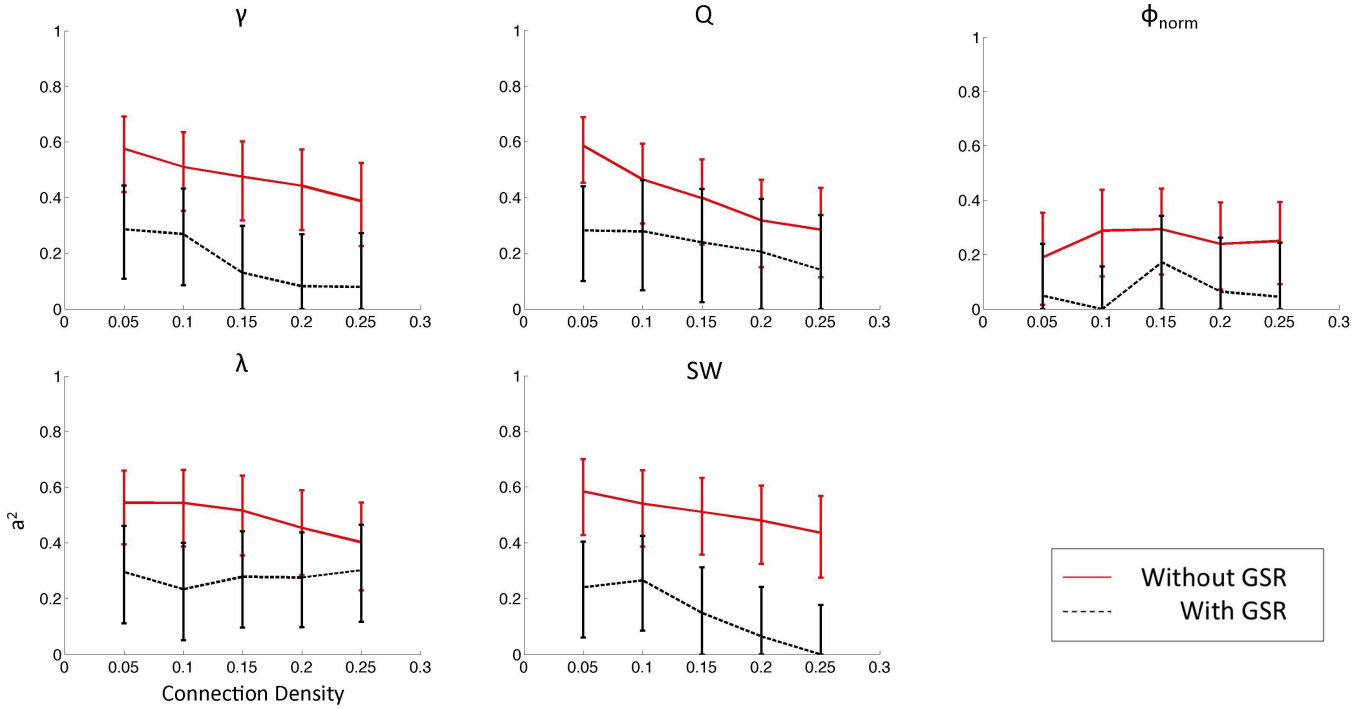

Figure 2.3: Additive genetic variance components across graph measures and thresholds estimated both without (solid line) and with (dashed line) global signal regression (GSR). Heritability estimates are much reduced with GSR implemented.

In addition, we found strong phenotypic correlations among the different network measures (Table 2.3). Without GSR, all graph measures were significantly correlated with the others, with the highest correlation at k=10% being 0.92 between γ and Q. With GSR implemented the correlations were lower (highest was 0.63 between γ and Q), suggesting that global signal fluctuations represent a common source of variance for the different graph measures. With GSR, Q and λ were negatively correlated, reflecting the trade-off between separation of and integration between modules. A similar pattern of correlations was seen across k both with and without GSR, other than for λ with GSR implemented, where λ is negatively correlated with γ at higher k (Supplementary Tables 2.3a-d).

A multivariate genetic analysis was used to estimate the shared genetic contribution across graph measures. Without GSR, a single genetic factor, A1, accounted for most of the genetic variance in all of the graph measures at all connection densities ($A1/A_{total}$=93%, 87% for Q and λ respectively at k=10%). With GSR implemented, 40% of the genetic variance (12% of the total variance) in Q was accounted for by a second genetic factor A2, which also accounted for 97% of the genetic variance in λ (Figure 2.5). The path coefficients for the second genetic factor, were the opposite sign for Q and λ, meaning that if this factor increases modularity, then the same factor will reduce λ. At higher connection densities the independent genetic factors (A2, A3) were reduced (Supplementary Tables 2.3a-d) and not significant, and most of variance was attributed to a single genetic factor, A1. This is related to the increasing correlations between the graph measures at higher connection densities.

Table 2.3. Multivariate genetic analyses of Mean Clustering (γ), Modularity (Q), and Global Efficiency (**λ**) at k=10%.

	Phenotypic Correlation		h^2	Breakdown of Total Variance (as Cholesky Decomposition), shown as a % with 95% Confidence Intervals					
				Additive Genetic Sources			Unshared Environmental Sources		
	ϒ	**Q**		A1	A2[a]	A3	E1	E2	E3
Without GSR									
ϒ	1.00		52	52 (37,64)			48 (36,63)		
Q	0.92 (0.91,0.93)	1.00	49	45 (31,57)	3 (0,6)		38 (27,52)	12 (9,16)	
λ	0.72 (0.67,0.76)	0.62 (0.56,0.67)	55	49 (33,66)	0 (0,3)	7 (0,6)	10 (4,21)	1 (0,5)	34 (26,44)
With GSR									
ϒ	1.00		27	27 (9,43)			73 (57,91)		
Q	0.64 (0.59,0.69)	1.00	29	18 (2,39)	12 (1,24)		25 (13,42)	47 (35,60)	
λ	0.26 (0.19,0.34)	-0.36 (-0.43,-0.29)	25	1 (0,12)	24 (5,43)	0 (0,9)	7 (1,18)	27 (15,44)	41 (33,49)

[a] Factor A2 has opposing effects (+ve for Q, but –ve for λ)

Multivariate models also revealed overlapping environmental influences/ experimental error on the different graph measures. Without GSR, The environmental influences on γ and Q overlapped, with sources influencing environmental variance in γ accounting for 75% ($E1/E_{total}$) of the environmental variance in Q. This same factor accounted for only 23% of the environmental variance in λ. A second environmental factor accounted for 23% of the environmental variance in Q, and 3% of the environmental variance in λ, and a final unique environmental factor accounted for the remaining 75% of the environmental variance in λ. With GSR implemented, the overlapping environmental/error influences were much reduced, with the majority of environmental variance in Q and λ attributed to E2 and E3 respectively, implying that without GSR implemented, much of E1 is due to global signal.

Test-Retest Reliabilities

Supplementary Table S2.2 gives the test retest reliabilities of all measures. These ranged from low to moderate (ICC= -0.21 to 0.41). In general, ICCs increased with increasing connection density, and there was no systematic difference between the ICCs of measures without GSR (mean(SD)=0.12(0.17)) and with GSR (0.15(0.11)), indicating that test-retest reliability was not a factor behind the higher observed heritabilities for measures without GSR.

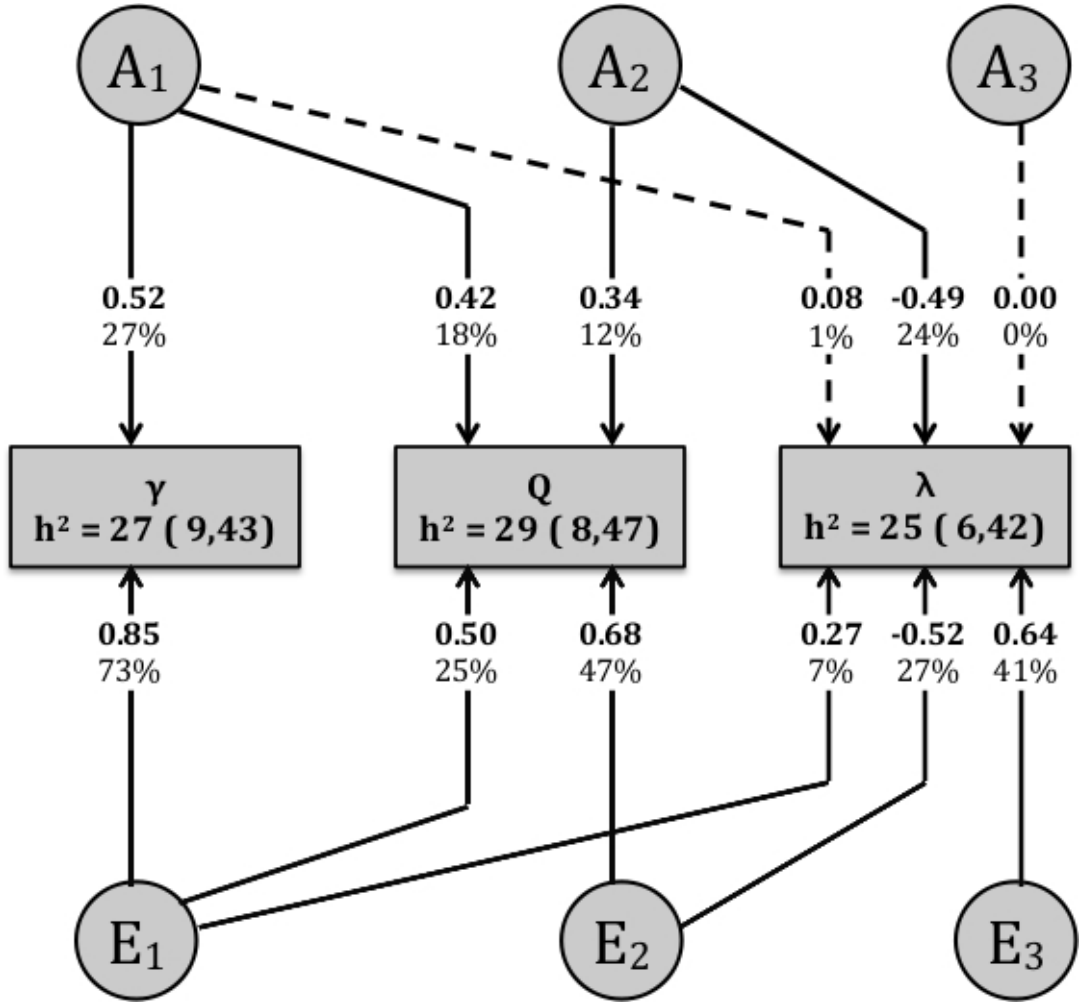

Figure 2.5: Path diagram for multivariate genetic model showing genetic and environmental sources of covariation between three graph measures, with parameter estimates given for k=10%, GSR implemented. Path labels give standardized path coefficients (bold) and variance components (the square of the path coefficients) of each factor. Thus, the genetic factor influencing γ also accounts for 18% of the total variation in Q (60% of the genetic variation), and 1% of the variation in λ. Q has a second genetic factor accounting for 12% of its variation, which also accounts for 24% of the variation in λ. Whereas overlapping genetic factors accounted for much of genetic variation in the graph measures, separate environmental factors account for the majority of environmental variance in Q (47%) and λ (41%). Heritability (the sum of sources of genetic variance for each variable; h^2) is shown for each variable. Non-significant path coefficients shown by dotted arrows.

Discussion

This study shows that network characteristics of resting state functional activity are partially under genetic influence, and that heritability estimates vary substantially depending on methodological choices. We found that γ (h^2 =47 to 61%), Q (h^2=38-59%), λ (h^2=52-64%) and σ (h^2=51-59%) were strongly influenced by genetic factors at connection densities ranging between k=5-15%, with heritability reducing at k>15%. Heritability estimates were substantially lower when global signal regression was implemented h^2 (γ=0-26%, Q=0-28%, ϕ_{norm}=0%, λ =23-30%, σ=0-27%) and there was little difference between considering weighted graphs or binary graphs, other than for ϕ_{norm}. Furthermore, these heritable traits were moderately correlated (|r|=0.62-0.92, without GSR, 0.27-0.63 with GSR) and largely influenced by overlapping genetic factors.

The heritability of global efficiency is largely consistent with prior studies of rs-fMRI graph measures. Fornito et al. (2011) found a heritability of 60(CI:17, 83)% (without GSR) for cost efficiency in 58 adults (cost efficiency reflects the trade off between the need for efficiency in a network and the cost of wiring). In 86 young children (mean age 12), van den Heuvel et al. (2013) estimated a heritability of 42(CI:5,73)% for λ, but no genetic influence on γ (without GSR). While the results for λ are similar, the participants were younger, and genetic and environmental effects on a trait can change with age (e.g. Bartels et al., 2002; Lenroot et al., 2009). Furthermore, their analysis was performed using voxel-wise networks, where each voxel constitutes a network node. Such networks differ topologically from anatomically informed networks, and they are 'scale-free' (van den Heuvel et al., 2008) – i.e., dominated by very highly connected hubs (Barabasi and Albert, 1999). In contrast to the previous two studies, we detect significant heritability of γ. This may represent methodological differences (van den Heuvel et al. (2013) did not correct for white matter signal, csf signal or motion confounds), but may also reflect that the previous two studies were underpowered, emphasizing the necessity of large sample sizes for heritability estimates. We performed power calculations based on the effect sizes in our sample, and determined that the sample sizes (number of twin pairs) required to reject the null hypothesis of no genetic component at a significance level of 0.05, with a power of 50% were (203, 97, 482, 5531 for λ(no GSR), γ(no GSR), λ(GSR), γ(GSR) respectively, k=10%), indicating that our study was underpowered for detecting heritability with GSR implemented, but sufficiently powered without GSR implemented.

Our heritability estimates are similar to those for other functional-imaging derived measures such as activation in N-Back working memory tasks, (h^2 ranging from 0 to 65%) (Blokland et al.,

2011), connectivity in the default mode network h^2 = 42±17% (Glahn et al., 2010), graph metrics derived from EEG measurements (h^2 ranging from 25 to 63%; Smit et al., 2010). They are lower than for cognitive phenotypes such as intelligence ($h^2 \sim$ 50-80%) (Plomin and Spinath, 2004), performance on working memory tasks ($h^2 \sim$ 40-60%) (e.g., Ando et al., 2001; Polderman et al., 2006).

γ, λ and σ may be collectively described as the small-world properties of networks. Small-world networks allow strong contact between groups of nodes with common functionality and simultaneously allow highly efficient information transfer via a small number of long range connections (Watts and Strogatz, 1998). Many studies (e.g. Salvador et al., 2005; Achard et al., 2006) have reported that the small-world architecture applies to human brain functional networks, and we observe the same in this data set (mean (SD) γ = 2.02 (0.80), mean λ =0.77 (0.07), k=10%, Table 2.2). This study demonstrates that this favorable set-up is substantially conferred by genetic factors. Furthermore, as we increase the connection density of the networks, and the small world properties of the graph reduce (γ decreases, λ increases), we see a corresponding drop-off in heritability, suggesting an underlying genetic influence which is only observed when the chosen connection density appropriately balances removal of weak and confounding connections with avoidance of network fragmentation. We believe this balance is best achieved at lower thresholds at around k=10%, as this is where we observe highest penetrance of genetic effects, and highest small-world properties.

In addition to high clustering and high efficiency, brain networks are modular (Beckmann et al., 2005; He et al., 2009): the nodes separate into modules with many strong connections between nodes within the same module, and relatively few between modules. Modularity measures this separation into distinct sub-networks with particular functions such as the visual, sensorimotor, and default mode networks, etc. Here we find a genetic contribution to modularity of (h^2=0-59%), a result not previously observed in other studies of the heritability of functional connectivity.

Recently, brain functional networks have been observed to display a 'rich-club' organization, whereby the network hubs (nodes with the largest number of connections) are highly connected to each other, forming a network core (van den Heuvel and Sporns, 2011); most of the shortest paths between nodes in the network pass via this rich club. Such organisation is hypothesized to give the network higher resilience against targeted attack of hubs (Kaiser et al., 2007; van den Heuvel and Sporns, 2011). Here, we did not find strong evidence that the rich club coefficient is heritable. ϕ_{norm} showed the most variability between the binary and weighted analysis, did not show the tendency to randomness as connection density increased as did the other graph measures, and yielded the lowest heritability parameters. Thus, ϕ_{norm} appears to be the least promising phenotype for use as a genetic biomarker, however, it is important to note that in the

context of brain imaging, ϕ_{norm} was originally defined on structural data (van den Heuvel and Sporns, 2011), not resting state functional data.

The network measures were correlated (Table 2.3), suggesting that common genetic or environmental factors might produce an advantageous network structure. Without GSR, the genetic source influencing γ also accounts for 93% and 87% of the genetic variance in Q and λ respectively. This may represent a single set of genetic processes giving rise to distinct network characteristics, or it may represent a common underlying factor to all graph measures, unrelated to network architecture, which has not been accounted for, such as the global signal. With GSR implemented, genetic influences were partitioned into two main factors, with one influencing γ and Q, and the second influencing Q and λ. γ and Q both measure features of network segregation and would be expected to be highly correlated and share common genetic underpinnings. More interestingly, Q and λ, were significantly negatively correlated and almost all of the genetic variation in λ, was accounted for by the second genetic factor influencing Q. Further, the set of genes which contributed positively to Q, negatively influence λ, indicating that this set of genes may regulate to trade-off between the separation of and the integration between modules. The phenotypic correlations between graph measures were also mediated in part by environmental factors. γ and Q and λ were all influenced to varying degrees by overlapping environmental factors or correlated measurement error, so all phenotypic correlations between graph measures have both genetic and environmental origins.

An important implication of this study is that the heritability of graph measures is substantially reduced with global signal regressed out. The origin of the global signal is uncertain, but it may have non-neuronal (cardiac, respiratory), as well as neuronal (e.g. ascending arousal systems) contributions (Fox et al., 2009). Global signal fluctuations are considered by many as a nuisance confound giving rise to artificial correlations between unrelated time series. There is ongoing debate as to the nature of anti-correlations introduced by global signal regression (Murphy et al., 2009; Fox et al., 2009) For this reason, we have carried out the analysis both with and without GSR. The results of this paper imply that a large proportion of the heritability estimates are dependent on these global signal fluctuations, and further, that global signal represents a common cause of variance in the different graph measures, with all graph measures strongly correlated and sharing a largely identical set of genetic influences when global signal is not accounted for. The two papers reporting heritability of network efficiency (Fornito et al., 2011; van den Heuvel et al., 2013), did not account for global signal, and reported similar estimates to those in this study without global signal accounted for. It is not clear which feature of the global

signal contributes to the enhanced heritability estimates for the graph measures. Since global signal regression is designed to remove physiological, non-neuronal contributions to the BOLD signal, itself a complex combination of neuronal, vascular and metabolic factors (Liu, 2013), this raises the possibility that the high heritability of graph measures seen here, and in previous studies (Fornito et al., 2011; van den Heuvel et al., 2013), may primarily represent the graph characteristics of vascular, as opposed to neural networks.

The current study has some limitations. The sample size is modest for establishing the importance of genetics and environment for phenotype as indicated by relatively wide confidence intervals, particularly for DZ twins where the confidence intervals spanned zero. Our multivariate analysis may suggest one set of genes regulating the trade-off between network modularity and network efficiency, with another set of genes influencing γ, but this finding is not robust to choice of threshold or binarising. Secondly the difference in heritability estimates when global signal regression is implemented may indicate that a proportion of the heritability is related to non-neuronal fluctuations in the BOLD signal, since GSR aims to remove such fluctuations. Indeed, γ and Q increase when global signal regression is implemented (λ_{binary} increases, $\lambda_{weighted}$ reduces), perhaps reflecting that the resulting graphs better 'capture' the underlying favorable network properties. Some non-neuronal influences can be ruled out as contributing to the heritability estimates. Head-motion was corrected for both at the subject level by regressing 6 head-motion parameters from voxel time series, and at the group level by inclusion of a mean-motion covariate. Overall levels of functional connectivity (and their neuronal and non-neuronal origins) are implicitly controlled for by normalizing graph measures to those of random graphs with the same overall level of functional connectivity (and other low level network characteristics such as degree distribution). We have taken a relatively simple approach to thresholding, simply retaining a certain percentage of edges whilst not removing edges that would cause the graph to fragment. To account for differences in network properties with the arbitrarily chosen connection density, we have calculated results over a range of connection densities. Some authors remove the arbitrary choice of threshold with techniques such as using weighted measures on unthresholded weighted graphs, or extracting the minimum spanning tree, which retains each node's strongest edge, then adds the minimum number of necessary edges required to fully connect the graph (e.g. Alexander-Bloch et al., 2010). Such approaches go some way to avoiding the confound of between group differences in percolation threshold (threshold at which graph fragments). We used the more common approach of a percentage threshold, whilst reducing the effects of percolation threshold by retaining crucial edges (e.g. Lord et al., 2012). We did not investigate the effect of parcellation strategy on heritability, and only considered the AAL template. One limitation of the AAL template

is that it consists of neuroanatomical regions of differing sizes, and consequently differing signal to noise ratios. Higher SNR can increase estimates of functional connectivity, and consequently increase the degree of high SNR nodes, giving them a disproportionate influence over network properties. More importantly, the value of graph measures changes considerably with spatial scale of the parcellation (size of nodes). For example, small worldness varies from ~2 at the spatial scale of the AAL to ~50 for a 4000 node sub-parcellation of the AAL template (Zalesky et al., 2010). More generally, organisational structure relevant to information processing emerges across many orders of magnitude in spatial scale, from molecules, synapses, neurons, nuclei, networks, layers, maps, up to systems (Churchland and Sejnowski, 1988). Whilst the AAL atlas extracts networks of large scale cognitive systems, voxel-wise networks (e.g. van den Heuvel et al., 2008) may capture the interactions of nuclei and cortical maps. Thus, it should be stressed that our results pertain only to large scale systems-level networks. Although investigation of different spatial scales would be of great interest, the number of connections scales with the number of nodes squared, with a corresponding increase in computation time, and the sample sizes typically used in genetic studies would make this very computationally expensive. Finally, the test-retest reliabilities of these metrics ranged from low to moderate low (ICC=-0.21 to 0.41). This is in line with reliabilities measured elsewhere for graph metrics on resting state fMRI (Wang et al., 2011; Braun et al., 2012). The ICCs are lower than those of psychometric measures and slightly lower than those of task-based fMRI BOLD signal derived measures. For example, Plichta et al. (2012) estimated reliabilities of ROI average BOLD signal at 0.56-0.62 for a reward task, 0.44-0.57 for an n-back working memory task, and -0.02-0.16 for a face matching task, while Caceres et al. (2009) estimated median ICCs for an auditory task at 0.07 (whole brain) and 0.35 (auditory network); and for an n-back task at 0.27 (whole brain) and 0.49 (n-back network). The contrast between low test-retest reliabilities of λ (table S1e), and moderate MZ twin correlations (table 2.2) is seemingly contradictory, in that a participant and their co-twin have a more similar λ than the same participant scanned at two different time points. This discrepancy is not a result of outliers (outliers were winsorised in the case of the MZ sample, and removed from the test-retest sample). It may be due to different numbers of participants for the test-retest and the MZ sample (53 and 84 respectively), and indeed, ICCs and MZ correlations lie within each-other's confidence intervals for the majority of measures (though not for λ). One further speculative possibility is that it is a consequence of the dependency of resting state connectivity on prior cognitive state (Waites et al., 2005; Harrison et al., 2008; Hasson et al., 2009). In our experimental protocol, test and retest are not equivalent trials in two respects. Task engagement prior to resting scans is known to affect subsequent resting state connectivity (Waites et al., 2005; Hasson et al., 2009). Our participants undertook an N-Back working memory task prior to their resting state scan. This was the case in

both test and retest trials, however, the retest trial is subject to habituation effects in the task experiment and increased task performance (Blokland et al., 2011), which may alter connectivity the rest experiment. Similarly, simple familiarity with the scanning experience can reduce anxiety and externally focused attention at rest, contributing further to the dissimilarity between test and retest trials. If such habituation artifacts do account for the low observed test-retest reliability, then they appear to have more effect on measures of functional integration (λ), than measures of network segregation/modular structure (γ, mod, ϕ_{norm}).

Despite these limitations, to date this is the largest study of twins with fMRI resting state scans, allowing the strongest and most comprehensive current estimates of network heritability. We find the first evidence of heritability of γ and Q, and strong evidence that λ is heritable. We used a range of the most common and consensual processing procedures for both resting state fMRI and graph theory, to make these results as applicable as possible to prior studies using these graph measures.

References

Achard, S., Salvador, R., Whitcher, B., Suckling, J., Bullmore, E., 2006. A resilient, low-frequency, small-world human brain functional network with highly connected association cortical hubs. J Neurosci 26, 63-72.

Alexander-Bloch, A.F., Gogtay, N., Meunier, D., Birn, R., Clasen, L., Lalonde, F., Lenroot, R., Giedd, J., Bullmore, E.T., 2010. Disrupted modularity and local connectivity of brain functional networks in childhood-onset schizophrenia. Front Syst Neurosci 4, 147.

Ando, J., Ono, Y., Wright, M.J., 2001. Genetic structure of spatial and verbal working memory. Behav Genet 31, 615-624.

Barabasi, A.L., Albert, R., 1999. Emergence of scaling in random networks. Science 286, 509-512.

Bartels, M., Rietveld, M.J., Van Baal, G.C., Boomsma, D.I., 2002. Genetic and environmental influences on the development of intelligence. Behav Genet 32, 237-249.

Beckmann, C.F., DeLuca, M., Devlin, J.T., Smith, S.M., 2005. Investigations into resting-state connectivity using independent component analysis. Philos Trans R Soc Lond B Biol Sci 360, 1001-1013.

Blokland, G.A., McMahon, K.L., Thompson, P.M., Martin, N.G., de Zubicaray, G.I., Wright, M.J., 2011. Heritability of working memory brain activation. J Neurosci 31, 10882-10890.

Braun, U., Plichta, M.M., Esslinger, C., Sauer, C., Haddad, L., Grimm, O., Mier, D., Mohnke, S., Heinz, A., Erk, S., Walter, H., Seiferth, N., Kirsch, P., Meyer-Lindenberg, A., 2012. Test-retest reliability of resting-state connectivity network characteristics using fMRI and graph theoretical measures. Neuroimage 59, 1404-1412.

Caceres, A., Hall, D.L., Zelaya, F.O., Williams, S.C., Mehta, M.A., 2009. Measuring fMRI reliability with the intra-class correlation coefficient. Neuroimage 45, 758-768.

Churchland, P.S., Sejnowski, T.J., 1988. Perspectives on cognitive neuroscience. Science 242, 741-745.

Damoiseaux, J.S., Greicius, M.D., 2009. Greater than the sum of its parts: a review of studies combining structural connectivity and resting-state functional connectivity. Brain Struct Funct 213, 525-533.

de Zubicaray, G.I., Chiang, M.C., McMahon, K.L., Shattuck, D.W., Toga, A.W., Martin, N.G., Wright, M.J., Thompson, P.M., 2008. Meeting the Challenges of Neuroimaging Genetics. Brain Imaging Behav 2, 258-263.

Dennis, E.L., Jahanshad, N., Toga, A., Brown, J., Rudie, J., Bookheimer, S., Dapretto, M., Johnson, K., McMahon, K., de Zubicaray, G., 2011. Heritability of structural brain connectivity network measures in 188 twins. SFN 2011, Washington, D.C.

Fornito, A., Zalesky, A., Bassett, D.S., Meunier, D., Ellison-Wright, I., Yucel, M., Wood, S.J., Shaw, K., O'Connor, J., Nertney, D., Mowry, B.J., Pantelis, C., Bullmore, E.T., 2011. Genetic influences on cost-efficient organization of human cortical functional networks. J Neurosci 31, 3261-3270.

Fox, M.D., Raichle, M.E., 2007. Spontaneous fluctuations in brain activity observed with functional magnetic resonance imaging. Nat Rev Neurosci 8, 700-711.

Fox, M.D., Zhang, D., Snyder, A.Z., Raichle, M.E., 2009. The global signal and observed anticorrelated resting state brain networks. J Neurophysiol 101, 3270-3283.

Glahn, D.C., Winkler, A.M., Kochunov, P., Almasy, L., Duggirala, R., Carless, M.A., Curran, J.C., Olvera, R.L., Laird, A.R., Smith, S.M., Beckmann, C.F., Fox, P.T., Blangero, J., 2010. Genetic control over the resting brain. Proc Natl Acad Sci U S A 107, 1223-1228.

Harrison, B.J., Pujol, J., Ortiz, H., Fornito, A., Pantelis, C., Yucel, M., 2008. Modulation of brain resting-state networks by sad mood induction. PLoS One 3, e1794.

Hasson, U., Nusbaum, H.C., Small, S.L., 2009. Task-dependent organization of brain regions active during rest. Proc Natl Acad Sci U S A 106, 10841-10846.

He, Y., Wang, J., Wang, L., Chen, Z.J., Yan, C., Yang, H., Tang, H., Zhu, C., Gong, Q., Zang, Y., Evans, A.C., 2009. Uncovering intrinsic modular organization of spontaneous brain activity in humans. PLoS One 4, e5226.

Honey, C.J., Sporns, O., Cammoun, L., Gigandet, X., Thiran, J.P., Meuli, R., Hagmann, P., 2009. Predicting human resting-state functional connectivity from structural connectivity. Proc Natl Acad Sci U S A 106, 2035-2040.
Kaiser, M., Martin, R., Andras, P., Young, M.P., 2007. Simulation of robustness against lesions of cortical networks. Eur J Neurosci 25, 3185-3192.
Lancichinetti, A., Fortunato, S., 2012. Consensus clustering in complex networks. Sci Rep 2, 336.
Lebel, C., Walker, L., Leemans, A., Phillips, L., Beaulieu, C., 2008. Microstructural maturation of the human brain from childhood to adulthood. Neuroimage 40, 1044-1055.
Lenroot, R.K., Schmitt, J.E., Ordaz, S.J., Wallace, G.L., Neale, M.C., Lerch, J.P., Kendler, K.S., Evans, A.C., Giedd, J.N., 2009. Differences in genetic and environmental influences on the human cerebral cortex associated with development during childhood and adolescence. Hum Brain Mapp 30, 163-174.
Li, Y., Liu, Y., Li, J., Qin, W., Li, K., Yu, C., Jiang, T., 2009. Brain anatomical network and intelligence. PLoS Comput Biol 5, e1000395.
Liu, T.T., 2013. Neurovascular factors in resting-state functional MRI. Neuroimage 80, 339-348.
Lord, A., Horn, D., Breakspear, M., Walter, M., 2012. Changes in community structure of resting state functional connectivity in unipolar depression. PLoS One 7, e41282.
Maslov, S., Sneppen, K., 2002. Specificity and stability in topology of protein networks. Science 296, 910-913.
Meunier, D., Lambiotte, R., Fornito, A., Ersche, K.D., Bullmore, E.T., 2009. Hierarchical modularity in human brain functional networks. Front Neuroinform 3, 37.
Murphy, K., Birn, R.M., Handwerker, D.A., Jones, T.B., Bandettini, P.A., 2009. The impact of global signal regression on resting state correlations: are anti-correlated networks introduced? Neuroimage 44, 893-905.
Neale, M., Baker, S., Xie, G., Maes, H., 2002. Mx: Statistical modeling, 6th ed. .
Newman, M.E., 2006. Modularity and community structure in networks. Proc Natl Acad Sci U S A 103, 8577-8582.
Plichta, M.M., Schwarz, A.J., Grimm, O., Morgen, K., Mier, D., Haddad, L., Gerdes, A.B., Sauer, C., Tost, H., Esslinger, C., Colman, P., Wilson, F., Kirsch, P., Meyer-Lindenberg, A., 2012. Test-retest reliability of evoked BOLD signals from a cognitive-emotive fMRI test battery. Neuroimage 60, 1746-1758.
Plomin, R., Spinath, F.M., 2004. Intelligence: genetics, genes, and genomics. J Pers Soc Psychol 86, 112-129.
Polderman, T.J.C., Stins, J.F., Posthuma, D., Gosso, M.F., Verhulst, F.C., Boomsma, D.I., 2006. The phenotypic and genotypic relation between working memory speed and capacity. Intelligence 34, 549-560.
Rubinov, M., Sporns, O., 2010. Complex network measures of brain connectivity: uses and interpretations. Neuroimage 52, 1059-1069.
Salvador, R., Suckling, J., Schwarzbauer, C., Bullmore, E., 2005. Undirected graphs of frequency-dependent functional connectivity in whole brain networks. Philos Trans R Soc Lond B Biol Sci 360, 937-946.
Smit, D.J., Boersma, M., van Beijsterveldt, C.E., Posthuma, D., Boomsma, D.I., Stam, C.J., de Geus, E.J., 2010. Endophenotypes in a dynamically connected brain. Behav Genet 40, 167-177.
Smit, D.J., Stam, C.J., Posthuma, D., Boomsma, D.I., de Geus, E.J., 2008. Heritability of "small-world" networks in the brain: a graph theoretical analysis of resting-state EEG functional connectivity. Hum Brain Mapp 29, 1368-1378.
Smith, S.M., Fox, P.T., Miller, K.L., Glahn, D.C., Fox, P.M., Mackay, C.E., Filippini, N., Watkins, K.E., Toro, R., Laird, A.R., Beckmann, C.F., 2009. Correspondence of the brain's functional architecture during activation and rest. Proc Natl Acad Sci U S A 106, 13040-13045.
Sporns, O., 2014. Contributions and challenges for network models in cognitive neuroscience. Nat Neurosci 17, 652-660.
Stam, C.J., Reijneveld, J.C., 2007. Graph theoretical analysis of complex networks in the brain. Nonlinear Biomed Phys 1, 3.

Stevens, A.A., Tappon, S.C., Garg, A., Fair, D.A., 2012. Functional brain network modularity captures inter- and intra-individual variation in working memory capacity. PLoS One 7, e30468.
Tzourio-Mazoyer, N., Landeau, B., Papathanassiou, D., Crivello, F., Etard, O., Delcroix, N., Mazoyer, B., Joliot, M., 2002. Automated anatomical labeling of activations in SPM using a macroscopic anatomical parcellation of the MNI MRI single-subject brain. Neuroimage 15, 273-289.
van den Heuvel, M.P., Sporns, O., 2011. Rich-club organization of the human connectome. J Neurosci 31, 15775-15786.
van den Heuvel, M.P., Stam, C.J., Boersma, M., Hulshoff Pol, H.E., 2008. Small-world and scale-free organization of voxel-based resting-state functional connectivity in the human brain. Neuroimage 43, 528-539.
van den Heuvel, M.P., Stam, C.J., Kahn, R.S., Hulshoff Pol, H.E., 2009. Efficiency of functional brain networks and intellectual performance. J Neurosci 29, 7619-7624.
van den Heuvel, M.P., van Soelen, I.L., Stam, C.J., Kahn, R.S., Boomsma, D.I., Hulshoff Pol, H.E., 2013. Genetic control of functional brain network efficiency in children. Eur Neuropsychopharmacol 23, 19-23.
Van Dijk, K.R., Sabuncu, M.R., Buckner, R.L., 2012. The influence of head motion on intrinsic functional connectivity MRI. Neuroimage 59, 431-438.
van Wijk, B.C., Stam, C.J., Daffertshofer, A., 2010. Comparing brain networks of different size and connectivity density using graph theory. PLoS One 5, e13701.
Waites, A.B., Stanislavsky, A., Abbott, D.F., Jackson, G.D., 2005. Effect of prior cognitive state on resting state networks measured with functional connectivity. Hum Brain Mapp 24, 59-68.
Wang, J., Zuo, X., He, Y., 2010. Graph-based network analysis of resting-state functional MRI. Front Syst Neurosci 4, 16.
Wang, J.H., Zuo, X.N., Gohel, S., Milham, M.P., Biswal, B.B., He, Y., 2011. Graph theoretical analysis of functional brain networks: test-retest evaluation on short- and long-term resting-state functional MRI data. PLoS One 6, e21976.
Watts, D.J., Strogatz, S.H., 1998. Collective dynamics of 'small-world' networks. Nature 393, 440-442.
Wright, M.J., Martin, N.G., 2004. Brisbane Adolescent Twin Study: Outline of study methods and research projects. Australian Journal of Psychology 56, 65-78.
Zalesky, A., Fornito, A., Bullmore, E., 2012. On the use of correlation as a measure of network connectivity. Neuroimage 60, 2096-2106.
Zalesky, A., Fornito, A., Harding, I.H., Cocchi, L., Yucel, M., Pantelis, C., Bullmore, E.T., 2010. Whole-brain anatomical networks: does the choice of nodes matter? Neuroimage 50, 970-983.

Supplementary Material

Tables S2.1a and S2.1b: Phenotypic and Genetic data for binary graphs. Computed without (Table S1a) and with (Table S1b) global signal regression.

Phenotype		Twin Correlations (95% CI)			Model fit (AIC)				Variance estimates (%) from best fitting model (95% CI)		
k		Mean(SD)	MZ (N= 84 pairs)	DZ (N= 89 pairs)	ACE	AE	CE	E	A	C	E
5	**Y**	3.10(1.62)	0.46 (0.32,0.59)	0.13 (-0.01,0.26)	387.62	**385.62**	398.58	422.56	59(44,70)	-	41(30,56)
	Q	0.46(0.10)	0.40 (0.25,0.53)	0.17 (0.03,0.30)	387.83	**385.84**	390.67	419.08	54(39,65)	-	46(35,61)
	φ_{norm}	1.61(0.27)	-0.12 (-0.28,0.05)	0.02 (-0.12,0.16)	345.21	343.21	343.21	**341.21**	-	-	100(100,100)
	λ	0.67(0.08)	0.45 (0.30,0.57)	0.16 (0.02,0.29)	393.43	**391.43**	399.91	431.18	59(44,69)	-	41(31,56)
	σ	2.19(1.29)	0.47 (0.33,0.59)	0.11 (-0.03,0.25)	389.35	**387.35**	401.41	424.29	59(44,70)	-	41(30,56)
10	**Y**	2.00(0.79)	0.40 (0.25,0.54)	0.14 (-0.00,0.27)	381.90	**379.90**	386.37	409.02	52(36,64)	-	48(36,64)
	Q	0.38(0.09)	0.33 (0.17,0.47)	0.13 (-0.01,0.26)	388.57	**386.75**	388.00	407.12	43(26,56)	-	57(44,74)
	φ_{norm}	1.43(0.22)	0.01 (-0.16,0.18)	0.09 (-0.05,0.23)	370.79	369.18	368.79	**367.42**	-	-	100(100,100)
	λ	0.78(0.07)	0.40 (0.25,0.53)	0.18 (0.05,0.32)	385.09	**383.17**	389.37	422.90	61(47,71)	-	39(29,53)
	σ	1.61(0.71)	0.43 (0.28,0.55)	0.14 (-0.00,0.27)	381.03	**379.03**	387.24	411.99	55(40,67)	-	45(33,60)
15	**Y**	1.65(0.51)	0.36 (0.21,0.50)	0.14 (0.00,0.28)	384.95	**383.01**	385.77	408.34	47(32,60)	-	53(40,68)
	Q	0.32(0.08)	0.27 (0.11,0.42)	0.12 (-0.02,0.26)	379.47	**377.91**	377.96	392.52	38(20,52)	-	62(48,80)
	φ_{norm}	1.32(0.16)	0.06 (-0.11,0.23)	0.14 (-0.00,0.27)	337.41	336.62	**335.41**	336.56	-	12(0,25)	88(75,100)
	λ	0.84(0.06)	0.42 (0.28,0.55)	0.20 (0.06,0.33)	375.08	**373.37**	379.28	418.46	64(50,73)	-	36(27,50)
	σ	1.41(0.49)	0.40 (0.24,0.53)	0.16 (0.02,0.29)	381.26	**379.31**	383.15	410.21	52(37,64)	-	48(36,63)
20	**Y**	1.46(0.36)	0.33 (0.17,0.47)	0.14 (0.00,0.28)	385.12	**383.42**	384.46	404.52	43(27,56)	-	57(44,73)
	Q	0.28(0.07)	0.21 (0.04,0.36)	0.14 (-0.00,0.27)	384.67	384.59	**382.67**	393.51	-	28(13,41)	72(59,87)
	φ_{norm}	1.27(0.12)	0.17 (0.00,0.33)	0.09 (-0.05,0.22)	367.94	366.69	**365.94**	370.50	-	18(4,31)	82(69,96)
	λ	0.88(0.05)	0.40 (0.25,0.54)	0.22 (0.08,0.35)	372.05	**370.73**	374.11	412.19	60(47,71)	-	40(29,53)
	σ	1.31(0.37)	0.36 (0.21,0.50)	0.16 (0.03,0.30)	381.04	**379.39**	380.95	405.90	48(32,60)	-	52(40,68)
25	**Y**	1.34(0.27)	0.29 (0.13,0.44)	0.15 (0.01,0.28)	386.19	385.06	**384.51**	402.02	-	33(19,45)	67(55,81)
	Q	0.25(0.07)	0.19 (0.02,0.35)	0.12 (-0.02,0.26)	389.56	388.92	**387.56**	395.77	-	25(10,38)	75(62,90)
	φ_{norm}	1.22(0.09)	0.10 (-0.07,0.27)	0.15 (0.01,0.28)	377.89	377.71	**375.89**	379.61	-	17(3,30)	83(70,97)
	λ	0.91(0.04)	0.41 (0.26,0.54)	0.25 (0.12,0.38)	358.16	**357.31**	360.18	403.41	62(49,72)	-	38(28,51)
	σ	1.24(0.29)	0.33 (0.17,0.47)	0.18 (0.04,0.31)	381.21	380.35	**379.76**	403.22	-	37(24,49)	63(51,76)

Table S2.1a: Binary graphs, no global signal regression

Phenotype		Twin Correlations (95% CI)			Model fit (AIC)				Variance estimates (%) from best fitting model (95% CI)		
k		Mean(SD)	MZ (N= 84 pairs)	DZ (N= 89 pairs)	ACE	AE	CE	E	A	C	E
5	**Y**	6.30(1.40)	0.19 (0.02,0.35)	0.20 (0.06,0.33)	413.46	413.04	**411.46**	421.53	-	25(11,37)	75(63,89)
	Q	0.64(0.05)	0.10 (-0.07,0.26)	0.15 (0.01,0.29)	414.31	413.94	**412.31**	415.27	-	16(2,30)	84(70,98)
	φ_{norm}	1.84(0.48)	-0.03 (-0.19,0.14)	0.02 (-0.12,0.16)	392.66	390.66	390.66	**388.66**	-	-	100(100,100)
	λ	0.67(0.06)	0.31 (0.15,0.46)	0.03 (-0.11,0.16)	421.73	**419.73**	423.67	427.79	30(12,46)	-	70(54,88)
	σ	4.25(1.13)	0.20 (0.03,0.36)	0.13 (-0.01,0.27)	427.71	**425.80**	426.16	431.80	26(8,42)	-	74(58,92)
10	**Y**	3.90(0.51)	0.20 (0.03,0.35)	0.10 (-0.04,0.24)	388.08	**386.13**	386.62	391.76	26(8,42)	-	74(58,92)
	Q	0.55(0.04)	0.15 (-0.02,0.31)	-0.02 (-0.16,0.12)	432.94	430.94	432.18	**430.81**	-	-	100(100,100)
	φ_{norm}	1.67(0.47)	-0.01 (-0.17,0.16)	0.01 (-0.13,0.15)	393.79	391.79	391.79	**389.79**	-	-	100(100,100)
	λ	0.82(0.04)	0.24 (0.08,0.39)	0.01 (-0.13,0.15)	416.18	**414.18**	416.49	418.58	23(5,40)	-	77(60,95)
	σ	3.19(0.48)	0.21 (0.05,0.37)	0.12 (-0.02,0.26)	398.61	**396.79**	396.96	403.70	27(10,43)	-	73(57,90)
15	**Y**	2.93(0.26)	0.09 (-0.08,0.25)	0.01 (-0.13,0.15)	392.27	390.27	390.51	**389.41**	-	-	100(100,100)
	Q	0.48(0.04)	0.20 (0.04,0.36)	0.01 (-0.13,0.15)	416.15	**414.15**	416.12	416.62	22(2,41)	-	78(59,98)
	φ_{norm}	1.57(0.36)	0.03 (-0.14,0.19)	0.08 (-0.06,0.22)	388.97	387.39	386.97	**386.22**	-	-	100(100,100)
	λ	0.88(0.03)	0.27 (0.11,0.42)	0.02 (-0.12,0.16)	373.70	**371.70**	374.06	379.03	27(10,42)	-	73(58,90)
	σ	2.57(0.24)	0.12 (-0.04,0.29)	0.06 (-0.08,0.20)	390.93	389.05	**388.96**	390.13	-	13(0,27)	87(73,100)
20	**Y**	2.40(0.16)	0.12 (-0.05,0.28)	-0.06 (-0.20,0.08)	399.79	397.79	398.49	**396.62**	-	-	100(100,100)
	Q	0.42(0.04)	0.18 (0.01,0.34)	-0.01 (-0.15,0.13)	420.38	**418.38**	419.95	419.30	18(0,37)	-	82(63,100)
	φ_{norm}	1.57(0.35)	0.01 (-0.16,0.18)	-0.08 (-0.21,0.06)	440.25	438.25	438.25	**436.25**	-	-	100(100,100)
	λ	0.92(0.02)	0.32 (0.16,0.46)	0.02 (-0.12,0.16)	369.38	**367.38**	370.49	378.53	30(14,44)	-	70(56,86)
	σ	2.21(0.14)	0.09 (-0.08,0.25)	0.00 (-0.14,0.14)	381.78	379.78	380.14	**378.86**	-	-	100(100,100)
25	**Y**	2.05(0.12)	0.15 (-0.02,0.31)	-0.07 (-0.21,0.07)	416.65	414.65	415.83	**414.11**	-	-	100(100,100)
	Q	0.37(0.04)	0.20 (0.04,0.36)	0.05 (-0.09,0.18)	407.48	**405.48**	406.67	409.30	23(4,40)	-	77(60,96)
	φ_{norm}	1.67(0.37)	0.17 (0.00,0.33)	-0.01 (-0.15,0.13)	160.91	**158.91**	159.82	159.46	22(0,45)	-	78(55,100)
	λ	0.95(0.02)	0.30 (0.14,0.44)	0.03 (-0.11,0.17)	365.63	**363.63**	365.86	374.08	29(13,43)	-	71(57,87)
	σ	1.96(0.10)	0.06 (-0.11,0.22)	-0.05 (-0.18,0.09)	402.15	400.15	400.31	**398.32**	-	-	100(100,100)

Table S2.1b: Binary graphs, global signal regression

Phenotype		Without GSR		With GSR	
k		Weighted	Binary	Weighted	Binary
5	**ϒ**	0.04 (-0.23,0.31)	0.09 (-0.18,0.35)	0.07 (-0.20,0.34)	0.04 (-0.24,0.31)
	Q	0.00 (-0.27,0.27)	-0.03 (-0.30,0.24)	0.21 (-0.06,0.46)	0.22 (-0.05,0.47)
	ϕ_{norm}	0.06 (-0.21,0.33)	-0.00 (-0.27,0.27)	0.31 (0.05,0.54)	0.07 (-0.20,0.34)
	λ	-0.21 (-0.45,0.07)	-0.18 (-0.43,0.10)	-0.03 (-0.29,0.25)	-0.01 (-0.28,0.26)
	σ	0.00 (-0.27,0.27)	0.05 (-0.22,0.32)	-0.03 (-0.30,0.24)	-0.03 (-0.30,0.24)
10	**ϒ**	0.12 (-0.15,0.38)	0.12 (-0.16,0.38)	-0.00 (-0.27,0.27)	0.01 (-0.26,0.28)
	Q	0.12 (-0.15,0.38)	0.19 (-0.08,0.44)	0.07 (-0.20,0.34)	0.12 (-0.15,0.38)
	ϕ_{norm}	0.27 (0.00,0.51)	0.06 (-0.22,0.33)	0.25 (-0.02,0.49)	0.27 (-0.01,0.50)
	λ	-0.15 (-0.40,0.13)	-0.06 (-0.33,0.22)	0.11 (-0.17,0.37)	0.14 (-0.13,0.40)
	σ	0.10 (-0.18,0.36)	0.10 (-0.17,0.36)	-0.01 (-0.28,0.26)	-0.03 (-0.30,0.24)
15	**ϒ**	0.23 (-0.05,0.47)	0.22 (-0.05,0.47)	0.10 (-0.18,0.36)	0.12 (-0.16,0.38)
	Q	0.21 (-0.06,0.45)	0.19 (-0.08,0.44)	0.24 (-0.04,0.48)	0.32 (0.06,0.54)
	ϕ_{norm}	0.20 (-0.08,0.44)	0.20 (-0.08,0.45)	0.13 (-0.16,0.39)	0.08 (-0.20,0.34)
	λ	-0.17 (-0.42,0.11)	-0.09 (-0.35,0.19)	0.15 (-0.13,0.40)	0.12 (-0.15,0.38)
	σ	0.18 (-0.09,0.43)	0.19 (-0.08,0.44)	0.06 (-0.22,0.32)	0.06 (-0.21,0.33)
20	**ϒ**	0.28 (0.01,0.51)	0.28 (0.01,0.51)	0.24 (-0.03,0.49)	0.31 (0.04,0.53)
	Q	0.20 (-0.07,0.45)	0.20 (-0.07,0.45)	0.33 (0.07,0.55)	0.28 (0.01,0.51)
	ϕ_{norm}	0.41 (0.15,0.61)	0.28 (0.00,0.52)	0.14 (-0.13,0.40)	0.16 (-0.12,0.41)
	λ	-0.20 (-0.45,0.08)	-0.12 (-0.38,0.16)	0.16 (-0.12,0.41)	0.17 (-0.11,0.42)
	σ	0.24 (-0.03,0.48)	0.25 (-0.02,0.49)	0.20 (-0.08,0.45)	0.26 (-0.01,0.50)
25	**ϒ**	0.35 (0.09,0.57)	0.34 (0.08,0.56)	0.30 (0.03,0.53)	0.31 (0.04,0.54)
	Q	0.28 (0.02,0.52)	0.24 (-0.03,0.48)	0.24 (-0.03,0.48)	0.23 (-0.05,0.47)
	ϕ_{norm}	0.33 (0.06,0.55)	0.25 (-0.04,0.49)	-0.11 (-0.37,0.17)	0.11 (-0.17,0.37)
	λ	-0.19 (-0.44,0.09)	-0.03 (-0.31,0.25)	0.18 (-0.09,0.43)	0.16 (-0.11,0.42)
	σ	0.30 (0.03,0.53)	0.30 (0.03,0.53)	0.24 (-0.03,0.48)	0.29 (0.01,0.52)

Table S2.2: Test-retest reliabilities for all metrics over all processing methodologies

Tables S2.3a – S2.3d. Multivariate genetic analyses of Mean Clustering (γ), Modularity (Q), and Global Efficiency (λ) across the whole range of connection densities.

Phenotype		Phenotypic Correlation		Genetic Correlation		Environmental Correlation		h^2	Breakdown of Total Variance (as Cholesky Decomposition), shown as a % with 95% Confidence Intervals					
									Additive Genetic Sources			Unshared Environmental Sources		
k		**Y**	**Q**	**Y**	**Q**	**Y**	**Q**		A1	A2	A3	E1	E2	E3
5	**Y**	1.00		0 [a]		1.00		0[a]	0			62 (51,75)		
	Q	0.89 (0.88,0.91)	1.00	0	0	0.84 (0.79,0.88)	1.00	0	0	0		34 (26,45)	15 (12,18)	
	λ	0.70 (0.66,0.74)	0.57 (0.51,0.62)	0	0	0.58 (0.48,0.67)	0.34 (0.21,0.45)	0	0	0	0	20 (13,30)	05 (02,09)	34 (27,42)
10	**Y**	1.00		1.00		1.00		52	52 (37,64)			48 (36,63)		
	Q	0.92 (0.90,0.93)	1.00	0.97 (0.93,1.00)	1.00	0.88 (0.83,0.91)	1.00	49	45 (31,57)	3 (0,6)		38 (27,52)	12 (9,16)	
	λ	0.72 (0.68,0.76)	0.62 (0.57,0.67)	0.93 (0.84,1.00)	0.88 (0.76,1.00)	0.47 (0.32,0.60)	0.34 (0.17,0.49)	55	49 (33,66)	0 (0,3)	7 (0,6)	10 (4,21)	1 (0,5)	34 (26,44)
15	**Y**	1.00		1.00		1.00		49	49 (34,61)			51 (39,66)		
	Q	0.94 (0.93,0.95)	1.00	0.96 (0.91,0.99)	1.00	0.92 (0.89,0.94)	1.00	41	36 (21,49)	4 (1, 6)		48 (36,65)	9 (7,12)	
	λ	0.68 (0.64,0.72)	0.59 (0.54,0.64)	0.89 (0.77,1.00)	0.81 (0.64,0.97)	0.46 (0.31,0.59)	0.39 (0.23,0.54)	51	41 (25,59)	1 (0, 12)	9 (0,20)	11 (4,21)	0 (0, 3)	39 (29,50)
20	**Y**	1.00		1.00		1.00		47	47 (32,59)			53 (41,68)		
	Q	0.94 (0.93,0.95)	1.00	0.97 (0.94,1.00)	1.00	0.93 (0.90,0.95)	1.00	33	31 (16,44)	2 (0, 4)		56 (42,73)	9 (7,12)	
	λ	0.63 (0.58,0.67)	0.54 (0.48,0.59)	0.84 (0.69,0.98)	0.77 (0.55,0.97)	0.43 (0.28,0.56)	0.37 (0.21,0.51)	46	33 (18,51)	3 (0,24)	11 (0,22)	10 (4,21)	0 (0, 3)	44 (34,56)
25	**Y**	1.00		1.00		1.00		41	41 (26,54)			59 (46,74)		
	Q	0.95 (0.94,0.96)	1.00	0.99 (0.95,1.00)	1.00	0.94 (0.91,0.95)	1.00	29	28 (14,42)	1 (0, 3)		61 (47,78)	9 (7,11)	
	λ	0.56 (0.50,0.61)	0.47 (0.41,0.53)	0.82 (0.64,0.99)	0.72 (0.46,0.98)	0.35 (0.19,0.49)	0.31 (0.16,0.45)	42	29 (14,47)	14 (0,27)	0 (0,18)	7 (2,16)	0 (0, 2)	51 (40,63)

Table S2.3a: Weighted graphs, no global signal regression.

[a] best fitting model was CE.

Phenotype		Phenotypic Correlation		Genetic Correlation		Environmental Correlation		h^2	Breakdown of Total Variance (as Cholesky Decomposition), shown as a % with 95% Confidence Intervals					
									Additive Genetic Sources			Unshared Environmental Sources		
k		**Y**	**Q**	**Y**	**Q**	**Y**	**Q**		A1	A2	A3	E1	E2	E3
5	**Y**	1.00		1.00		1.00		29	29 (11,44)			71 (56,89)		
	Q	0.66 (0.62,0.71)	1.00	0.82 (0.55,0.97)	1.00	0.58 (0.47,0.68)	1.00	31	20 (5,48)	10 (2,21)		23 (13,37)	46 (36,56)	
	λ	0.39 (0.32,0.46)	-0.17 (-0.24,-0.09)	0.19 (-0.42,0.54)	-0.41 (-0.81,0.02)	0.51 (0.36,0.63)	-0.06 (-0.23,0.12)	31	1 (0,11)	31 (10,49)	0 (0,13)	18 (8,32)	13 (6,25)	38 (29,49)
10	**Y**	1.00		1.00		1.00		27	27 (9,43)			73 (57,91)		
	Q	0.64 (0.59,0.69)	1.00	0.77 (0.37,0.98)	1.00	0.58 (0.45,0.69)	1.00	29	18 (2,39)	12 (1,24)		25 (13,42)	47 (35,60)	
	λ	0.26 (0.19,0.34)	-0.36 (-0.43,-0.29)	0.16 (-0.49,0.67)	-0.50 (-0.86,0.14)	0.30 (0.13,0.46)	-0.31 (-0.46,-0.14)	25	01 (0,12)	24 (5,43)	0 (0,9)	07 (1,18)	27 (15,44)	41 (33,49)
15	**Y**	1.00		1.00		1.00		14	14 (0,31)			86 (69,100)		
	Q	0.64 (0.59,0.69)	1.00	0.78 (-1.00,1.00)	1.00	0.60 (0.49,0.70)	1.00	24	16 (0,43)	9 (0,22)		29 (16,47)	48 (36,62)	
	λ	0.02 (-0.06,0.10)	-0.55 (-0.61,-0.49)	-0.19 (-1.00,1.00)	-0.68 (-1.00,-0.11)	0.09 (-0.08,0.26)	-0.49 (-0.62,-0.34)	29	1 (0,40)	21 (0,45)	7 (0,18)	1 (0, 5)	33 (20,52)	37 (28,47)
20	**Y**	1.00		1.00		1.00		13	13 (0,30)			87 (70,100)		
	Q	0.74 (0.70,0.77)	1.00	0.97 (-1.00,1.00)	1.00	0.70 (0.62,0.77)	1.00	21	22 (0,44)	1 (0, 9)		42 (26,61)	40 (31,48)	
	λ	-0.31 (-0.38,-0.24)	-0.66 (-0.70,-0.61)	-0.69 (-1.00,0.05)	-0.83 (-1.00,-0.42)	-0.21 (-0.37,-0.05)	-0.57 (-0.68,-0.44)	29	15 (0,47)	15 (0,35)	0 (0,17)	3 (0, 12)	25 (15,40)	43 (33,53)
25	**Y**	1.00		1.00		1.00		13	13 (1,31)			87 (69,99)		
	Q	0.82 (0.79,0.84)	1.00	0.99 (0.33,1.00)	1.00	0.79 (0.73,0.84)	1.00	14	15 (0,35)	0 (0, 6)		55 (38,72)	32 (25,37)	
	λ	-0.58 (-0.63,-0.52)	-0.72 (-0.76,-0.68)	-0.95 (-1.00,-0.51)	-0.90 (-1.00,-0.47)	-0.48 (-0.60,-0.35)	-0.68 (-0.76,-0.57)	31	29 (5, 52)	3 (0,20)	0 (0,17)	17 (7, 31)	17 (9, 26)	37 (28,47)

Table S2.3b: Weighted graphs, global signal regression

Phenotype		Phenotypic Correlation		Genetic Correlation		Environmental Correlation		h^2	Breakdown of Total Variance (as Cholesky Decomposition), shown as a % with 95% Confidence Intervals					
									Additive Genetic Sources			Unshared Environmental Sources		
k		**Y**	**Q**	**Y**	**Q**	**Y**	**Q**		A1	A2	A3	E1	E2	E3
5	**Y**	1.00		1.00		1.00		57	57 (40,70)			60 (47,75)		
	Q	0.90 (0.89,0.92)	1.00	1.00 (0.95,1.00)	1.00	0.78 (0.72,0.86)	1.00	54	54 (36,66)	0 (0,6)		62 (47,79)	10 (8,13)	
	λ	0.71 (0.67,0.75)	0.59 (0.53,0.64)	0.86 (0.76,0.96)	0.87 (0.71,0.99)	0.53 (0.35,0.66)	0.25 (0.06,0.45)	58	44 (28,62)	15 (0,25)	0 (0,25)	14 (8,24)	0 (1, 1)	23 (17,31)
10	**Y**	1.00		1.00		1.00		53	53 (39,65)			47 (35,61)		
	Q	0.92 (0.90,0.93)	1.00	0.97 (0.93,1.00)	1.00	0.87 (0.83,0.91)	1.00	46	43 (29,56)	3 (0,6)		41 (29,56)	13 (10,16)	
	λ	0.76 (0.72,0.79)	0.65 (0.59,0.70)	0.94 (0.86,1.00)	0.89 (0.78,1.00)	0.51 (0.37,0.64)	0.38 (0.22,0.53)	61	56 (40,72)	0 (0,11)	6 (0,15)	11 (5,20)	1 (0,3)	28 (21,37)
15	**Y**			1.00		1.00		49	49 (34,61)			51 (39,66)		
	Q	0.93 (0.92,0.94)		0.96 (0.92,1.00)	1.00	0.92 (0.88,0.94)	1.00	38	34 (19,47)	3 (0, 6)		50 (37,67)	10 (7,13)	
	λ	0.75 (0.71,0.78)	0.66 (0.61,0.70)	0.92 (0.82,1.00)	0.84 (0.70,0.98)	0.55 (0.41,0.67)	0.51 (0.36,0.63)	63	54 (37,72)	1 (0, 14)	9 (0,18)	12 (6,21)	0 (0, 1)	26 (19,35)
20	**Y**	1.00		1.00		1.00		46	46 (31,58)			54 (42,69)		
	Q	0.94 (0.93,0.95)	1.00	0.97 (0.92,1.00)	1.00	0.93 (0.90,0.95)	1.00	31	28 (14,41)	2 (0, 5)		59 (44,76)	9 (7, 12)	
	λ	0.75 (0.71,0.78)	0.64 (0.59,0.69)	0.90 (0.81,0.99)	0.78 (0.61,0.97)	0.58 (0.45,0.69)	0.56 (0.43,0.67)	61	51 (34,68)	8 (0,22)	4 (0,14)	14 (7,23)	0 (0, 1)	26 (19,34)
25	**Y**	1.00		1.00		1.00		40	40 (25,53)			60 (47,75)		
	Q	0.94 (0.93,0.95)	1.00	0.98 (0.93,1.00)	1.00	0.93 (0.90,0.95)	1.00	27	26 (11,39)	1 (0, 4)		62 (47,79)	10 (8,13)	
	λ	0.75 (0.71,0.78)	0.64 (0.59,0.68)	0.90 (0.80,1.00)	0.80 (0.62,1.00)	0.62 (0.50,0.72)	0.57 (0.44,0.68)	63	51 (34,69)	12 (0,23)	0 (0,14)	14 (8,24)	0 (0, 1)	23 (17,31)

Table S2.3c: Binary graphs, no global signal regression

Phenotype		Phenotypic Correlation		Genetic Correlation		Environmental Correlation		h^2	Breakdown of Total Variance (as Cholesky Decomposition), shown as a % with 95% Confidence Intervals					
									Additive Genetic Sources			Unshared Environmental Sources		
k		**Y**	**Q**	**Y**	**Q**	**Y**	**Q**		A1	A2	A3	E1	E2	E3
5	**Y**	1.00		1.00		1.00		30	30 (13,45)			70 (55,87)		
	Q	0.70 (0.66,0.74)	1.00	0.73 (0.22,0.99)	1.00	0.69 (0.59,0.76)	1.00	18	9 (00,23)	8 (0,17)		38 (24,56)	44 (34,55)	
	λ	0.40 (0.33,0.47)	0.02 (-0.06,0.10)	0.29 (-0.23,0.63)	-0.24 (-0.94,0.35)	0.47 (0.32,0.60)	0.10 (-0.07,0.27)	30	3 (01,14)	14 (0,43)	14 (0,30)	16 (7,29)	6 (2,15)	48 (36,62)
10	**Y**	1.00		1.00		1.00		26	26 (7,42)			74 (58,93)		
	Q	0.58 (0.52,0.63)	1.00	0.67 (0.67,1.00)	1.00	0.55 (0.42,0.67)	1.00	17	8 (0,28)	9 (0,23)*		28 (14,47)	57 (44,70)	
	λ	0.30 (0.22,0.37)	-0.36 (-0.43,-0.29)	0.36 (-0.24,0.96)	-0.44 (-0.90,0.88)	0.28 (0.11,0.44)	-0.35 (-0.49,-0.19)	24	3 (0,22)	20 (0,38)	0 (0,10)	6 (1,17)	28 (16,44)	42 (33,50)
15	**Y**			1.00		1.00		9	9 (0,26)			91 (74,100)		
	Q	0.55 (0.49,0.61)		0.61 (-1.00,1.00)	1.00	0.55 (0.42,0.65)	1.00	22	9 (0,35)	14 (0,27)		25 (13,41)	54 (42,69)	
	λ	0.08 (0.00,0.16)	-0.56 (-0.61,-0.50)	0.22 (-1.00,1.00)	-0.64 (-0.95,0.02)	0.05 (-0.11,0.21)	-0.56 (-0.67,-0.43)	26	1 (0,33)	23 (0,40)	0 (0,13)	0 (0, 3)	34 (0,50)	37 (29,46)
20	**Y**	1.00		1.00		1.00		11	11 (0,31)			89 (69,100)		
	Q	0.69 (0.64,0.73)	1.00	0.82 (-1.00,1.00)	1.00	0.67 (0.57,0.75)	1.00	18	12 (0,37)	6 (0,17)		39 (23,57)	45 (35,55)	
	λ	-0.19 (-0.27,-0.11)	-0.63 (-0.68,-0.58)	-0.50 (-1.00,1.00)	-0.90 (-1.00,-0.56)	-0.16 (-0.32,0.01)	-0.59 (-0.69,-0.47)	31	7 (0,44)	20 (0,37)	1 (0,13)	2 (0, 7)	27 (17,40)	39 (31,47)
25	**Y**	1.00		1.00		1.00		15	15 (1,33)			85 (67,99)		
	Q	0.82 (0.79,0.84)	1.00	0.99 (0.74,1.00)	1.00	0.79 (0.72,0.84)	1.00	23	23 (3,40)	0 (0, 6)		47 (32,65)	29 (23,35)	
	λ	-0.45 (-0.51,-0.38)	-0.67 (-0.71,-0.63)	-0.83 (-1.00,-0.36)	-0.89 (-1.00,-0.63)	-0.38 (-0.51,-0.24)	-0.61 (-0.71,-0.50)	30	19 (2, 41)	8 (0,23)	0 (0,15)	10 (3, 19)	17 (10,26)	42 (33,51)

Table S2.3d: Binary graphs, global signal regression

3 Chapter 3: Heritability of Fronto-Parietal Effective connectivity in Working Memory

This paper has been submitted to Human Brain Mapping in January 2015, and is under review. The paper has been replicated here. The contents have been altered only slightly to reflect formatting changes.

Heritability of Fronto-Parietal Effective Connectivity in Working Memory

Benjamin Sinclair[1,2,3], Nick G. Martin[3], Paul M. Thompson[4], Marta Garrido[1,5], Michael Breakspear[3], Greig I. de Zubicaray[2], Margaret J. Wright[3], Katie L. McMahon[1]

1 Centre for Advanced Imaging, The University of Queensland, Brisbane, QLD 4072, Australia
2 School of Psychology, The University of Queensland, Brisbane, QLD 4072, Australia
3 QIMR Berghofer Medical Research Institute, Brisbane, QLD 4029, Australia
4 Imaging Genetics Center, Dept. of Neurology, Keck School of Medicine, University of Southern California, Los Angeles, CA 90095, USA
5 Queensland Brain Institute, The University of Queensland, Brisbane, QLD 4072, Australia

Abbreviated Title: Heritability of Working Memory Connectivity
Keywords: Heritability, Effective Connectivity; Dynamic Causal Modeling, Working Memory, Test-Retest Reliability

Please address correspondence to:
Ben Sinclair,
Centre for Advanced Imaging,
University of Queensland, Brisbane,
QLD 4072, Australia
+61 415314218
b.sinclair@uq.edu.au

Abstract

Working memory performance is impaired in a number of psychiatric disorders, and is moderately to strongly heritable. The neural correlates of working memory may therefore serve as useful endophenotypes for psychiatric disease. A number of recent studies have implicated causal influences (effective connectivity) between frontal and parietal brain regions as a mechanism underlying working memory execution. We investigate the heritability of fronto-parietal effective connectivity during working memory, to see if this neural correlate is promising as an endophenotype, using a large cohort of twins (194 monozygotic (MZ), 206 dizygotic (DZ) and 152 unpaired twins, age range 21-29). To measure fronto-parietal effective connectivity we use dynamic causal modeling, currently one of the most widely-used methodologies for investigating the causal influences of one brain region on another. We used a two region DCM, including right dorsolateral prefrontal cortex (dlPFC) and right parietal cortex (PC) to measure fronto-parietal connectivity. Our best model was one in which stimulus presentation drove the PC, WM load drove the dlPFC, and WM load modulated both forward and backward connections. We find no evidence of a heritable component for the modulation in fronto-parietal connectivity, with low and non-significant twin correlations (PC to dlPFC modulation: MZ correlation=0.08, DZ correlation=-0.05; dlPFC to PC modulation MZ correlation=-0.14, DZ correlation=-0.05), and all variance in the connectivity attributable to unique environment and/or modeling/experimental error. The forward and backward modulations had low test-retest reliabilities (0.12 and 0.30 respectively).

Key words: working memory, dynamic causal modeling, genetics, heritability, effective connectivity, test-retest reliability

---

Introduction

Working memory (WM) is a key component of cognition, defined as the mechanism by which information is held and manipulated over short periods of time (Baddeley, 1992). It is believed to facilitate higher-order cognitive functions, such as decision-making and goal directed behavior. Further, WM abnormalities are a hallmark of schizophrenia (Carter et al., 1996; Lee and Park, 2005), and WM is particularly susceptible to Alzheimer's disease

(Baddeley et al., 1991), thus the neural correlates of WM may be a promising biomarker for psychiatric disease.

The neural correlates of working memory are well studied. Meta-analyses of the N-Back WM task by Owen et al. (2005) report consistent activation of posterior parietal cortex (PPC), dorsolateral prefrontal cortex (dlPFC), ventrolateral prefrontal cortex (vlPFC), premotor cortex and frontal pole. Consensus on the functional roles of these regions has not been reached. Some attribute the dlPFC a central role in strategic reorganization of memory contents (Bor et al., 2003; Owen et al., 2005), whilst meta-analyses by Wager and Smith (2003) propose that the dlPFC is more involved in continuous updating and temporal order memory. The PPC, part of the dorsal spatial visual processing stream (Goodale and Milner, 1992) plays a role in the storage of spatial information (Wager and Smith, 2003; Muller and Knight, 2006), and is also involved in switching of spatial attention (Corbetta et al., 1995; Cabeza and Nyberg, 2000), and a wide range of executive operations (Wager and Smith, 2003). There is also some degree of lateralization in WM, with right hemisphere more involved in spatial working memory and left hemisphere activated more strongly by verbal WM (D'Esposito et al., 1998), thought this lateralization is dependent on executive demand (Wager and Smith, 2003). More recently, increased connectivity between specific regions has been identified as facilitating WM. Honey et al. (2002) found increased connectivity between frontal and parietal regions with increased WM load using structural equation modeling, and similarly Woodward et al. (2006) observe a load enhanced network consisting of superior parietal, inferior prefrontal, occipital and anterior cingulate regions using a constrained principle component analysis.

In this paper we employ dynamic causal modeling (DCM; Friston et al. (2003)), to measure directed connectivity in working memory networks. DCM is a technique adapted from control theory, in which the causal influence of a set of brain regions on each other is modeled by linear differential equations, whose parameters are estimated via a Bayesian inversion scheme. There have been a number of recent studies investigating WM in a DCM framework. Ma et al. (2012) report task-related increase in directed connectivity from posterior parietal cortex to inferior frontal cortex and middle frontal gyrus and similarly, Dima et al. (2014) found WM-load increases in connectivity from right PC to right dlPFC. Conversely, Deserno et al. (2012) report a modulation of the backward (dlPFC to PC connection). Using DCM for an N-Back WM task to compare schizophrenic patients to healthy controls, they found that connectivity from dlPFC to PC is increased in response to higher WM

load in healthy subjects, but that this task dependent modulation was absent in schizophrenic patients, suggesting a possible pathological mechanism for reduced WM capacity in SZ patients. This disease-association motivated the current study in which we assess the suitability of fronto-parietal effective connectivity, as measured with DCM, as an imaging endophenotype (Gottesman and Gould, 2003; Meyer-Lindenberg and Weinberger, 2006).

Working memory performance is a strongly heritable phenotype ($h^2 \sim 40\text{-}60\%$) (e.g., Ando et al., 2001; Polderman et al., 2006). Additionally, voxel-wise BOLD activation during WM performance is heritable (h^2 up to 65%, Blokland et al., 2011). To date, no study has looked at the heritability of functional or effective connectivity during WM, though gene-association studies have revealed a genetic influence on some features of WM connectivity. Esslinger et al. (2011) report a lack of decoupling, measured as an increased Pearson's correlation, between dorsolateral prefrontal cortex (dlPFC) and hippocampus during working memory task for subjects with a schizophrenia risk allele on gene ZNF804A.

In this study, we investigate the heritability of frontal-parietal connections using a large sample of twins (N=452), scanned with functional MRI whilst undertaking an N-Back WM task. Given the behavioral heritability of WM, and the role that frontal-parietal connectivity seems to play in facilitating WM, we expect the task-dependent modulation of connectivity to be heritable.

Methodology

Participants. 452 subjects (97 monozygotic (MZ) twin pairs (mean age 24.1, 60 female, 37 male), 103 dizygotic (DZ) twin pairs (mean age 23.7, 36 female pairs, 17 male pairs, 50 mixed gender pairs), and 52 single twins) were recruited from the Queensland Twin Imaging Study (QTIM) (de Zubicaray et al. 2008), under approval of the Human Research Ethics Committees of the Queensland Institute of Medical Research, University of Queensland, and Uniting Health Care, Wesley Hospital. Written informed consent was obtained for each participant. Twins were scanned in the same session or within a week of each other. Participants were excluded if they reported any history of psychiatric disease, brain injury, substance abuse or MR incompatibility.

Experimental Paradigm. Our experimental procedure has been described previously Blokland et al. (2011). Participants undertook a spatial N-Back test of working memory

(Callicott et al., 1998), with 0-Back and 2-Back conditions. In this experiment, participants are shown numbers between 1 and 4, in fixed positions within a diamond, in random order. During the 0-Back condition, participants must report the number with which they were presented, and during the 2-Back condition, participants must report the number with which they were presented two trials previously. Alternating 0-Back and 2-Back blocks lasted 16 seconds each, with 16 trials per block.

Image Acquisition. Imaging was conducted on a 4 Tesla Bruker Medspec whole body scanner (Bruker). Functional magnetic resonance images (fMRI) were acquired with a T2*-weighted gradient echo, echo planar imaging (GE-EPI) sequence (repetition time TR = 2100 ms; echo time TE = 30 ms; flip angle = 90°; field of view FOV = 230 mm x 230 mm, pixel size 3.6x3.6mm, 36 coronal 3.0mm slices with 0.6mm gap). In one continuous run, 127 axial brain volumes were acquired while they completed the spatial N-Back task. Within the same session, a T1-weighted 3D structural image was acquired (MPRAGE, TR = 1500 ms; TE = 3.35 ms; inversion time TI=700ms; flip angle = 8°; FOV = 230 mm^3, pixel size 0.9x0.9x0.9mm).

Image Processing. Images were preprocessed in SPM8 (www.fil.ion.ucl.ac.uk). For each subject, the first 5 EPI volumes were removed to allow for steady state magnetization, all EPI volumes coregistered to the first time point to remove inter-scan movement, the mean image from all coregistered images was calculated and registered to the subjects T1 image. Using these registration parameters, all EPIs were registered to the T1 image of the participant. To transform all images into standard space, the T1 images were non-linearly registered to MNI coordinates using the DARTEL algorithm. Using the resulting deformation fields, the EPI images of all subjects were then transformed to standard space. Finally, images were smoothed with a $4mm^3$ Gaussian kernel and global signal effects were estimated and removed using a voxel-level general linear model (Macey et al., 2004).

Statistical Parametric Mapping. For each subject, a block-design fixed effects analysis was conducted. Two regressors were entered into a general liner model, a delta comb function modeling the stimulus presentation (one number presented at one second intervals), and a boxcar function modeling the working memory load (2-Back/0-Back conditions). Each regressor was convolved with a canonical hemodynamic response function. T-statistic contrast images were calculated to measure the main effect of task-condition (2-Back>0Back), and these images were entered into second level random effects analysis used to measure group-wise activation, with the resulting group-wise t-statistic map thresholded at $p<0.05$

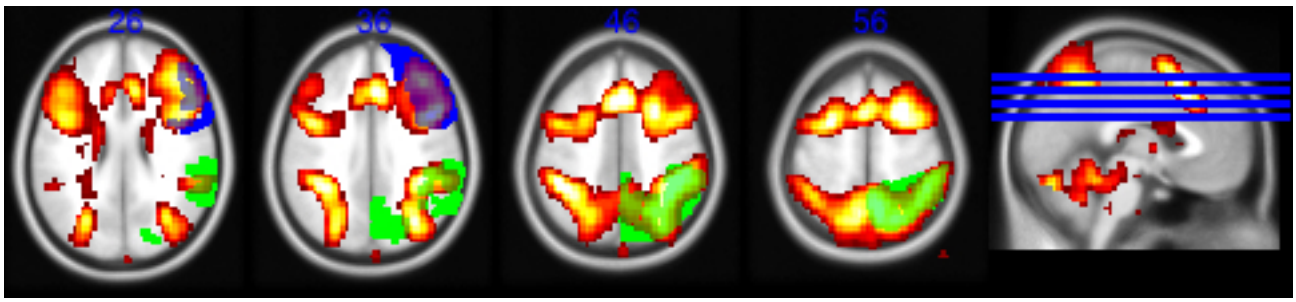

Figure 3.1: Regions of interest for dynamic causal models were calculated as the intersection of the group-wise activation map (red-yellow) and anatomical regions defined by the WFU Pick Atlas depicted in blue (dorsolateral prefrontal cortex) and green (parietal cortex). MNI slice coordinates labeled above (mm).

with a family wise error (FWE) correction for multiple comparisons. The group-wise activation map showed robust activation in Inferior and Superior Parietal Cortex and dorsolateral Prefrontal Cortex (Figure 3.1).

Volume of Interest Selection. A simple two region DCM, including only right dlPFC and right PC was used to measure fronto-parietal connectivity. We initially explored models including the visual cortex, as in Deserno et al. (2012). However, we observed no activation in response to stimulus presentation in the visual cortex for a large number of subjects, and since our hypothesis regarded fronto-parietal connectivity, and not connectivity with the visual cortex, we dropped the visual cortex from our models. The right hemisphere was selected as deficits in fronto-parietal connectivity in SZ were specific to the right hemisphere in Deserno et al. (2012), and there is evidence that spatial working memory is right-lateralized (D'Esposito et al., 1998, Wager and Smith, 2003). Volumes of interest were extracted using a combination of anatomical and functional criteria. Anatomical regions of interest were extracted from the WFU Pick Atlas (www.fmri.wfubmc.edu), with the dlPFC defined as the union of BA9 and BA46, with medial sections of BA9 manually removed, and parietal cortex defined as the union of BA7 and BA40. These ROIs were masked with the group-wise task activation map. For each subject, the maximally activated voxel within the resulting ROI was surrounded with a sphere of radius 6mm, and the first eigenvariate within the sphere taken as the representative time series of the brain region.

Dynamic Causal Modeling. DCM models the change in neuronal activity in a region as arising from contributions from direct driving input from experimental manipulations, C, intrinsic connectivity between regions, A, and context-dependent changes in those connections, B. This hidden neuronal activity is mapped to an observed BOLD response via a

hemodynamic model. Posterior distributions for neuronal coupling and hemodynamic model parameters are estimated simultaneously by inverting the forward model with a Bayesian inversion scheme (Friston et al., 2003). We used deterministic, linear DCM, using the DCM10 toolbox as implemented in SPM12, to generate maximum *a posteriori* estimates for the parameters A, B and C.

Since we do not know *a priori* which regions are functionally connected, how those connections alter with context and which nodes are directly driven by experimental manipulations, in DCM one specifies a range of plausible hypotheses and compares them for goodness of fit. Assuming the presence of bi-directional intrinsic connections between PC and dlPFC, all possible combinations of driving input from stimulus presentation, driving input from the 2-Back condition, and task-related modulations in connectivity by the 2-Back condition amounts to 64 different possible network configurations. This model space was constrained by applying two model assumptions. Firstly that each experimental manipulation, stimulus presentation and working memory load, directly drives the system through some entry node (i.e. models missing one of these driving inputs were excluded), and secondly that each experimental manipulation enters at only one node, with effects on other nodes arising through the connectivity between nodes. These assumptions reduce the model space from 64 to 16 models, depicted in Figure 3.2. The model set is split into four families, with membership determined by the direction of the task-dependent modulation. Models 1-4 have no task-dependent connectivity modulations (NM), in models 5-8 the PC to dlPFC (forward; FW) connection is modulated, in models 9-12 the dlPFC to PC (backward; BW) connection is modulated, and in models 13-16, both connections are modulated (bi-directional; BD).

Bayesian Model Section. The best family of models, and best individual model were determined using Bayesian model selection (BMS; Penny et al., 2004), implemented in DCM12. BMS compares the model evidence (probability of the data given the model, integrated over all model parameters) of alternative DCMs. This approach inherently penalizes model complexity. We use the variational Bayes version of BMS described in Stephan et al. (2009), to perform group-wise random effects model comparison. BMS was implemented at the family level (Penny et al., 2010), to determine which modulation is most likely, integrating over all other model features, and also at the individual model level. The individual model with the highest exceedance probability (Ep; probability that the model has a higher posterior probability than any other model) was retained for genetic analysis.

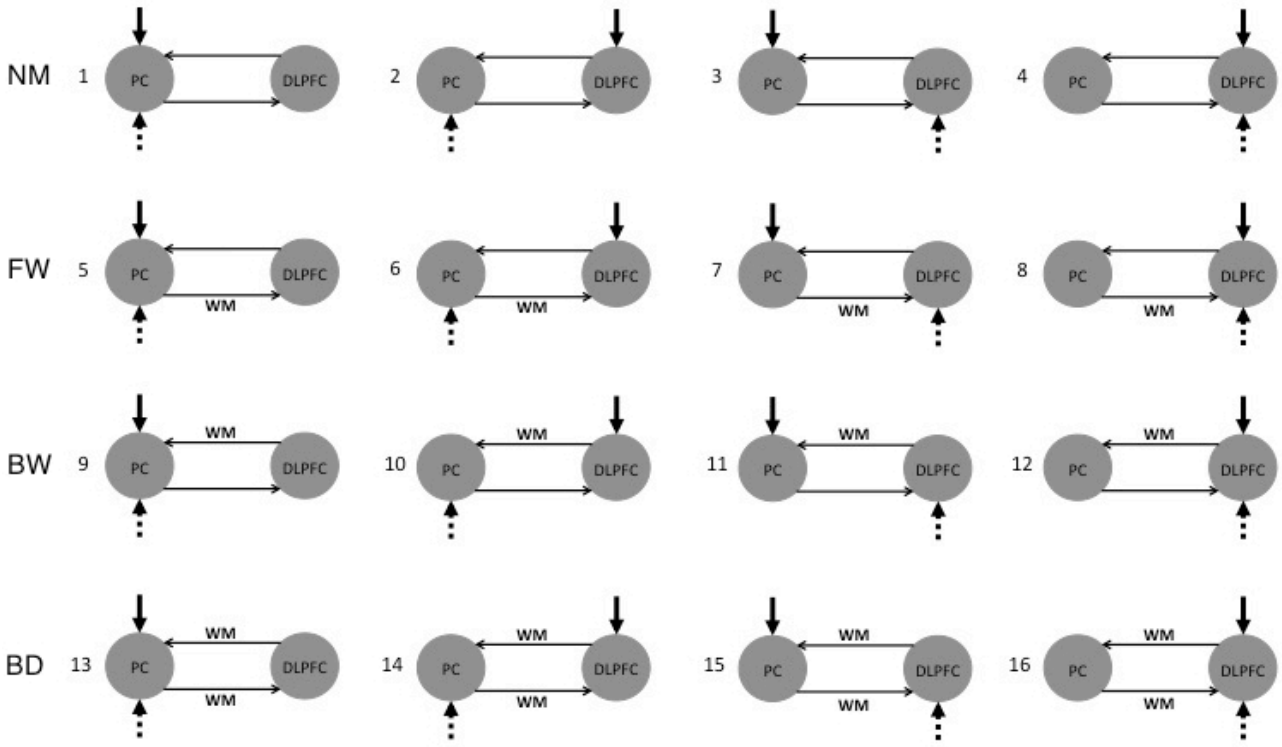

Figure 3.2: DCM model space. Stimulus driving input indicated by solid vertical arrow, task driving input indicated by dashed arrow, intrinsic connections indicated by arrows between nodes, and task modulation of connection indicated by 'WM' over arrow. Models 1-4 have no task-dependent connectivity changes, in models 5-8 the forward connection is altered with WM load, in models 9-12 the backward connection is modulated, and in models 13-16 both forward and backward connection are modulated.

Genetic modeling. We first calculated correlations between twin pairs for the parameters of the winning model, using maximum likelihood fitting in Mx (Neale et al., 2002), with sex, age and mean motion included as covariates. We then used structural equation models (SEM) to estimate to what extent the variance in the load-dependent connectivity modulations was attributable to additive genetic (where allelic contributions add linearly to a phenotype), A, common environment, C, and unique environment/residual modeling error, E (Neale et al., 2002). Structural equation modeling fits a predicted covariance structure based on linear relationships between latent genetic and environmental variables, to the observed covariance between twin phenotypes. The SEMs were fitted to the data using a maximum likelihood fitting implemented in Mx (Neale et al., 2002). Initially, variance models including all components (ACE model) were fitted, including age, sex and mean motion analysis (average across all volumes of $\sqrt{x^2 + y^2 + z^2}$; Van Dijk et al., 2012) as covariates. Parameters were successively dropped from the model and reduced models were tested for goodness of fit using the log likelihood ratio test and Akaike Information Criterion (AIC).

Test-Retest Reliability: A subset of 40 of the twins were rescanned an average of 3.9 months after their first scan, allowing a measurement of the test-retest reliability of the DCM parameters. Performing the same experimental paradigm and imaging procedure we fitted the best model from the 452 subjects (model 15), to obtain DCM parameters for the second session, and used them to calculate the test-retest reliability of the connectivity measures, quantified by the intra-class coefficients (ICCs).

Results

Bayesian Model Selection

The bidirectional model family (Models 13-16), with WM-load modulations of both forward and backward connections outperformed the other models (Ep=100%). The family of backward models had higher evidence than the family of forward models, and the family with no modulations had the least evidence. Within the bidirectional model family, model 15 had the highest exceedance probability (Ep=97.7%; Figure 3.3), with the stimulus input driving the PC and the task driving the dlPFC.

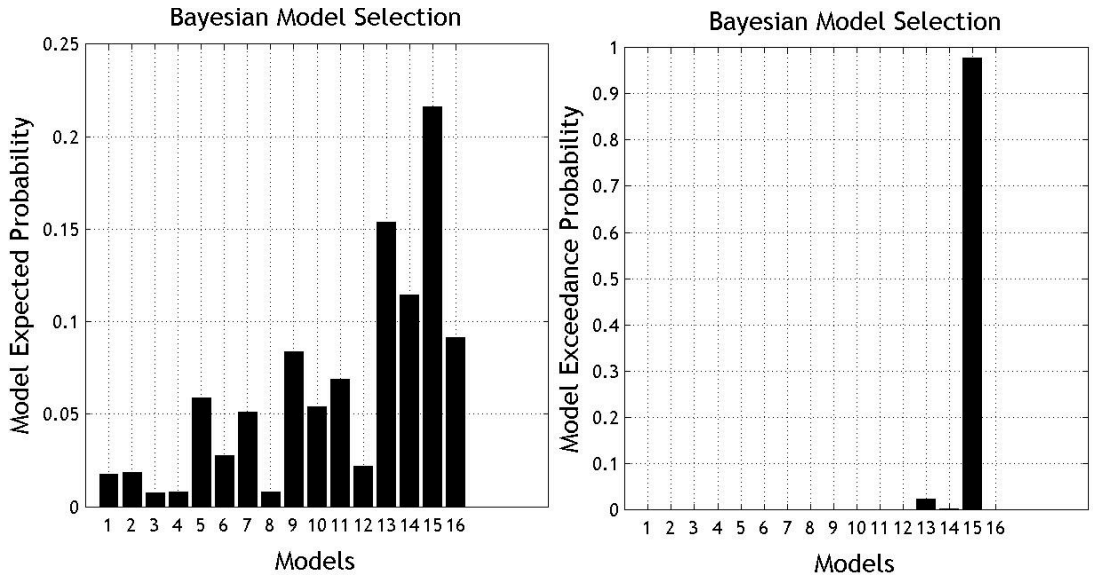

Figure 3.3: Model expected probabilities (left), and exceedance probabilities (right). Models with WM modulation both forward and backward modulations had higher model expected probability than those with modulation of backward connections (models 9-12) which in turn had higher expected probabilities than those with WM modulation of forward connections (models 5-8). The model with highest evidence was model 15, with WM modulation of both forward and backward connections, stimulus input into PC and WM input into dlPFC.

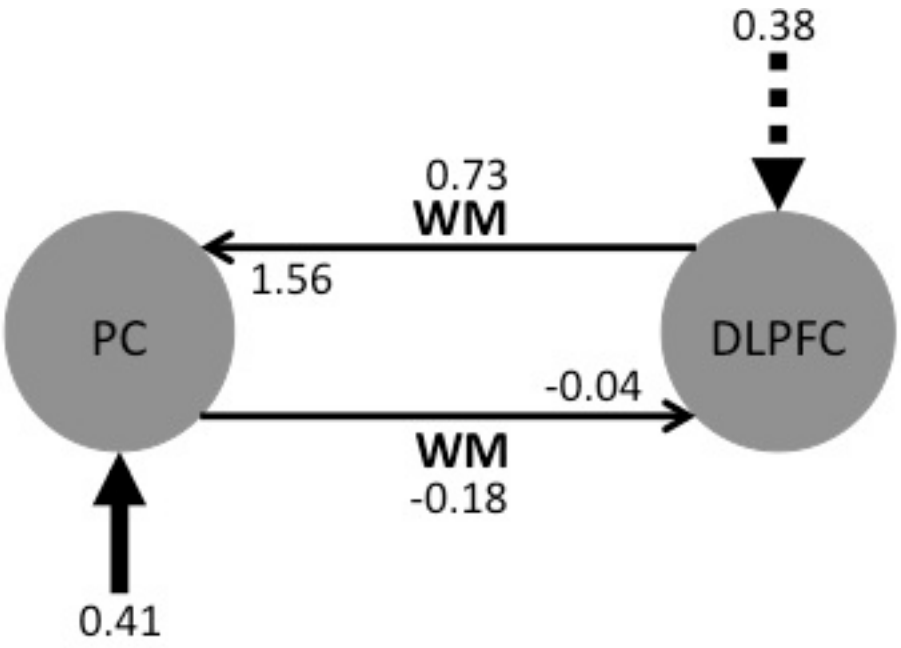

Figure 3.4: Average parameters across the sample for model 15.

DCM Parameters

The mean parameters across the 452 subjects of model 15 are shown in Figure 3.4. In this model, the stimulus presentation drives the network via the parietal cortex, and WM load drives the network via the dlPFC. dlPFC exerts a strong excitatory input to PC, and this influence is strongly increased during the 2B condition. Conversely, the PC exerts a relatively weak inhibitory influence on the dlPFC, and this influence is increased during 2B condition.

Genetic Modeling

Twin correlations were small and non-significant, indicating no genetic influence. As expected from the twin pair correlations, genetic modeling (Table 3.1) showed that the variance for both forward and back projections was due to unique environmental influences, which includes experimental (measurement) error.

Test-Retest Reliabilities And Posterior Correlations

To shed light on whether the large E component was more likely due to unique environmental influences, or experimental error, we examined the test-retest reliability. We found low test-retest reliabilities for the task-dependent modulations, intrinsic connections, driving stimuli and decay constants, with the highest ICC being 0.30 for the task modulation of the PC to

dlPFC connection (Table 3.2). These low ICCs indicate that the main contribution to the large E component is experimental error, rather than unique environmental influence.

Table 3.2 gives the posterior correlations between parameter estimates. There are numerous significant negative correlations, the largest being -0.65 between 2B driving input to dlPFC and 2B modulation on PC to dlPFC, implying that the increase in activity during 2B of the dlPFC may be explained by either direct driving of the region by the task, or an increase in connectivity from PC to dlPFC during the task, and that there is a high degree of co-linearity between these two possible factors.

Table 3.1: Means, twin correlations, and variance component estimates of the connectivity parameters from the best fitting model 15. MZ and DZ pairs were low and not significant, with wide confidence intervals.

	Mean (SD)	Twin Correlations		Model Fit				Variance components, expressed as % of total variance		
		MZ (97 pairs)	DZ (103 pairs)	-2LL	df	χ^2 test p-value	AIC	A	C	E
2B on PC to dlPFC (B_{212})	-0.18 (0.38)	0.08 (-0.10,0.26)	-0.05 (-0.22,0.12)							
ACE				1121.80	445	-	231.80	4 (0,21)	0(0,0)	96 (79,100)
AE				1121.80	446	1.00	229.80	4 (0,21)	-	96 (79,100)
CE				1122.01	446	0.64	230.01	-	1(0,15)	99 (85,100)
E				1122.04	447	0.89	228.04	-	-	100 (100,100)
2B on dlPFC to PC (B_{122})	0.73 (1.80)	-0.14 (-0.32,0.04)	-0.05 (-0.22,0.12)							
ACE				1273.84	445	-	383.84	0 (0,8)	0 (0,7)	100 (92,100)
AE				1273.84	446	1.00	381.84	0 (0,8)	-	100 (92,100)
CE				1273.84	446	1.00	381.84	-	0 (0,7)	100 (93,100)
E				1273.84	447	1.00	379.84	-	-	100 (100,100)

Table 3.2: Test-retest reliabilities of all model parameters for best fitting model 15, and posterior correlations between model parameters.

Model Parameter	ICC (95% CIs)	Posterior Parameter Correlation (95% CIs)							
		A_{21}	A_{12}	A_{11}	A_{22}	B_{212}	B_{122}	C_{11}	C_{22}
PC to dlPFC (A_{21})	0.15 (-0.17,0.44)	1.00 (1.00,1.00)	-	-	-	-	-	-	-
dlPFC to PC (A_{12})	-0.03 (-0.34,0.28)	-0.29 (-0.37,-0.20)	1.00 (1.00,1.00)	-	-	-	-	-	-
PC decay constant (A_{11})	-0.01 (-0.32,0.29)	0.03 (-0.06,0.13)	0.02 (-0.07,0.12)	1.00 (1.00,1.00)	-	-	-	-	-
dlPFC decay constant (A_{22})	-0.22 (-0.49,0.10)	-0.36 (-0.44,-0.28)	0.09 (-0.00,0.18)	0.02 (-0.07,0.12)	1.00 (1.00,1.00)	-	-	-	-
2B on PC to dlPFC (B_{212})	0.30 (-0.01,0.56)	-0.33 (-0.41,-0.25)	0.07 (-0.03,0.16)	0.08 (-0.01,0.17)	-0.03 (-0.12,0.07)	1.00 (1.00,1.00)	-	-	-
2B on dlPFC to PC (B_{122})	0.12 (-0.20,0.42)	0.11 (0.02,0.20)	-0.32 (-0.40,-0.24)	-0.06 (-0.15,0.03)	-0.03 (-0.12,0.07)	-0.11 (-0.20,-0.02)	1.00 (1.00,1.00)	-	-
Stimulus driving input to PC (C_{11})	0.01 (-0.30,0.31)	-0.02 (-0.12,0.07)	0.10 (0.01,0.19)	-0.16 (-0.25,-0.07)	-0.12 (-0.21,-0.03)	0.10 (0.01,0.19)	-0.01 (-0.10,0.08)	1.00 (1.00,1.00)	-
2B driving input to dlPFC (C_{22})	-0.03 (-0.34,0.28)	-0.03 (-0.13,0.06)	0.03 (-0.06,0.12)	-0.33 (-0.41,-0.25)	-0.07 (-0.16,0.03)	-0.65 (-0.70,-0.59)	0.13 (0.04,0.22)	0.19 (0.10,0.28)	1.00 (1.00,1.00)

Discussion

Fronto-parietal connectivity has been frequently associated with working memory (Chafee and Goldman-Rakic, 1998; Quintana and Fuster, 1999; Honey et al., 2002), and has recently been observed to be disrupted in schizophrenia (Deserno et al., 2012), motivating our assessment of its suitability as an endophenotype. In the largest sample to date (N=452), we performed dynamic causal modeling of data from a spatial N-Back working memory task, in order to estimate the genetic influence on task-induced changes in fronto-parietal connectivity. We found a task-related modulation of PC to dlPFC (forward) and dlPFC to PC (backward) connections, with the backward connection being larger in magnitude. We find no evidence that the task-dependent changes in fronto-parietal connectivity are influenced by genetic variation, and that the DCM parameters had low test-retest reliability.

The lack of heritability is surprising given related studies on fronto-parietal connectivity during WM. The BOLD activation in frontal and parietal regions in our data set was heritable, as was working memory performance itself (Blokland et al., 2008; Blokland et al., 2011). In other samples, it has been shown that the structural connections between frontal and parietal cortex are genetically influenced. Karlsgodt et al. (2010) found fractional anisotropy (FA; a measure of white matter integrity) in the superior longitudinal fasciculus, the primary white matter tract linking frontal and parietal cortices, to be heritable (h^2=59%), and to share common genetic influences with spatial working memory performance.

We found that most variance in the metrics was due to unique environmental variance and/or modeling/experimental error, E. Although it is not possible to separate unique environmental variance and modeling/experimental error using the twin design ACE model, post-hoc analyses lead us to believe there is a large contribution from modeling/experimental error to the parameter estimate. We found low test-retest reliability of all DCM parameters (ICC≤0.3). This could indicate a strong practice effect often seen in executive tasks (Basso et al., 1999; Lemay et al., 2004; Lowe and Rabbitt, 1998), a poor performance of our experimental procedure to reveal the underlying connectivity modulations, or an absence of those connectivity modulations (e.g. Harding et al. (2014) find no WM-load fronto-parietal connectivity modulations). There have been two prior studies on the test-retest reliabilities of DCM parameters. Schuyler et al. (2010) find high reliabilities of DCM parameters (ICC=0.5-0.9) in a task requiring identification of angry or happy faces/voices, for scanning sessions 5 minutes apart, whereas Rowe et al. (2010) find very low reliability in an action selection task (r^2=0.02-0.17), for scanning sessions weeks apart. Rowe et al. (2010) suggest that the difference in reliabilities compared to the Schuyler et al. (2010) study may arise from the difference in inter-scan interval, the simplicity of the Schuyler et al. (2010) models, in which only feed-forward mechanisms are present, and substantial posterior covariance between model parameters in their study. Posterior covariance between parameters can indicate that one parameter may be able to compensate for the value of another whilst maintaining overall model evidence, such that the anti-correlated values of each parameter could vary substantially between sessions. These considerations are important for the present study, since the models involve both feed-forward and feedback mechanisms, and there is strong posterior covariance between model parameters (Table 3.2). A high degeneracy between model parameters not only allows for large variation between scans, but also large variation between twins, potentially hindering the estimation of genetic effects. Post-hoc analysis of the

test-retest reliabilities of the simpler unidirectional models 7 and 11 (Supplementary Table S3.1), gave higher posterior correlations than for the bidirectional model 15, and test-retest reliabilities were not systematically higher, suggesting that parameter degeneracy associated with bidirectional models was not a cause of low test-retest reliabilities.

The DCM model with highest evidence suggested that WM load serves as a driving input into the dlPFC, with the dlPFC driving the PC, more strongly during 2B as compared to 0B condition. Although our winning model included modulations of both forward (PC to dlPFC) and backward (dlPFC to PC) modulation, the backward modulation was much greater in magnitude, and the model family including only backward modulations had more evidence than those including only forward modulations. The modulation of the backward connection is consistent with the top-down architecture proposed by Curtis and D'Esposito (2003), in which persistent activity in the dlPFC acts to focus attention on stimulus representations stored in the parietal cortex, and consistent with the biophysical model and fMRI observations of Edin et al. (2009), whereby lateral parietal inhibition which limits WM capacity at low load, is overcome by excitatory input from the dlPFC at higher loads. Backward modulation was also observed in healthy controls in the DCM studies of Deserno et al., 2012 (numeric N-Back task). However, a forward mechanism was observed in the winning models of both Ma et al., 2012 (numeric delayed match to sample task) and Dima et al., 2014 (verbal N-Back task) and no fronto-parietal modulations were observed by Harding et al. (2014) (verbal N-Back task). While Dima et al. (2014) constrained their model space to only allow (WM-load) driving input into the parietal cortex, Ma et al. (2012) tested the most likely region of WM input with connectivity modulations absent, and found this to be the parietal cortex. The study of (Ma, et al., 2012) differed from the present study in that the task paradigm was a delayed matching to sample task, and the networks used in DCM were considerably more complex, involving 8 bilateral regions of interest. It is noted that none of the previous studies employed a spatial N-Back working memory task.

One limitation of this study is the simplicity of the DCM models utilized. Working memory consists of numerous sub-processes, among them encoding, information manipulation, maintenance and retrieval. As depicted in Figure 3.1, the N-Back working memory task activates a large number of brain regions. By modeling the activity of only two regions, we potentially fail to account for multiple sources of variance/covariance in the data (Eichler, 2005; Waldorp et al., 2011). However, two region DCMs have been successfully implemented in the past to investigate the N-Back WM task (Bernal-Casas et al., 2013),

demonstrating multi-site reproducibility of winning model and parameter estimates. A related limitation is that in restricting our model space, we rejected models in which both dlPFC and PC are driven by external task input, and interregional connectivity is absent. This was based on the suggested importance of fronto-parietal connections and modulations in prior literature. However, given the low reliability of our connectivity parameters, and the absence of direct fronto-parietal modulations in Harding et al. (2014), such models may be worthy of consideration in future work. A second limitation of this study is that the experimental design was optimized to find differences between 0B and 2B conditions, whereas the contrast on stimulus presentation (one per second) is relatively poorly distinguished. The inter-trial interval of one second is less than the duration of the hemodynamic response function, which may pose difficulties in tracking the propagation of activity induced by external stimuli, with the BOLD response at each node being a superposition of influences from multiple stimuli. However, since DCM is a continuous time modeling approach which explicitly models the fast hidden neuronal states and the hemodynamic response function, a short inter-stimulus time should not preclude the application of DCM (Valdes-Sosa et al., 2011).

In summary, contrary to our hypothesis, we do not observe heritability of fronto-parietal connectivity modulations in working memory. The task-induced changes in the connectivity between dlPFC and PC seen in our winning model have very low test-retest reliabilities, limiting the inferences that can be made from the heritability analysis. More work is needed to establish the reliability of different working memory task settings and DCM modeling choices. This is the largest ever study on effective connectivity in working memory, and the first study to look at the heritability of DCM connectivity estimates in any cognitive domain.

References

Ando, J., Ono, Y., Wright, M.J. (2001) Genetic structure of spatial and verbal working memory. Behavior genetics, 31:615-24.

Baddeley, A. (1992) Working memory. Science, 255:556-9.

Baddeley, A.D., Bressi, S., Della Sala, S., Logie, R., Spinnler, H. (1991) The decline of working memory in Alzheimer's disease. A longitudinal study. Brain : a journal of neurology, 114 (Pt 6):2521-42.

Basso, M.R., Bornstein, R.A., Lang, J.M. (1999) Practice effects on commonly used measures of executive function across twelve months. The Clinical neuropsychologist, 13:283-92.

Bernal-Casas, D., Balaguer-Ballester, E., Gerchen, M.F., Iglesias, S., Walter, H., Heinz, A., Meyer-Lindenberg, A., Stephan, K.E., Kirsch, P. (2013) Multi-site reproducibility of prefrontal-hippocampal connectivity estimates by stochastic DCM. NeuroImage, 82:555-63.

Blokland, G.A., McMahon, K.L., Hoffman, J., Zhu, G., Meredith, M., Martin, N.G., Thompson, P.M., de Zubicaray, G.I., Wright, M.J. (2008) Quantifying the heritability of task-related brain activation and performance during the N-back working memory task: a twin fMRI study. Biological psychology, 79:70-9.

Blokland, G.A., McMahon, K.L., Thompson, P.M., Martin, N.G., de Zubicaray, G.I., Wright, M.J. (2011) Heritability of working memory brain activation. The Journal of neuroscience : the official journal of the Society for Neuroscience, 31:10882-90.

Bor, D., Duncan, J., Wiseman, R.J., Owen, A.M. (2003) Encoding strategies dissociate prefrontal activity from working memory demand. Neuron, 37:361-7.

Cabeza, R., Nyberg, L. (2000) Imaging cognition II: An empirical review of 275 PET and fMRI studies. Journal of cognitive neuroscience, 12:1-47.

Callicott, J.H., Ramsey, N.F., Tallent, K., Bertolino, A., Knable, M.B., Coppola, R., Goldberg, T., van Gelderen, P., Mattay, V.S., Frank, J.A., Moonen, C.T., Weinberger, D.R. (1998) Functional magnetic resonance imaging brain mapping in psychiatry: methodological issues illustrated in a study of working memory in schizophrenia. Neuropsychopharmacology : official publication of the American College of Neuropsychopharmacology, 18:186-96.

Carter, C., Robertson, L., Nordahl, T., Chaderjian, M., Kraft, L., O'Shora-Celaya, L. (1996) Spatial working memory deficits and their relationship to negative symptoms in unmedicated schizophrenia patients. Biological psychiatry, 40:930-2.

Chafee, M.V., Goldman-Rakic, P.S. (1998) Matching patterns of activity in primate prefrontal area 8a and parietal area 7ip neurons during a spatial working memory task. Journal of neurophysiology, 79:2919-40.

Corbetta, M., Shulman, G.L., Miezin, F.M., Petersen, S.E. (1995) Superior parietal cortex activation during spatial attention shifts and visual feature conjunction. Science, 270:802-5.

Curtis, C.E., D'Esposito, M. (2003) Persistent activity in the prefrontal cortex during working memory. Trends in cognitive sciences, 7:415-423.

D'Esposito, M., Aguirre, G.K., Zarahn, E., Ballard, D., Shin, R.K., Lease, J. (1998) Functional MRI studies of spatial and nonspatial working memory. Brain research. Cognitive brain research, 7:1-13.

Deserno, L., Sterzer, P., Wustenberg, T., Heinz, A., Schlagenhauf, F. (2012) Reduced prefrontal-parietal effective connectivity and working memory deficits in schizophrenia. The Journal of neuroscience : the official journal of the Society for Neuroscience, 32:12-20.

Dima, D., Jogia, J., Frangou, S. (2014) Dynamic causal modeling of load-dependent modulation of effective connectivity within the verbal working memory network. Human brain mapping, 35:3025-35.

Edin, F., Klingberg, T., Johansson, P., McNab, F., Tegner, J., Compte, A. (2009) Mechanism for top-down control of working memory capacity. Proceedings of the National Academy of Sciences of the United States of America, 106:6802-7.
Eichler, M. (2005) A graphical approach for evaluating effective connectivity in neural systems. Philosophical transactions of the Royal Society of London. Series B, Biological sciences, 360:953-67.
Esslinger, C., Kirsch, P., Haddad, L., Mier, D., Sauer, C., Erk, S., Schnell, K., Arnold, C., Witt, S.H., Rietschel, M., Cichon, S., Walter, H., Meyer-Lindenberg, A. (2011) Cognitive state and connectivity effects of the genome-wide significant psychosis variant in ZNF804A. NeuroImage, 54:2514-23.
Friston, K.J., Harrison, L., Penny, W. (2003) Dynamic causal modelling. NeuroImage, 19:1273-302.
Goodale, M.A., Milner, A.D. (1992) Separate visual pathways for perception and action. Trends in neurosciences, 15:20-25.
Gottesman, II, Gould, T.D. (2003) The endophenotype concept in psychiatry: etymology and strategic intentions. The American journal of psychiatry, 160:636-45.
Harding, I.H., Yücel, M., Harrison, B.J., Pantelis, C., Breakspear, M. (2014) Effective Connectivity within the Frontoparietal Control Network Differentiates Cognitive Control and Working Memory. NeuroImage.
Honey, G.D., Fu, C.H., Kim, J., Brammer, M.J., Croudace, T.J., Suckling, J., Pich, E.M., Williams, S.C., Bullmore, E.T. (2002) Effects of verbal working memory load on corticocortical connectivity modeled by path analysis of functional magnetic resonance imaging data. NeuroImage, 17:573-82.
Karlsgodt, K.H., Kochunov, P., Winkler, A.M., Laird, A.R., Almasy, L., Duggirala, R., Olvera, R.L., Fox, P.T., Blangero, J., Glahn, D.C. (2010) A multimodal assessment of the genetic control over working memory. The Journal of neuroscience : the official journal of the Society for Neuroscience, 30:8197-202.
Lee, J., Park, S. (2005) Working memory impairments in schizophrenia: a meta-analysis. Journal of abnormal psychology, 114:599-611.
Lemay, S., Bedard, M.A., Rouleau, I., Tremblay, P.L. (2004) Practice effect and test-retest reliability of attentional and executive tests in middle-aged to elderly subjects. The Clinical neuropsychologist, 18:284-302.
Lowe, C., Rabbitt, P. (1998) Test/re-test reliability of the CANTAB and ISPOCD neuropsychological batteries: theoretical and practical issues. Cambridge Neuropsychological Test Automated Battery. International Study of Post-Operative Cognitive Dysfunction. Neuropsychologia, 36:915-23.
Ma, L., Steinberg, J.L., Hasan, K.M., Narayana, P.A., Kramer, L.A., Moeller, F.G. (2012) Working memory load modulation of parieto-frontal connections: evidence from dynamic causal modeling. Human brain mapping, 33:1850-67.
Macey, P.M., Macey, K.E., Kumar, R., Harper, R.M. (2004) A method for removal of global effects from fMRI time series. NeuroImage, 22:360-6.
Meyer-Lindenberg, A., Weinberger, D.R. (2006) Intermediate phenotypes and genetic mechanisms of psychiatric disorders. Nature reviews. Neuroscience, 7:818-27.
Muller, N.G., Knight, R.T. (2006) The functional neuroanatomy of working memory: contributions of human brain lesion studies. Neuroscience, 139:51-8.
Owen, A.M., McMillan, K.M., Laird, A.R., Bullmore, E. (2005) N-back working memory paradigm: a meta-analysis of normative functional neuroimaging studies. Human brain mapping, 25:46-59.
Penny, W.D., Stephan, K.E., Daunizeau, J., Rosa, M.J., Friston, K.J., Schofield, T.M., Leff, A.P. (2010) Comparing families of dynamic causal models. PLoS computational biology, 6:e1000709.

Penny, W.D., Stephan, K.E., Mechelli, A., Friston, K.J. (2004) Comparing dynamic causal models. NeuroImage, 22:1157-72.
Polderman, T.J.C., Stins, J.F., Posthuma, D., Gosso, M.F., Verhulst, F.C., Boomsma, D.I. (2006) The phenotypic and genotypic relation between working memory speed and capacity. Intelligence, 34:549-560.
Quintana, J., Fuster, J.M. (1999) From perception to action: temporal integrative functions of prefrontal and parietal neurons. Cerebral cortex, 9:213-21.
Rowe, J.B., Hughes, L.E., Barker, R.A., Owen, A.M. (2010) Dynamic causal modelling of effective connectivity from fMRI: are results reproducible and sensitive to Parkinson's disease and its treatment? NeuroImage, 52:1015-26.
Schuyler, B., Ollinger, J.M., Oakes, T.R., Johnstone, T., Davidson, R.J. (2010) Dynamic Causal Modeling applied to fMRI data shows high reliability. NeuroImage, 49:603-11.
Stephan, K.E., Penny, W.D., Daunizeau, J., Moran, R.J., Friston, K.J. (2009) Bayesian model selection for group studies. NeuroImage, 46:1004-17.
Valdes-Sosa, P.A., Roebroeck, A., Daunizeau, J., Friston, K. (2011) Effective connectivity: influence, causality and biophysical modeling. NeuroImage, 58:339-61.
Van Dijk, K.R., Sabuncu, M.R., Buckner, R.L. (2012) The influence of head motion on intrinsic functional connectivity MRI. NeuroImage, 59:431-8.
Wager, T.D., Smith, E.E. (2003) Neuroimaging studies of working memory: a meta-analysis. Cognitive, affective & behavioral neuroscience, 3:255-74.
Waldorp, L., Christoffels, I., van de Ven, V. (2011) Effective connectivity of fMRI data using ancestral graph theory: dealing with missing regions. NeuroImage, 54:2695-705.
Woodward, T.S., Cairo, T.A., Ruff, C.C., Takane, Y., Hunter, M.A., Ngan, E.T. (2006) Functional connectivity reveals load dependent neural systems underlying encoding and maintenance in verbal working memory. Neuroscience, 139:317-25.

Supplementary Material

Table S3.1: ICCs of DCM parameters for models 15, 7 and 11.

Parameter	Model 15 (BD)	Model 7 (FW)	Model 11 (BW)
A11	-0.01(-0.32,0.29)	0.34(0.04,0.59)	-0.04(-0.34,0.27)
A21	0.15(-0.17,0.44)	0.25(-0.07,0.52)	0.14(-0.18,0.43)
A12	-0.03(-0.34,0.28)	0.41(0.11,0.64)	-0.03(-0.34,0.28)
A22	-0.22(-0.49,0.10)	-0.10(-0.39,0.22)	-0.09(-0.39,0.22)
B212	0.30(-0.01,0.56)	0.03(-0.28,0.34)	-
B122	0.12(-0.20,0.42)	-	0.06(-0.25,0.37)
C11	0.01(-0.30,0.31)	0.06(-0.25,0.36)	-0.05(-0.36,0.26)
C22	-0.03(-0.34,0.28)	0.01(-0.30,0.32)	0.21(-0.11,0.49)

Table S3.2: ICCs of DCM parameters using region of interest selection methods from Deserno et al., 2012 and Ma et al., 2012.

Parameter	Deserno et al. 2012	Ma et al. 2012
A11	-0.01(-0.32,0.29)	0.10(-0.23,0.41)
A21	0.15(-0.17,0.44)	-0.09(-0.40,0.25)
A12	-0.03(-0.34,0.28)	-0.25(-0.53,0.08)
A22	-0.22(-0.49,0.10)	0.09(-0.23,0.40)
B212	0.30(-0.01,0.56)	0.31(-0.01,0.57)
B122	0.12(-0.20,0.42)	-0.02(-0.34,0.31)
C11	0.01(-0.30,0.31)	-0.09(-0.40,0.23)
C22	-0.03(-0.34,0.28)	0.30(-0.02,0.57)

4 Chapter 4: Genetics Influences on Functional Connectivity in Working Memory Networks

This paper has been submitted to the Journal of Neuroscience in August 2015. The paper has been replicated here. The contents have been altered only slightly to reflect formatting changes.

Genetic Influences on Functional Connectivity in Working Memory Networks

Benjamin Sinclair[1,2,3], Nick G. Martin[3], Paul M. Thompson[4], Greig I. de Zubicaray[2], Margaret J. Wright[3], Katie L. McMahon[1]

1 Centre for Advanced Imaging, University of Queensland, Brisbane, QLD 4072, Australia
2 School of Psychology, University of Queensland, Brisbane, QLD 4072, Australia
3 QIMR Berghofer Medical Research Institute, Brisbane, QLD 4029, Australia
4 Imaging Genetics Center, Dept. of Neurology, Keck School of Medicine, University of Southern California, Los Angeles, CA 90095, USA

Please address correspondence to:
Ben Sinclair,
Centre for Advanced Imaging,
University of Queensland, Brisbane,
QLD 4072, Australia
+61 415314218
b.sinclair@uq.edu.au

Conflicts of interest: None real or perceived.

Abstract

The dorsolateral prefrontal cortex (dlPFC) is a robustly activated region during a range of working memory (WM) tasks. Its connectivity with the rest of the brain during working memory has been reported to be predictive of task performance and associated with disease genetic risk factors. Here we probe the connectivity profile of the right dlPFC during working memory in a large sample of twins (N=827, 134 monozygotic (MZ) pairs; 165 dizygotic (DZ) pairs; 229 unpaired), and measure the heritability of a number of right dlPFC connections previously reported as implicated in WM, to the left dlPFC, right parietal cortex, left hippocampus, medial frontal cortex and posterior cingulate cortex. We observe the expected positive coupling between dlPFC and task-positive network regions, and negative coupling with the default mode network. Changes in connectivity with working memory load were less significant, with increased contralateral dlPFC connectivity, and increased dlPFC-posterior cingulate cortex anti-correlation. We estimate weak heritability of dlPFC connectivity to contralateral dlPFC (h^2=36%), ipsilateral parietal cortex (24%), posterior cingulate cortex (37%) and medial frontal cortex (26%).

Key words: working memory, functional connectivity, genetics, heritability

1. Introduction

Convergent evidence suggests that working memory (WM) function is facilitated by the interaction of a distributed network of functionally related brain regions (Schlosser et al., 2006; Fuster, 2009). Functional connectivity (FC) correlates the time series data of different brain regions to measure large scale brain interactions. As opposed to effective connectivity, which models the causal influence of one neuronal population on another, FC measures the statistical dependencies between activity of disparate brain anatomy (Friston, 2011), and thus cannot be said to make any inference on neural mechanisms. Despite this conceptual limitation, functional connectivity has proven useful in disease group classification (Meyer-Lindenberg et al., 2005; Koshino et al., 2005), and is predictive of cognitive performance across a range of domains (Hampson et al., 2006a; Hampson et al., 2006b; He et al., 2007).

Working memory is a strongly heritable cognitive process. Accuracy in working memory tasks is a heritable phenotype (h^2=40-60%; Ando et al., 2001, Polderman et al., 2006). Recently it has been shown that variation in brain activation in N-Back working memory tasks has a moderate to strong genetic component (mean h^2=23%, max h^2=65%) (Blokland et al., 2011). Since brain connectivity is thought to underlie working memory execution, and many aspects of working memory are strongly heritable, it is reasonable to hypothesize that WM-associated connectivity is a heritable feature, and may be a useful endophenotype for understanding the genetic architecture of WM. However, little work has been done to establish the genetic effects on WM-related brain connectivity.

Most prior studies of WM FC have looked at the connectivity of the dorsolateral prefrontal cortex (dlPFC), which is a key node in WM performance. It is robustly activated in a range of paradigms (Owen et al., 2005), with its activation related to performance measures (Pessoa et al., 2002; Sakai et al., 2002). Its connectivity with other brain regions is thought to have a mechanistic role in facilitating WM (Chafee and Goldman-Rakic, 1998; Gazzaley et al., 2004; Zanto et al., 2011). Further, abnormalities in dlPFC connectivity with left hippocampus (Meyer-Lindenberg et al., 2005) and right parietal cortex (Deserno et al., 2012) have been observed in schizophrenic patients. We investigate the strength and heritability of WM task connections of the right dlPFC with right parietal cortex (rPC) and left hippocampus.

At rest, the brain is intrinsically organized into two anti-correlated networks (Fox et al., 2005), one referred to as the "task-positive network" including a set of regions routinely activated across a range of cognitive domains such as the dlPFC, posterior parietal cortex, anterior cingulate cortex (Dosenbach et al., 2006; Cole and Schneider, 2007), and the "task-negative network" or default mode network (DMN), including regions routinely deactivated (Shulman et al., 1997; Raichle et al., 2001) such as medial frontal cortex (MFC), posterior cingulate cortex (PCC) and lateral parietal cortices. The anti-correlation between these networks persists during task-performance (Kelly et al., 2008; Whitfield-Gabrieli and Nieto-Castanon, 2012) which may be involved in task-related suppression of the DMN. Although most work in the working memory literature has focused on the interactions between task-positive regions, there is growing interest in the role of task-positive to task-negative interaction in cognition. Interestingly, task-negative regions have been reported to display connectivity with the dlPFC which is predictive of task performance in a verbal WM task (Hampson et al., 2010). In particular, the strength of anti-correlation between dlPFC and MFC,

a robustly deactivated region, is correlated with task performance. Similarly, the anti-correlation between task-positive and task-negative regions has been linked to behavioral variability in response inhibition tasks (Kelly et al., 2008). In this study we look at the functional connectivity between dlPFC and two task-negative regions, the MFC and PCC.

Although no work has yet measured the heritability of functional connectivity during working memory, a couple of studies have found genetic association with some features of dlPFC connectivity. Esslinger et al. (2009) found that inter-hemispheric dlPFC and dlPFC-hippocampal connectivity was correlated with genotype of the schizophrenia risk gene ZNF804, and Tan et al. (2007) found dlPFC-PC functional connectivity was modulated by interactions between dopaminergic and glutamatergic genes.

Based on previous research into WM-related brain connectivity, patient data, and genetic studies, we expect positive correlations between the right dlPFC with the left dlPFC and right PC, and negative correlations to MFC, PCC and left hippocampus during working memory performance, and we expect that the FC of right dlPFC with left dlPFC, right PC, left hippocampus, MFC and PCC during WM will be heritable, and that load dependent changes in these connections will also be heritable.

2. Materials and Methods

Participants. 906 subjects were recruited from the Queensland Twin Imaging Study (QTIM) (de Zubicaray et al., 2008), under approval of the Human Research Ethics Committees of the Queensland Institute of Medical Research, University of Queensland, and Uniting Health Care, Wesley Hospital. Written informed consent was obtained for each participant. Twins were scanned in the same session or within a week of each other. Participants were excluded if they reported any history of psychiatric disease, brain injury, substance abuse or MR incompatibility. Data from 79 subjects were excluded due to excessive head motion (translation>3mm, rotation>2°) leaving a final sample size of 827 subjects (134 monozygotic (MZ) pairs; 165 dizygotic (DZ) pairs; 229 unpaired; mean age 22.9 (SD 2.7)).

Experimental Paradigm. Participants undertook the widely-used N-Back test of working memory (Callicott et al., 1998), with 0-Back (0B) and 2-Back (2B) conditions. In this experiment, participants are shown numbers between 1 and 4 in random order appearing on a colored diamond, with each unique number always appearing in the same location on the diamond grid (see Blokland et al 2011). During the 0B condition, participants must report the number with which they were presented, and during the 2B condition, participants must report the number with which they were presented two trials previously. The 0 and 2 back conditions were in blocks of 16 trials (16s), and alternated throughout the run, with 8 blocks of each condition.

Image Acquisition. Imaging was conducted on a 4 Tesla Bruker Medspec whole body scanner (Bruker). Participants undertook an fMRI scan, whilst performing the working memory task. The imaging sequence was a T2*-weighted gradient echo, echo planar imaging (GE-EPI) sequence (repetition time TR = 2100 ms; echo time TE = 30 ms; flip angle = 90°; field of view FOV = 230 mm x 230 mm, pixel size 3.6x3.6mm, 36 coronal 3.0mm slices with 0.6mm gap, 127 volumes). Prior to the fMRI scan a T1-weighted 3D structural image was acquired (MPRAGE, TR = 1500 ms; TE = 3.35 ms; inversion time TI=700ms; flip angle = 8°; FOV = 230 mm^3, pixel size 0.9x0.9x0.9mm).

Image Processing. Images were processed in SPM8 (www.fil.ion.ucl.ac.uk/spm/). For each subject, the first 5 EPI volumes were removed to allow for steady state magnetization, and all images slice time corrected. All EPI volumes coregistered to the first time point to remove inter-scan movement, the mean image from all coregistered images was calculated and registered to the subjects T1 image. T1 images were transformed into standard space, using the DARTEL algorithm, and the resulting deformation fields applied to the EPI images. Finally, images were smoothed with an $8mm^3$ Gaussian kernel.

Statistical Parametric Mapping. For each subject activation in response to the 0- and 2-back conditions was measured using a general linear model. A contrast was generated for working memory load (2B greater than 0B). This was taken and entered into a group wise random effects analysis, to measure group-wise activation, with the resulting t-statistic map thresholded at $p<0.05$ with a family wise error (FWE) correction for multiple comparisons. The resulting group-wise activation map showed activation in inferior and superior parietal

cortex, dlPFC and deactivation in medial frontal cortex (MFC), posterior cingulate cortex (PCC) and hippocampus (Figure 4.2).

dlPFC Seed Region. The right dlPFC seed region was extracted using a combination of anatomical and functional criteria. Anatomical regions of interest were extracted from the WFU Pick Atlas (www.fmri.wfubmc.edu), with the dlPFC defined as the union of BA9 and BA46, with medial sections of BA9 manually removed. The maximum groupwise activation for the 2B>0B condition within the dlPFC was at MNI coordinates [42,36,24]. For each subject, the nearest local maximum to this coordinate was surrounded with a sphere of radius 6mm, and the first eigenvariate within the sphere taken as the representative time series for the right dlPFC.

Functional Connectivity Analysis. Functional connectivity analysis was undertaken in the *conn fmri* toolbox (Whitfield-Gabrieli and Nieto-Castanon, 2012). For each subject, time series were despiked, linearly detrended and high-pass filtered at 1/128 Hz. The first 5 principle components of signal from white matter and CSF were removed, using the compcor algorithm, an alternative to removing global signal which nonetheless removes much of the artificial global signal related correlation (Behzadi et al., 2007), along with 6 motion parameters and their first derivatives.

Finally, Pearson's correlation coefficient of the dlPFC seed time series with every voxel was taken to quantify functional connectivity. Functional connectivity was calculated within each condition by partitioning the time series into time points falling within each condition, allowing for haemodynamic delay. This was carried out using weighted correlations specific to each condition, with weights calculated by convolving the boxcar functions for 0B and 2B conditions with a haemodynamic response function (hrf). Since time points at the boundary between conditions will contain contributions from both 0B and 2B conditions, the robustness of our results were assessed by repeating the procedure convolving with a Hanning filter, rather than a hrf, which is simply a rectangular filter which disregards points close to the boundary. We also measured the effect of regressing out task-related variance, which is carried out when a single correlation across multiple task conditions is taken (e.g. Esslinger et al., 2011), and also helps reduce ramping up and ramping down effects at the boundary between conditions. The difference in correlation between conditions was also calculated for each subject, as a representation of connectivity change during working

memory load. Fisher-transformed subject dlPFC connectivity maps for 0B, 2B and 2B-0B were taken forward to a second level random effects analysis, to calculate group connectivity.

Target ROIs. To quantify the functional connectivity of the right dlPFC to the regions of interest, we averaged the Fisher-transformed correlation coefficient over all voxels contained within the region. The target ROIs were defined anatomically using the WFU Pick Atlas, and were right parietal cortex (PC; BA 7 and BA 40), left dlPFC (BA 9 and BA 46, with medial BA 9 manually removed), left hippocampus, bilateral PCC (BA 23 and BA 31), and bilateral MFC (BA 9 and BA 10). To restrict averaging to regions connected with the dlPFC, each anatomical region was masked with each of the three group-wise connectivity profiles, 0B, 2B, 2B>0B, and the largest cluster in the composite mask retained. For the 0B and 2B conditions, in the left dlPFC and right PC, only significantly positively correlated voxels were retained, and in the left hippocampus, PCC and MFC only significantly negatively correlated voxels were retained. For the 2B-0B condition, left dlPFC and MFC were masked with voxels showing a significant increase in correlation (2B>0B), and PCC, left hippocampus and right PC were masked with voxels showing a significant decrease in correlation (0B>2B), as this was the pattern of connectivity changes observed in those regions (see Figure 4.2; bottom panel).

Heritability. Monozygotic and dizygotic twin correlations were calculated using maximum likelihood fitting implemented in Mx (Neale et al., 2002), with sex, age and mean motion (average across all volumes of $\sqrt{x^2 + y^2 + z^2}$; Van Dijk et al., 2012) included as covariates. We then used structural equation models (SEM) to estimate to what extent the variance in the FC was attributable to additive genetic, A, common environment, C, and unique environment/measurement error, E (Neale et al., 2002). Structural equation modeling fits a predicted covariance structure based on linear relationships between latent variables, to the observed covariance between twin phenotypes. The phenotype, in our case FC, is modeled as a linear function of latent genetic and environmental variables, $P = aA + cC + eE$. The variance of the phenotype is given by $var(P) = a^2 + c^2 + e^2$, the covariance between MZ twin pairs as $cov(P_1,P_2)_{MZ} = a^2 + c^2$, and the covariance between DZ twins as $cov(P_1,P_2)_{DZ} = ½\ a^2 + c^2$, since on average DZ twins share 50% of their genetic polymorphisms. The path diagram embodying this covariance structure is shown in with Figure 4.1. The SEMs were fitted to the data using a maximum likelihood fitting implemented in Mx (Neale et al., 2002). Initially, variance models including all components (ACE model) were fitted, including age, sex and mean motion as covariates. Parameters were successively dropped from the model and reduced models were

tested for goodness of fit. The nested genetic models were then compared for model parsimony using the Akaike Information Criterion (AIC). To correct for multiple comparisons, an effective number of independent tests was estimated from the phenotype correlation matrix, and a Bonferonni correction applied based on the effective number of independent tests to give an adjusted significance threshold required to keep Type I error rates at 5% and corresponding confidence intervals (Nyholt, 2004). The uncorrected 95% confidence intervals on each parameter are reported, and heritability estimates exceeding the significance threshold once corrected for multiple comparisons are indicated.

Test-retest reliability. A subset of 48 subjects were rescanned an average of 3.5(SD 1.4) months after the first scan, to measure the test-retest reliability of the connectivity measures, quantified with the intra-class correlation coefficient.

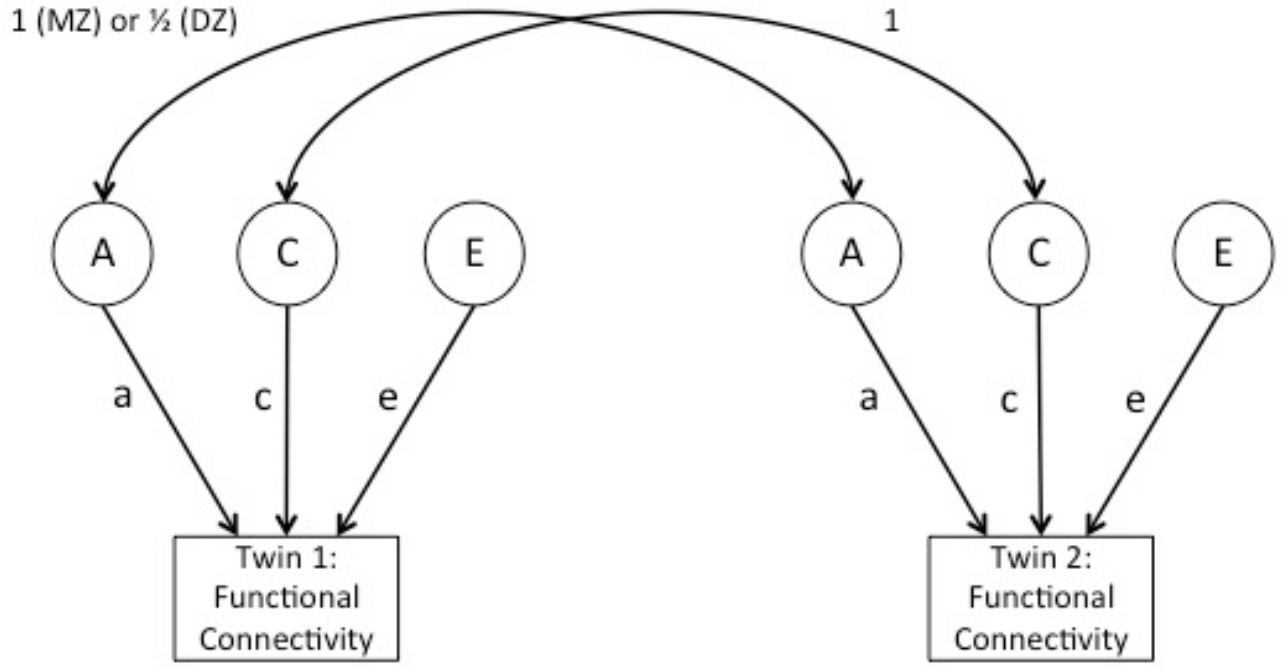

Figure 4.1: Path Diagram for genetic modeling. In this structural equation modeling, (observed) variance in functional connectivity parameters is modeled as arising from (hidden) additive genetic factors (A), common environmental factors (C), and unique environmental factors (E). The covariance in additive genetic factors is set to 1 for monozygotic (MZ) twins and ½ for dizygotic (DZ) twins.

3. Results

Functional Connectivity

Figure 4.2 shows the connectivity profile of the dlPFC during WM, and the change in connectivity between 0B and 2B conditions. For the 2B condition we see positive correlation with the majority of WM-activated regions, including superior and inferior parietal cortex (peak maxima, MNI coordinates (50, 30, 48)), left dlPFC (-46, 26, 30), middle/anterior cingulate cortex (4, 24, 44) and insula (38 22, -2). We also see negative correlations with many areas of the task-negative/default mode network, including medial frontal cortex (-2, 56,2), posterior cingulate cortex (-6, -48, 28) and angular gyrus (-48, -62, 30). The connectivity profile for the 0B condition was very similar to the 2B condition, and the bottom panel of Table 4.1 shows that the average FC across the regions of interest changes very little between conditions, with the standard deviations crossing zero.

Nonetheless, due to our large sample size and high power to detect small changes, we do observe significant changes in FC between 2B and 0B conditions in some regions. Increases in correlation are observed in the left dlPFC (-52, 20, 24), anterior precuneus (-4,-52,44) which go from positively correlated to more positively correlated, and superior regions of the medial frontal cortex (-6,56,38) and left angular gyrus (-46, -66, 22), which go from negatively correlated to more negatively correlated. Reductions in correlation are present in Posterior cingulate cortex (2,-28,28), anterior cingulate cortex (0,30,22) and posterior precuneus (12,-68,40).

Heritability

Table 1 gives heritability estimates for dlPFC connectivity and the five ROIs for the 0B, 2B and 2B>0B conditions. During the 2B condition, right PC (h^2=24%), dlPFC (h^2=36%), PCC (h^2=37%) and MFC (h^2=26%) have small but significant estimates of additive genetic variance. For hippocampus, the best fitting model was one without additive genetic component. In some cases where an AE model was chosen as the best model, there was little difference in the AIC values of the AE and CE models ($\Delta AIC<2$), giving little evidence to choose between the two. During the baseline condition, a similar pattern of genetic and environmental influences was present. The variance in change in connectivity between 2B

and 0B for all regions was attributed to unique environmental/ measurement error for all regions.

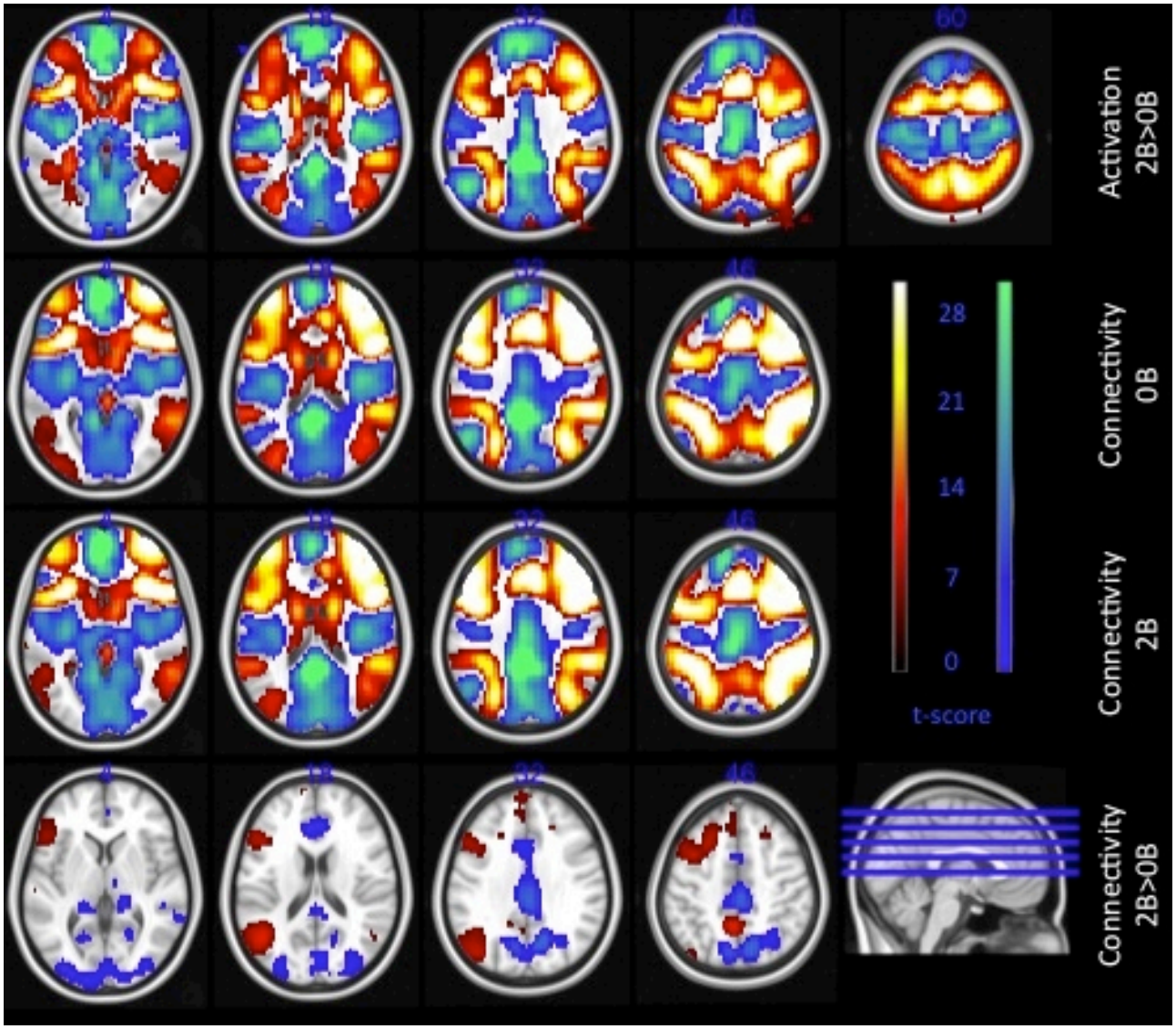

Figure 4.2: Group wise activation (top panel), and connectivity profiles with dlPFC seed (bottom three panels). Positive activation/connections in red-yellow, negative activations/connections in blue-green. The t-statistics were thresholded at FWE $p<0.05$, corrected for multiple comparisons.

Table 4.1: Means, twin correlations and genetic modeling for functional connectivity with the right dorsolateral prefrontal cortex, averaged over regions of interest.

Region	Mean (SD)	Twin Correlations (95% CIs)		Aikike's Information Criterion				ACE estimates from best fitting model, expressed as % (95% CIs)		
	827 subjects	MZ (134 pairs)	DZ (165 pairs)	ACE	AE	CE	E	A	C	E
0B										
right PC	0.24(0.13)	0.18 (0.05,0.31)	0.02 (-0.09,0.13)	641.67	**639.67**	642.39	644.69	22(6,36)	-	78(64,94)
left dlPFC	0.20(0.12)	0.18 (0.05,0.31)	0.01 (-0.10,0.12)	673.90	**671.90**	674.10	676.32	19(4,33)	-	81(67,96)
left hippocampus	-0.09(0.12)	0.03 (-0.11,0.16)	0.06 (-0.05,0.16)	607.86	606.23	605.86	**605.03**	-	-	100(100,100)
PCC	-0.14(0.12)	0.12 (-0.01,0.25)	0.06 (-0.05,0.17)	602.24	**600.24**	600.87	603.89	19(3,33)	-	81(67,97)
MFC	-0.17(0.12)	0.19 (0.06,0.32)	0.09 (-0.02,0.20)	602.71	**600.71**	602.86	610.09	26(11,39)*	-	74(61,89)
2B										
right PC	0.24(0.13)	0.16 (0.03,0.29)	0.10 (-0.01,0.20)	601.89	**599.94**	600.63	607.78	24(9,37)*	-	76(63,91)
left dlPFC	0.21(0.12)	0.31 (0.19,0.43)	0.15 (0.04,0.25)	633.83	**632.07**	633.68	658.29	36(24,48)*	-	64(52,76)
left hippocampus	-0.09(0.12)	0.05 (-0.08,0.19)	0.01 (-0.11,0.12)	588.19	586.19	586.40	**584.82**	-	-	100(100,100)
PCC	-0.16(0.12)	0.23 (0.10,0.36)	0.10 (-0.01,0.21)	532.52	**530.52**	535.84	549.08	37(22,50)*	-	63(50,78)
MFC	-0.16(0.13)	0.20 (0.06,0.32)	0.07 (-0.04,0.18)	577.80	**575.80**	578.74	584.73	26(11,39)*	-	74(61,89)
2B-0B										
right PC	-0.06(0.12)	0.11 (-0.02,0.24)	-0.02 (-0.13,0.09)	687.66	685.66	686.58	**685.25**	-	-	100(100,100)
left dlPFC	0.05(0.13)	0.09 (-0.05,0.22)	0.04 (-0.07,0.15)	665.44	**663.46**	663.57	663.77	11(0,25)	-	89(75,100)
left hippocampus	-0.04(0.18)	-0.04 (-0.17,0.10)	-0.06 (-0.17,0.05)	701.75	699.75	699.75	**697.75**	-	-	100(100,100)
PCC	-0.06(0.13)	-0.02 (-0.16,0.11)	0.03 (-0.09,0.14)	689.52	687.52	687.52	**685.52**	-	-	100(100,100)
MFC	0.05(0.14)	0.08 (-0.05,0.21)	0.03 (-0.08,0.14)	670.32	668.32	668.44	**668.23**	-	-	100(100,100)

* Exceeds multiple comparisons threshold for 5% Type I error rate.
Best fitting model indicated in bold font.

Test retest reliabilities are given in Table 4.2. Reliabilities were low to moderate, ranging from -0.30 to 0.51. Test-retest reliabilities (and heritability estimates) were lowest in the hippocampus, and lowest for the 2B-0B contrast. We note that the hippocampus was the smallest of the ROIs considered, and that the segmentation of the hippocampus extracted from the WFU Pick Atlas did not overlap well with our functional connectivity cluster in the hippocampus (Supplementary Figure S4.1).

Table 4.2: Test retest reliabilities for the mean functional connectivity with the right dorsolateral prefrontal cortex over each region, for each condition, quantified as the intra-class correlation between session 1 and session 2.

Region	Intra Class Correlation		
	0B	**2B**	**2B-0B**
right PC	0.15 (-0.13,0.41)	0.45 (0.19,0.65)	0.18 (-0.11,0.44)
left dlPFC	0.41 (0.14,0.62)	0.47 (0.22,0.66)	0.13 (-0.16,0.39)
left hippocampus	0.03 (-0.25,0.31)	-0.02 (-0.30,0.26)	-0.30 (-0.53,-0.02)
PCC	0.51 (0.27,0.69)	0.28 (0.00,0.52)	0.20 (-0.08,0.46)
MFC	0.38 (0.12,0.60)	0.28 (-0.00,0.52)	0.09 (-0.20,0.36)

Processing variations accounting for boundary effects

Groupwise correlation maps (Supplementary figure S4.2), heritability estimates (Supplementary Table S4.1) and test-retest reliabilities (Table S4.2) when using a Hanning filter to remove time points near condition boundaries are almost identical to those when using a more conventional hrf filter to de-weight boundary time points, indicating that results were not confounded by boundary effects. Regressing out task-related variance did not substantially alter the connectivity profiles for 0B and 2B conditions, but produced an unexpected WM-load (2B>0B) reduction in functional connectivity with the right posterior parietal cortex (Figure S4.3). Test-retest reliabilities were substantially lower (Table S4.4), while heritability estimates were similar (Table S4.3), other than for MFC, which was not heritable.

4. Discussion

This study shows a weak to moderate influence of genetic variation on the functional connectivity between right dlPFC with left dlPFC (h^2=36%), right PC (24%), PCC (37%) and MFC(26%) during working memory performance, but no genetic influence on load-dependent changes in connectivity. All connectivity measures had large unique environmental/ measurement error variance components.

Inter-hemispheric prefrontal connectivity is fundamental to integrative attentional processing and cognitive control (Banich, 1998; Gazzaniga, 2000). There are a number of genetic mechanisms which may contribute to the observed heritability of inter-hemispheric prefrontal connectivity. Glutamatergic, GABAergic and dopaminergic systems have all been implicated in working memory function. Glutamate is involved in cortico-cortical excitatory interactions, and genes regulating glutamate transmission are associated with spatial working memory performance (Donohoe et al., 2007). Dopamine modulates the excitability of prefrontal neurons, and its importance in WM has been long established (Sawaguchi and Goldman-Rakic, 1991; Goldman-Rakic, 1998). Genes involved in dopamine signaling, catechol-O-methyl transferase (COMT; dopamine catabolism) and DRD2 (codes for D2 receptor) are likewise related to WM activation (de Frias et al., 2010; Bertolino et al., 2010) and WM task performance (Goldberg et al., 2003; Stelzel et al., 2009). Inter-regional communication is also dependent on the integrity of the white matter pathways linking them (Honey et al., 2009). Fractional anisotropy in diffusion weighted MRI (a measure of tract integrity) in the anterior corpus callosum is a heritable trait (Chiang et al., 2009), so genetic effects on white matter microstructure may also contribute to the heritability of right-left dlPFC functional connectivity.

The heritability of inter-hemispheric dlPFC connectivity is in line with Woodward et al. (2009), who found reduced connectivity of right dlPFC with left middle frontal gyrus for schizophrenic (SZ) patients, and trend ($p<0.06$) towards reduced connectivity in unaffected siblings during a choice reaction time task, suggesting a genetic liability for reduced inter-hemispheric frontal connectivity. Inter-hemispheric dlPFC connectivity during WM has previously been associated with genetic risk for Schizophrenia. Esslinger et al. (2011) found inter-hemispheric dlPFC connectivity during combined 0B and 2B conditions of a numeric working memory task to be associated with the schizophrenia risk gene ZNF804A. However,

this association was also present during an emotion recognition task, and at rest, indicating that this particular genetic influence is independent of cognitive domain. We find similarly that total genetic influences are present during both stages of our task, the 0B condition which involves basic attentional processes and response selection, and the 2B condition involving the maintenance and manipulation elements of working memory. Thus it is not clear that the heritability pertains specifically to WM processes. This is noteworthy since it is common practice in task-related functional connectivity studies to measure the correlation in a single experimental condition, or to average across conditions.

Fronto-parietal connectivity is considered a core mechanism sub-serving WM (Chafee and Goldman-Rakic, 1998; Quintana and Fuster, 1999). Although structural connectivity between frontal and parietal regions has demonstrated heritability (Karlsgodt et al., 2010), the heritability of fronto-parietal functional connectivity has not previously been established. However, dlPFC functional connectivity to focal regions of the posterior parietal cortex (PPC; BA7 and BA40) has previously been associated with the epistatic interaction between COMT and glutamate receptor mgluR3 (GRM3) genotype (Tan et al., 2007) for combined 1B and 2B conditions in a numeric/spatial N-Back WM task. Fronto-parietal functional connectivity was estimated to be weakly heritable in the present study (h^2=24%), which is substantially lower than heritability of fractional anisotropy in the superior longitudinal fasciculus (h^2=59%; Karlsgodt et al., 2010).

We also find that the anti-correlations between dlPFC and default mode regions are heritable. The observed anti-correlation is believed to reflect the competition between cognitive control and default mode networks (Fox et al., 2005). This anti-correlation has been associated with behavioral variability, for example Kelly et al. (2008) find that variance in reaction time on a Flanker task is lower for subjects with greater anti-correlation between default mode network and task-positive attentional network, while Hampson et al. (2010) find a positive correlation between the strength of the dlPFC to MFC anti-correlation, and working memory performance. Our results indicate that the antagonistic relationship between these two networks may be influenced by genes, though the influence is small, and does not appear to be related to cognitive demand for the MFC in our data set.

The heritability observed in this study are along the lines of those seen in other functional neuro-imaging measures, such as working memory activation (mean h^2=23%,

Blokland et al., 2011), default mode network functional connectivity (h^2=42%; Glahn et al., 2010), and resting state network characteristics (h^2=0-60% Fornito et al., 2011; van den Heuvel et al., 2013). However, they are lower than corresponding measures of structural connectivity. White matter integrity in the frontal lobes has a heritability of 55% (Chiang et al., 2009), and white matter integrity in the superior longitudinal fasciculus connecting frontal and parietal regions has a heritability of 59% (Karlsgodt et al., 2010). It may therefore be that variation in functional connectivity is less heritable than corresponding structural connectivity, or that our functional connectivity measures have inherently more measurement error than structural measures.

There are a number of limitations of this study to take into account. The test-retest reliability of the connectivity estimates was low to moderate (ICC≤0.51). The four connectivity estimates with significant heritabilities during 2B (right PC, right dlPFC and PCC and MFC) had ICCs of 0.45, 0.47, 0.28 and 0.28 respectively. It is important to note that the test-retest reliability places an upper bound on the measure of heritability. Test-retest reliability gives an estimate of our precision in measuring an assumed constant underlying phenotype, and the ICC is conceptually similar to a regression R^2. 1-ICC can be considered as the variance explained by test unreliability (U), with the remainder (1-U) explained by genetic and environmental factors. For none of the metrics is the E variance component substantially greater than U, indicating that the majority of the E component is likely to represent measurement error, rather than unique environmental factors. Conversely, the similarity of the A estimates with (1-U) indicate that the unreliability of the measure restricted the estimate of A, and heritability estimates for the underlying connectivity may increase with a more reliable experimental measure.

A second limitation is that as with previous studies, we have used group-wise masks to restrict the target regions of interest. Whilst this step usually ensures that measures are averaged only over voxels related to the task, for our large sample of 827 subjects, the group-wise connectivity profiles are extensive, reflecting our power to detect small effects. The downside is that averaging over a large region will include voxels not necessarily significantly correlated at the subject level, and may average over functionally distinct regions. Future work could explore how the heritability and reliabilities change with subject-specific masks.

In summary, the interaction of the dlPFC with regions of the WM-network and default mode network shows a weak to moderate genetic influence, but these genetic influences may

also be present during the baseline condition, which should be taken into account in interpreting future task-based genetic-association studies. The significant heritability estimates provide some support for the ongoing practice of using functional connectivity as an endophenotype.

Acknowledgements

We thank the twins and siblings for their participation, Marlene Grace and Ann Eldridge for twin recruitment, Aiman Al Najjar and other radiographers for scanning, Kerrie McAloney and Daniel Park for research support, and staff in the Molecular Epidemiology Laboratory for DNA sample processing and preparation. This study was supported by the National Institute of Child Health and Human Development (R01 HD050735), and the National Health and Medical Research Council (NHMRC 486682, 1009064), Australia. Genotyping was supported by the NHMRC (grant 389875). BS is supported by ANZ Trustees PhD Scholarship in Medical Research. GZ is supported by an ARC Future Fellowship (FT0991634).

References

Ando, J., Ono, Y., Wright, M.J. (2001) Genetic structure of spatial and verbal working memory. Behavior genetics, 31:615-24.

Banich, M.T. (1998) The missing link: the role of interhemispheric interaction in attentional processing. Brain and cognition, 36:128-57.

Behzadi, Y., Restom, K., Liau, J., Liu, T.T. (2007) A component based noise correction method (CompCor) for BOLD and perfusion based fMRI. NeuroImage, 37:90-101.

Bertolino, A., Taurisano, P., Pisciotta, N.M., Blasi, G., Fazio, L., Romano, R., Gelao, B., Lo Bianco, L., Lozupone, M., Di Giorgio, A., Caforio, G., Sambataro, F., Niccoli-Asabella, A., Papp, A., Ursini, G., Sinibaldi, L., Popolizio, T., Sadee, W., Rubini, G. (2010) Genetically determined measures of striatal D2 signaling predict prefrontal activity during working memory performance. PloS one, 5:e9348.

Blokland, G.A., McMahon, K.L., Thompson, P.M., Martin, N.G., de Zubicaray, G.I., Wright, M.J. (2011) Heritability of working memory brain activation. The Journal of neuroscience : the official journal of the Society for Neuroscience, 31:10882-90.

Callicott, J.H., Ramsey, N.F., Tallent, K., Bertolino, A., Knable, M.B., Coppola, R., Goldberg, T., van Gelderen, P., Mattay, V.S., Frank, J.A., Moonen, C.T., Weinberger, D.R. (1998) Functional magnetic resonance imaging brain mapping in psychiatry: methodological issues illustrated in a study of working memory in schizophrenia. Neuropsychopharmacology : official publication of the American College of Neuropsychopharmacology, 18:186-96.

Chafee, M.V., Goldman-Rakic, P.S. (1998) Matching patterns of activity in primate prefrontal area 8a and parietal area 7ip neurons during a spatial working memory task. Journal of neurophysiology, 79:2919-40.

Chiang, M.C., Barysheva, M., Shattuck, D.W., Lee, A.D., Madsen, S.K., Avedissian, C., Klunder, A.D., Toga, A.W., McMahon, K.L., de Zubicaray, G.I., Wright, M.J., Srivastava, A., Balov, N.,

Thompson, P.M. (2009) Genetics of brain fiber architecture and intellectual performance. The Journal of neuroscience : the official journal of the Society for Neuroscience, 29:2212-24.
Cole, M.W., Schneider, W. (2007) The cognitive control network: Integrated cortical regions with dissociable functions. NeuroImage, 37:343-60.
de Frias, C.M., Marklund, P., Eriksson, E., Larsson, A., Oman, L., Annerbrink, K., Backman, L., Nilsson, L.G., Nyberg, L. (2010) Influence of COMT gene polymorphism on fMRI-assessed sustained and transient activity during a working memory task. Journal of cognitive neuroscience, 22:1614-22.
de Zubicaray, G.I., Chiang, M.C., McMahon, K.L., Shattuck, D.W., Toga, A.W., Martin, N.G., Wright, M.J., Thompson, P.M. (2008) Meeting the Challenges of Neuroimaging Genetics. Brain imaging and behavior, 2:258-263.
Deserno, L., Sterzer, P., Wustenberg, T., Heinz, A., Schlagenhauf, F. (2012) Reduced prefrontal-parietal effective connectivity and working memory deficits in schizophrenia. The Journal of neuroscience : the official journal of the Society for Neuroscience, 32:12-20.
Donohoe, G., Morris, D.W., Clarke, S., McGhee, K.A., Schwaiger, S., Nangle, J.M., Garavan, H., Robertson, I.H., Gill, M., Corvin, A. (2007) Variance in neurocognitive performance is associated with dysbindin-1 in schizophrenia: a preliminary study. Neuropsychologia, 45:454-8.
Dosenbach, N.U., Visscher, K.M., Palmer, E.D., Miezin, F.M., Wenger, K.K., Kang, H.C., Burgund, E.D., Grimes, A.L., Schlaggar, B.L., Petersen, S.E. (2006) A core system for the implementation of task sets. Neuron, 50:799-812.
Esslinger, C., Kirsch, P., Haddad, L., Mier, D., Sauer, C., Erk, S., Schnell, K., Arnold, C., Witt, S.H., Rietschel, M., Cichon, S., Walter, H., Meyer-Lindenberg, A. (2011) Cognitive state and connectivity effects of the genome-wide significant psychosis variant in ZNF804A. NeuroImage, 54:2514-23.
Esslinger, C., Walter, H., Kirsch, P., Erk, S., Schnell, K., Arnold, C., Haddad, L., Mier, D., Opitz von Boberfeld, C., Raab, K., Witt, S.H., Rietschel, M., Cichon, S., Meyer-Lindenberg, A. (2009) Neural mechanisms of a genome-wide supported psychosis variant. Science, 324:605.
Fornito, A., Zalesky, A., Bassett, D.S., Meunier, D., Ellison-Wright, I., Yucel, M., Wood, S.J., Shaw, K., O'Connor, J., Nertney, D., Mowry, B.J., Pantelis, C., Bullmore, E.T. (2011) Genetic influences on cost-efficient organization of human cortical functional networks. The Journal of neuroscience : the official journal of the Society for Neuroscience, 31:3261-70.
Fox, M.D., Snyder, A.Z., Vincent, J.L., Corbetta, M., Van Essen, D.C., Raichle, M.E. (2005) The human brain is intrinsically organized into dynamic, anticorrelated functional networks. Proceedings of the National Academy of Sciences of the United States of America, 102:9673-8.
Friston, K.J. (2011) Functional and effective connectivity: a review. Brain connectivity, 1:13-36.
Fuster, J.M. (2009) Cortex and memory: emergence of a new paradigm. Journal of cognitive neuroscience, 21:2047-72.
Gazzaley, A., Rissman, J., D'Esposito, M. (2004) Functional connectivity during working memory maintenance. Cognitive, affective & behavioral neuroscience, 4:580-99.
Gazzaniga, M.S. (2000) Cerebral specialization and interhemispheric communication: does the corpus callosum enable the human condition? Brain : a journal of neurology, 123 (Pt 7):1293-326.
Glahn, D.C., Winkler, A.M., Kochunov, P., Almasy, L., Duggirala, R., Carless, M.A., Curran, J.C., Olvera, R.L., Laird, A.R., Smith, S.M., Beckmann, C.F., Fox, P.T., Blangero, J. (2010) Genetic control over the resting brain. Proceedings of the National Academy of Sciences of the United States of America, 107:1223-8.

Goldberg, T.E., Egan, M.F., Gscheidle, T., Coppola, R., Weickert, T., Kolachana, B.S., Goldman, D., Weinberger, D.R. (2003) Executive subprocesses in working memory: relationship to catechol-O-methyltransferase Val158Met genotype and schizophrenia. Archives of general psychiatry, 60:889-96.

Goldman-Rakic, P.S. (1998) The cortical dopamine system: role in memory and cognition. Advances in pharmacology (San Diego, Calif.), 42:707.

Hampson, M., Driesen, N., Roth, J.K., Gore, J.C., Constable, R.T. (2010) Functional connectivity between task-positive and task-negative brain areas and its relation to working memory performance. Magnetic resonance imaging, 28:1051-7.

Hampson, M., Driesen, N.R., Skudlarski, P., Gore, J.C., Constable, R.T. (2006a) Brain connectivity related to working memory performance. The Journal of neuroscience : the official journal of the Society for Neuroscience, 26:13338-43.

Hampson, M., Tokoglu, F., Sun, Z., Schafer, R.J., Skudlarski, P., Gore, J.C., Constable, R.T. (2006b) Connectivity-behavior analysis reveals that functional connectivity between left BA39 and Broca's area varies with reading ability. NeuroImage, 31:513-9.

He, B.J., Snyder, A.Z., Vincent, J.L., Epstein, A., Shulman, G.L., Corbetta, M. (2007) Breakdown of functional connectivity in frontoparietal networks underlies behavioral deficits in spatial neglect. Neuron, 53:905-18.

Honey, C.J., Sporns, O., Cammoun, L., Gigandet, X., Thiran, J.P., Meuli, R., Hagmann, P. (2009) Predicting human resting-state functional connectivity from structural connectivity. Proceedings of the National Academy of Sciences of the United States of America, 106:2035-40.

Karlsgodt, K.H., Kochunov, P., Winkler, A.M., Laird, A.R., Almasy, L., Duggirala, R., Olvera, R.L., Fox, P.T., Blangero, J., Glahn, D.C. (2010) A multimodal assessment of the genetic control over working memory. The Journal of neuroscience : the official journal of the Society for Neuroscience, 30:8197-202.

Kelly, A.M., Uddin, L.Q., Biswal, B.B., Castellanos, F.X., Milham, M.P. (2008) Competition between functional brain networks mediates behavioral variability. NeuroImage, 39:527-37.

Koshino, H., Carpenter, P.A., Minshew, N.J., Cherkassky, V.L., Keller, T.A., Just, M.A. (2005) Functional connectivity in an fMRI working memory task in high-functioning autism. NeuroImage, 24:810-21.

Meyer-Lindenberg, A.S., Olsen, R.K., Kohn, P.D., Brown, T., Egan, M.F., Weinberger, D.R., Berman, K.F. (2005) Regionally specific disturbance of dorsolateral prefrontal-hippocampal functional connectivity in schizophrenia. Archives of general psychiatry, 62:379-86.

Neale, M., Baker, S., Xie, G., Maes, H. (2002) Mx: Statistical modeling, 6th ed. .

Nyholt, D.R. (2004) A simple correction for multiple testing for single-nucleotide polymorphisms in linkage disequilibrium with each other. American journal of human genetics, 74:765-9.

Owen, A.M., McMillan, K.M., Laird, A.R., Bullmore, E. (2005) N-back working memory paradigm: a meta-analysis of normative functional neuroimaging studies. Human brain mapping, 25:46-59.

Pessoa, L., Gutierrez, E., Bandettini, P., Ungerleider, L. (2002) Neural correlates of visual working memory: fMRI amplitude predicts task performance. Neuron, 35:975-87.

Polderman, T.J.C., Stins, J.F., Posthuma, D., Gosso, M.F., Verhulst, F.C., Boomsma, D.I. (2006) The phenotypic and genotypic relation between working memory speed and capacity. Intelligence, 34:549-560.

Quintana, J., Fuster, J.M. (1999) From perception to action: temporal integrative functions of prefrontal and parietal neurons. Cerebral cortex, 9:213-21.

Raichle, M.E., MacLeod, A.M., Snyder, A.Z., Powers, W.J., Gusnard, D.A., Shulman, G.L. (2001) A default mode of brain function. Proceedings of the National Academy of Sciences of the United States of America, 98:676-82.
Sakai, K., Rowe, J.B., Passingham, R.E. (2002) Active maintenance in prefrontal area 46 creates distractor-resistant memory. Nature neuroscience, 5:479-84.
Schlosser, R.G., Wagner, G., Sauer, H. (2006) Assessing the working memory network: studies with functional magnetic resonance imaging and structural equation modeling. Neuroscience, 139:91-103.
Shulman, G.L., Fiez, J.A., Corbetta, M., Buckner, R.L., Miezin, F.M., Raichle, M.E., Petersen, S.E. (1997) Common Blood Flow Changes across Visual Tasks: II. Decreases in Cerebral Cortex. Journal of cognitive neuroscience, 9:648-63.
Stelzel, C., Basten, U., Montag, C., Reuter, M., Fiebach, C.J. (2009) Effects of dopamine-related gene-gene interactions on working memory component processes. The European journal of neuroscience, 29:1056-63.
Tan, H.Y., Chen, Q., Sust, S., Buckholtz, J.W., Meyers, J.D., Egan, M.F., Mattay, V.S., Meyer-Lindenberg, A., Weinberger, D.R., Callicott, J.H. (2007) Epistasis between catechol-O-methyltransferase and type II metabotropic glutamate receptor 3 genes on working memory brain function. Proceedings of the National Academy of Sciences of the United States of America, 104:12536-41.
van den Heuvel, M.P., van Soelen, I.L., Stam, C.J., Kahn, R.S., Boomsma, D.I., Hulshoff Pol, H.E. (2013) Genetic control of functional brain network efficiency in children. European neuropsychopharmacology : the journal of the European College of Neuropsychopharmacology, 23:19-23.
Van Dijk, K.R., Sabuncu, M.R., Buckner, R.L. (2012) The influence of head motion on intrinsic functional connectivity MRI. NeuroImage, 59:431-8.
Whitfield-Gabrieli, S., Nieto-Castanon, A. (2012) Conn: a functional connectivity toolbox for correlated and anticorrelated brain networks. Brain connectivity, 2:125-41.
Woodward, N.D., Waldie, B., Rogers, B., Tibbo, P., Seres, P., Purdon, S.E. (2009) Abnormal prefrontal cortical activity and connectivity during response selection in first episode psychosis, chronic schizophrenia, and unaffected siblings of individuals with schizophrenia. Schizophr Res, 109:182-90.
Zanto, T.P., Rubens, M.T., Thangavel, A., Gazzaley, A. (2011) Causal role of the prefrontal cortex in top-down modulation of visual processing and working memory. Nature neuroscience, 14:656-61.

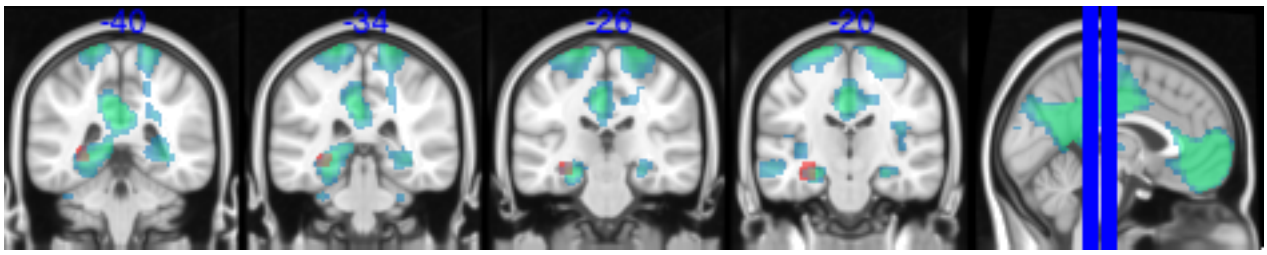

Figure S4.1: WFU Pick Atlas segmentation of the left hippocampus (red), overlaid on negative functional connectivity during 2B condition (blue-green). Segmentation does not overlap well with peak connectivity.

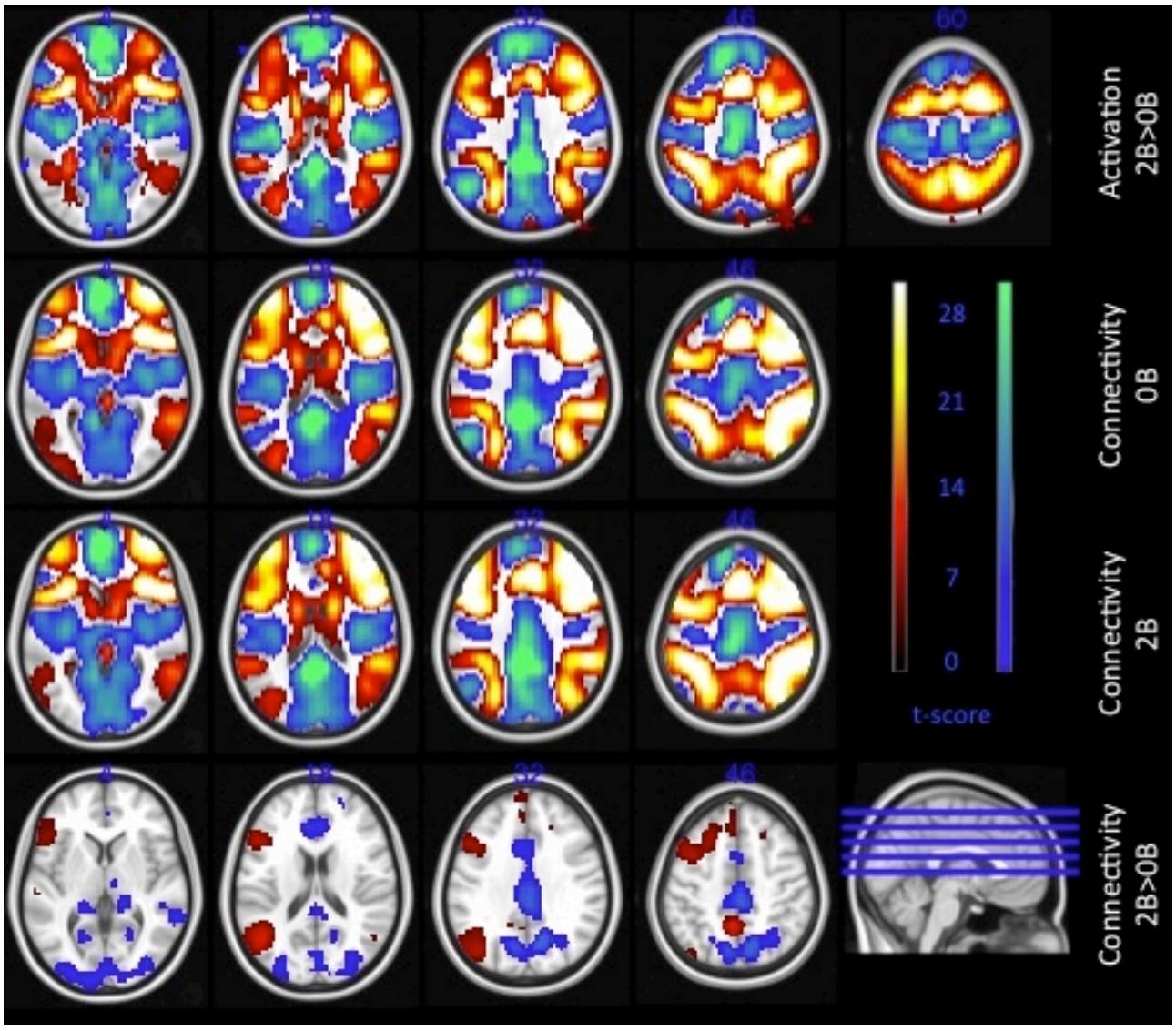

Figure S4.2: Using a Hanning filter to avoid interference between task conditions yields nearly identical correlation maps to Figure 2.

Table S4.1: Means, twin correlations and genetic modeling for functional connectivity with the right dorsolateral prefrontal cortex, averaged over regions of interest. Hanning filter used to partition conditions.

Region	Mean (SD)	Twin Correlations (95% CIs)		Aikike's Information Criterion				ACE estimates from best fitting model, expressed as % (95% CIs)		
	827 subjects	MZ (134 pairs)	DZ (165 pairs)	ACE	AE	CE	E	A	C	E
0B										
right PC	0.25(0.13)	0.19 (0.05,0.31)	0.01 (-0.10,0.12)	679.69	**677.69**	681.01	683.43	23(7,37)	-	77(63,93)
left dlPFC	0.21(0.13)	0.14 (0.00,0.27)	0.02 (-0.09,0.13)	662.95	**660.95**	662.28	663.36	16(1,30)	-	84(70,99)
left hippocampus	-0.09(0.12)	0.03 (-0.11,0.16)	0.05 (-0.06,0.16)	627.24	625.55	625.24	**624.30**	-	-	100(100,100)
PCC	-0.14(0.12)	0.13 (-0.01,0.26)	0.05 (-0.06,0.16)	604.06	**602.06**	602.84	605.65	19(3,33)	-	81(67,97)
MFC	-0.17(0.13)	0.22 (0.08,0.34)	0.08 (-0.03,0.18)	647.18	**645.18**	648.08	655.32	27(12,41)*	-	73(59,88)
2B										
right PC	0.24(0.14)	0.15 (0.01,0.27)	0.08 (-0.03,0.19)	645.81	**643.82**	644.60	649.85	22(7,36)	-	78(64,93)
left dlPFC	0.22(0.12)	0.30 (0.17,0.42)	0.16 (0.05,0.27)	622.16	**620.79**	621.28	646.55	36(24,48)*	-	64(52,76)
left hippocampus	-0.09(0.13)	0.02 (-0.11,0.16)	-0.01 (-0.12,0.10)	602.65	600.65	600.71	**598.72**	-	-	100(100,100)
PCC	-0.16(0.13)	0.24 (0.11,0.36)	0.11 (0.00,0.22)	550.80	**548.80**	553.99	568.76	38(23,51)*	-	62(49,77)
MFC	-0.16(0.13)	0.21 (0.07,0.33)	0.06 (-0.05,0.17)	631.94	**629.94**	633.99	640.62	28(13,42)*	-	72(58,87)
2B-0B										
right PC	-0.06(0.13)	0.13 (-0.01,0.26)	-0.06 (-0.17,0.05)	678.41	676.41	677.41	**675.54**	-	-	100(100,100)
left dlPFC	0.05(0.13)	0.07 (-0.06,0.21)	0.02 (-0.09,0.13)	662.92	660.92	661.18	**660.66**	-	-	100(100,100)
left hippocampus	-0.05(0.20)	-0.06 (-0.19,0.08)	-0.08 (-0.19,0.03)	694.40	692.40	692.40	**690.40**	-	-	100(100,100)
PCC	-0.07(0.15)	0.00 (-0.13,0.14)	0.02 (-0.09,0.13)	690.53	688.55	688.53	**686.56**	-	-	100(100,100)
MFC	0.05(0.15)	0.08 (-0.06,0.21)	0.03 (-0.08,0.14)	666.48	664.48	664.66	**664.16**	-	-	100(100,100)

* Exceeds multiple comparisons threshold for 5% Type I error rate.
Best fitting genetic model indicated in bold font.

Table S4.2: Test-retest reliabilities with Hanning filter implemented.

Region	Intra Class Correlation		
	0B	**2B**	**2B-0B**
right PC	0.16 (-0.12,0.42)	0.44 (0.18,0.64)	0.24 (-0.05,0.48)
left dlPFC	0.40 (0.13,0.61)	0.47 (0.22,0.67)	0.11 (-0.18,0.38)
left hippocampus	0.01 (-0.27,0.29)	0.01 (-0.27,0.29)	-0.34 (-0.56,-0.06)
PCC	0.47 (0.22,0.67)	0.25 (-0.04,0.50)	0.19 (-0.10,0.44)
MFC	0.37 (0.10,0.59)	0.22 (-0.06,0.48)	0.06 (-0.22,0.33)

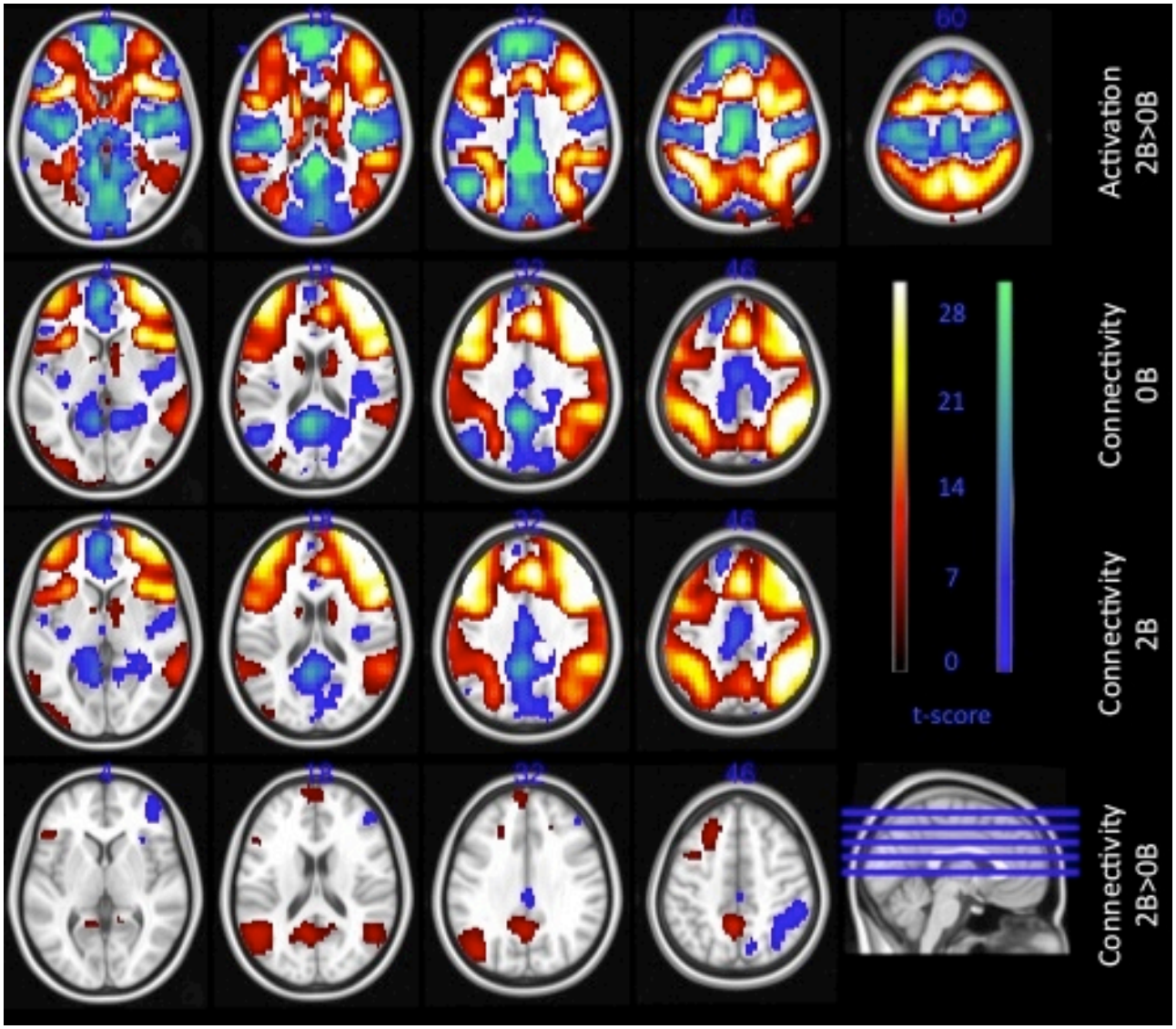

Figure S4.3: Group wise activation (top panel), and connectivity profiles with dlPFC seed (bottom three panels), with task related variance regressed out. With task related variance regressed out, the pattern of correlations during 0B and 2B remain very similar to those observed in Figure 2 (without task regression), demonstrating that condition specific correlations are not the result of common activation in response to task. The change in functional connectivity (bottom panel) has some differences to Figure 2. The connectivity with the posterior cingulate cortex goes from negative to less negative, and the connectivity with the right parietal cortex goes from positive to less positive. This pattern is unexpected and may be an introduced artifact by the task regression.

Table S4.3: Means, twin correlations and genetic modeling for functional connectivity with the right dorsolateral prefrontal cortex, averaged over regions of interest. Task-related variance regressed out.

Region	Mean (SD)	Twin Correlations (95% CIs)		Aikike's Information Criterion				ACE estimates from best fitting model, expressed as % (95% CIs)		
	827 subjects	MZ (134 pairs)	DZ (165 pairs)	ACE	AE	CE	E	A	C	E
0B										
right PC	0.15(0.09)	0.12 (-0.02,0.25)	0.03 (-0.08,0.14)	657.98	**655.98**	657.02	657.84	16(0,32)	-	84(68,100)
left dlPFC	0.14(0.10)	0.17 (0.04,0.30)	0.06 (-0.06,0.16)	653.51	**651.51**	652.88	657.73	22(7,35)	-	78(65,93)
left hippocampus	-0.05(0.10)	-0.00 (-0.14,0.13)	-0.04 (-0.15,0.07)	645.91	643.91	643.91	**641.91**	-	-	100(100,100)
PCC	-0.07(0.09)	0.10 (-0.03,0.23)	0.03 (-0.08,0.14)	601.79	**599.79**	600.67	601.00	15(0,31)	-	85(69,100)
MFC	-0.08(0.09)	0.06 (-0.08,0.19)	0.09 (-0.02,0.20)	687.83	686.80	**685.83**	687.26	-	11(0,22)	89(78,100)
2B										
right PC	0.13(0.09)	0.19 (0.05,0.31)	0.11 (-0.00,0.21)	582.79	**581.12**	581.20	591.78	27(12,40)*	-	73(60,88)
left dlPFC	0.14(0.10)	0.27 (0.14,0.39)	0.16 (0.05,0.27)	602.57	**600.93**	602.32	625.49	39(25,51)*	-	61(49,75)
left hippocampus	-0.04(0.11)	0.01 (-0.13,0.14)	-0.04 (-0.15,0.07)	606.22	604.22	604.22	**602.22**	-	-	100(100,100)
PCC	-0.06(0.10)	0.13 (-0.00,0.26)	0.04 (-0.07,0.15)	514.65	**512.65**	514.39	516.59	21(4,36)	-	79(64,96)
MFC	-0.07(0.09)	0.02 (-0.12,0.15)	0.06 (-0.05,0.17)	676.35	674.77	674.35	**673.29**	-	-	100(100,100)
2B-0B										
right PC	-0.04(0.12)	0.04 (-0.09,0.18)	-0.03 (-0.14,0.08)	698.90	696.90	696.95	**694.95**	-	-	100(100,100)
left dlPFC	0.04(0.15)	-0.05 (-0.19,0.08)	-0.04 (-0.15,0.07)	693.90	691.85	691.85	**689.85**	-	-	100(100,100)
left hippocampus	NE[a]	-	-	-	-	-	**-**	-	-	-
PCC	0.05(0.13)	0.02 (-0.12,0.15)	0.03 (-0.08,0.14)	681.22	679.29	679.22	**677.46**	-	-	100(100,100)
MFC	0.04(0.12)	0.03 (-0.10,0.17)	-0.02 (-0.13,0.10)	699.78	697.78	697.87	**695.90**	-	-	100(100,100)

[a] NE: not estimable, no group-wise significant correlations in relevant group-wise connectivity profile.
* Exceeds multiple comparisons threshold for 5% Type I error rate.
Best fitting genetic model indicated in bold font.

Table S4.4: Test retest reliabilities for the mean functional connectivity with the right dorsolateral prefrontal cortex over each region, for each condition, quantified as the intra-class correlation between session 1 and session 2, with task related variance regressed out. Test retest reliabilities are substantially lower than those in Table 4.2.

Region	Intra Class Correlation		
	0B	**2B**	**2B-0B**
right PC	0.00 (-0.28,0.28)	0.25 (-0.03,0.50)	-0.10 (-0.37,0.18)
left dlPFC	0.22 (-0.07,0.48)	0.13 (-0.16,0.40)	-0.01 (-0.29,0.27)
left hippocampus	-0.24 (-0.49,0.04)	-0.38 (-0.60,-0.11)	NE[a]
PCC	0.26 (-0.02,0.50)	0.05 (-0.24,0.33)	0.35 (0.08,0.58)
MFC	0.21 (-0.07,0.47)	-0.09 (-0.36,0.20)	0.04 (-0.24,0.32)

[a] NE: not estimable, no group-wise significant correlations in relevant group-wise connectivity profile.

5 Chapter 5: Discussion

5.1 Summary of results

In this thesis, I estimated the heritability of a variety of measures of brain functional connectivity, in order to assess their suitability as imaging endophenotypes. This was carried out using the largest MRI study of twins to date. The phenotypes chosen were selected on the basis of their prior association with psychiatric disorder, cognitive function, or genetic association studies indicating a genetic influence.

The most heritable phenotypes were the graph theory measures on resting state analysis, all graph measures considered bar one showed moderate to high heritability, (h^2=0.4-0.6). However, these findings were crucially dependent on whether or not global signal was regressed out, with heritability estimates much lower (yet still significant for some measures) with global signal removed (h^2=0.0-0.3). Resting state fMRI and functional connectivity measures are particularly susceptible to confounds, and a number of additional pre-processing steps must be taken as compared to task-activation fMRI, in order to remove the influence of motion (Van Dijk et al., 2012), and physiological artefacts (Van Dijk et al., 2010; Birn, 2012). By far the most contentious pre-processing step is the removal of global signal, with some researchers arguing that it represents an artifactual shared source of variance between different voxels (Zarahn et al., 1997; Fox et al., 2009), whilst others arguing that global signal regression introduces artificial correlational structures in the data (Murphy et al., 2009; Weissenbacher et al., 2009). Whilst the well-publicized anti-correlation between the task-positive network and default mode network (Fox et al., 2005) seems to be a generalized feature, not restricted to global-signal adjusted data (Fox et al., 2009, Hampson et al., 2010; Chai et al., 2012), the ground truth of other observed correlational structures after global signal regression has not been established. Furthermore, other work indicates that the global signal has neuronal contributions (Schölvinck et al., 2010), and is even related to psychiatric disorder (Hahamy et al., 2014). The results of this thesis may be interpreted as supporting either side of the debate. That the global signal has its own genetic influences increases its interpretability as a biologically meaningful phenotype. However, physiological confounds (head motion; Couvy-Duchesne et al., 2014, haemodynamic response function,

Shan et al., in preparation) are also heritable but this does not mean that they have meaning in terms of neuronal processing.

The phenotypes relating to connectivity during working memory were less heritable. Functional connectivity through time-series correlation yielded low estimates of connectivity with the (right PC: h^2=24%, left dlPFC: h^2=36%, PCC: h^2=37%, MFC: h^2=26%). These heritability estimates are more similar to those of resting-state graph measures with global signal removed.

Test-retest reliabilities for functional connectivity were low (ICCs≤0.51). On the one hand, since the test-retest reliability places an upper bound on the heritability, and should methodologies develop which increase the reliability of the measures and reduce measurement error, one can expect higher heritability estimates to emerge. On the other hand, such low heritabilities preclude the use of these measures as useful biomarkers, and emphasizes that more work needs to be done on improving the stability our measures of connectivity, before they can be considered disease biomarkers or used in genetic association studies.

The second study in this thesis uses dynamic causal modelling to probe functional connectivity during working memory. We found no evidence of heritability of fronto-parietal effective connectivity, and found that the connectivity parameters had low test-retest reliability. Dynamic causal modelling is an altogether more sophisticated methodology for measuring neuronal coupling, which explicitly models underlying neuronal activity and haemodynamics, which may free us from confounds associated with basing our inferences solely on the convoluted BOLD signal. One may speculate that this approach should yield more reliable and heritable phenotypes than those derived directly from the BOLD signal. Indeed this was one motivation for considering DCM, aside from its current prevalence in the neuroimaging community. However, I did not find higher reliability or heritability using DCM to characterise connectivity, as compared to using the more basic measure of Pearson's correlation between time series. This was in no way a systematic comparison of the two methods, nor a assessment of the validity of DCM, of which much has been written (Friston et al., 2003; Daunizeau et al., 2011; Lohmann et al., 2012; Friston et al., 2013).

Taken together, Chapters 3 and 4 suggest a low heritability of task-dependent modulation in functional connectivity. This is surprising given prior genetic association of individual variants with task-dependent functional connectivity (Pezawas et al., 2005; Heinz et al., 2005; Tan et al., 2007; Esslinger et al., 2011). In the case of Chapter 3, the null result may be due to the inadequate model space or sub-optimal experimental design. In the case of Chapter 3, a simplistic subtraction of functional connectivity between conditions is informative but not the ideal modelling procedure, superior alternatives exist such as psychophysiological interactions (Friston et al., 1997) and dynamic causal modelling (Friston et al., 2003). However, it is important to note that although (Pezawas et al., 2005; Heinz et al., 2005; Tan et al., 2007; Esslinger et al., 2011) used data acquired during task performance, they did not model task-dependent modulations. Their functional connectivity measurements were Pearson's correlations of time series across both during task and baseline conditions (Pezawas et al., 2005; Heinz et al., 2005; Esslinger et al., 2011), or during task conditions alone (Tan et al., 2007). Consistent with these observations, functional connectivity within single task conditions was shown to be heritable in Chapter 4. Chapters 3 and 4 have important implications for the prior candidate SNP studies of functional connectivity, where it is not clear whether the genetic effect pertained to the task, or simply to intrinsic connectivity between regions, which is known to be under strong genetic influence (Glahn et al., 2010; Fornito et al., 2011). Esslinger et al. (2011) demonstrated that the effect of the rs1344706 single nucleotide polymorphism in ZNF804A on inter-hemispheric dlPFC connectivity was indeed present at rest, but the effect on dlPFC-hippocampal connectivity was specific to WM. However, it was not clear whether this effect was specific to the maintenance and manipulation components of WM (2B condition), or more basic attentional and coding components during the baseline (0B condition).

This thesis provides both biological and technical contributions to the field of endophenotyping. On the biological side, I have established the heritability of graph measures and to a lesser extent of WM-related functional connectivity, which would suggest their suitability as imaging endophenotypes, and may indicate that they are on the etiological pathway from genes to disease (see future directions section for elaboration). However, these results are tempered by the low reliability observed, an issue which is often overlooked in neuroimaging genetic studies. On the technical side, I have demonstrated the sensitivity of heritability estimates to certain methodological choices, in particular the use of global signal

regression for resting state fMRI, and the importance of comparison to baseline in task-based fMRI.

In their paper "Endophenotypes for Psychiatric Disorders: Ready for Primetime?" Bearden and Freimer (2006) discuss the urgent need for quantitative and heritable intermediate phenotypes to complement if not eventually replace imprecise categorical psychiatric diagnosis. Meyer-Lindenberg (2009) put forward neural connectivity as a promising candidate for such endophenotypes with the justification that "features of connectivity often better account for behavioural effects of genetic variation than regional parameters of activation or structure". The results of this thesis suggest that the functional connectivity biomarkers considered here may not be particularly promising endophenotypes. Despite observing significant heritability for a number of measures, the heritability estimates are lower than those seen for brain structural features (Thompson et al., 2001; Peper et al., 2007) and white matter integrity (Chiang et al., 2009; Karlsgodt et al., 2010). The reliability of the biomarkers was also low. Thus, until functional connectivity measures are found which demonstrate both high heritability and acceptable reliability, they will not be ready for primetime.

5.2 Future directions

The aim of this thesis was to assess the viability of brain functional connectivity as an endophenotype, such that these features could then be used as imaging biomarkers, or to further investigate the genetic basis of brain network development. The most heritable phenotypes were the graph measures: mean clustering coefficient (γ), modularity (Q), global efficiency (λ) and small-world coefficient (σ), applied to resting state data, with the stipulation that global signal regression is not implemented. The next most heritable measures were inter-hemispheric dlPFC, and dlPFC-PCC functional connectivity during working memory. It would thus follow that these phenotypes are the most appropriate to be taken forward to genetic association studies, either via genome–wise association studies, or candidate gene studies. Identification of genome-wide significant SNPs would be a significant step in elucidating factors influencing the development of brain-wide integrated networks. Regarding the endophenotype concept, future genetic association studies targeting disease risk alleles, and multivariate genetic modelling of disease and endophenotype would elucidate whether these connectivity phenotypes are indeed on the pathway from genes to disease.

A couple of hypotheses have arisen throughout the course of this thesis which warrant testing. The large difference in heritability of graph measures seen with and without GSR raise the question whether global signal itself is heritable. Although global signal is a time-series, the heritability of which is not immediately measurable as a univariate statistic, a couple of studies have attempted to condense the global signal time series into a single quantitative phenotype. Fox et al. (2009) consider the variance of the global signal time series to investigate whether it can be explained in terms of the addition of the activity of various cortical subsystems, or whether it contains a separate contribution in addition to contributions from the main functional subsystems. Hampson et al. (2010) calculate a summary statistic of the global signal to use as a regressor at the group level as an alternative to global signal regression. Their measure is the mean voxel-wise correlation. With global signal removed, inter-voxel correlation is mean-centred at zero, and thus the positive bias in correlation values can be considered as directly measuring the magnitude of the effect of global signal.

The second hypothesis that has arisen is whether whole brain network measures show greater genetic penetrance than individual pairwise inter-regional connections. Contrasting the resting state study to the two working memory studies would suggest that the effects of genes are more apparent at the whole brain network level that the inter-regional connectivity level. However, the methodologies and experimental paradigms were non-comparable between the studies. Thus to test this hypothesis, the heritability of the graph measures could be compared to the heritability of individual connections measured during resting state with the same processing methodology used in chapter two. These pairwise connections were measured as an intermediate step in calculating the graph measures, so they are readily available for such analysis.

Regarding the pairwise connectivity phenotypes considered in chapters 3 and 4, sufficient heritability and reliability have not been established to pursue genetic-association studies. Future work should be focused on improving the reliability and validity of the phenotypes. One of the limitations of the DCM study was the simplicity of the models used, motivated in part by computational expense considerations within the time-limits of a PhD thesis, and also to reproduce the phenotypes of Deserno et al. (2012). Since this study was conducted, a number of other DCM studies have been published with different regions of interest. These

models may be tested on our data to see whether higher heritability and reliability emerge. In particular, the DCM study of Harding et al. (2014) use a large model space of 5 fronto-parietal network nodes and systematically test 4096 different model structures, giving greater generalizability and less sensitivity to subtle effects of individual models. They observe no modulation of dlPFC-PC connectivity with WM load, but rather find that the dorsal anterior cingulate cortex (ACC)/pre supplementary motor areas has WM load dependent connectivity with the rest of the fronto-parietal network. Although this was a verbal N-Back task, as compared to out numeric spatial N-Back task, and results may not generalise, we do see substantial activation of the anterior cingulate cortex in our data set, and DCM models including the ACC may show more promise as endophenotypes than the models considered in this thesis.

6 Bibliography

Abbott, L.F., Varela, J.A., Sen, K., Nelson, S.B. (1997) Synaptic depression and cortical gain control. Science, 275:220-4.

Achard, S., Salvador, R., Whitcher, B., Suckling, J., Bullmore, E. (2006) A resilient, low-frequency, small-world human brain functional network with highly connected association cortical hubs. The Journal of neuroscience : the official journal of the Society for Neuroscience, 26:63-72.

Alexander-Bloch, A.F., Gogtay, N., Meunier, D., Birn, R., Clasen, L., Lalonde, F., Lenroot, R., Giedd, J., Bullmore, E.T. (2010) Disrupted modularity and local connectivity of brain functional networks in childhood-onset schizophrenia. Frontiers in systems neuroscience, 4:147.

Anand, A., Li, Y., Wang, Y., Wu, J., Gao, S., Bukhari, L., Mathews, V.P., Kalnin, A., Lowe, M.J. (2005) Activity and connectivity of brain mood regulating circuit in depression: a functional magnetic resonance study. Biological psychiatry, 57:1079-88.

Ando, J., Ono, Y., Wright, M.J. (2001) Genetic structure of spatial and verbal working memory. Behavior genetics, 31:615-24.

Arfanakis, K., Cordes, D., Haughton, V.M., Moritz, C.H., Quigley, M.A., Meyerand, M.E. (2000) Combining independent component analysis and correlation analysis to probe interregional connectivity in fMRI task activation datasets. Magnetic resonance imaging, 18:921-30.

Arieli, A., Sterkin, A., Grinvald, A., Aertsen, A. (1996) Dynamics of ongoing activity: explanation of the large variability in evoked cortical responses. Science, 273:1868-71.

Atkinson, R.C., Shiffrin, R.M. (1968) Human memory: A proposed system and its control processes. Psychology of learning and motivation, 2:89-195.

Awh, E., Vogel, E.K., Oh, S.H. (2006) Interactions between attention and working memory. Neuroscience, 139:201-8.

Baddeley, A. (2000) The episodic buffer: a new component of working memory? Trends in cognitive sciences, 4:417-423.

Baddeley, A.D., Hitch, G. (1974) Working memory. Psychology of learning and motivation, 8:47-89.

Baldo, J.V., Shimamura, A.P. (2002) Frontal lobes and memory. The handbook of memory disorders, 2:363-379.

Barak, O., Tsodyks, M., Romo, R. (2010) Neuronal population coding of parametric working memory. The Journal of neuroscience : the official journal of the Society for Neuroscience, 30:9424-30.

Barch, D.M., Carter, C.S., Braver, T.S., Sabb, F.W., MacDonald, A., 3rd, Noll, D.C., Cohen, J.D. (2001) Selective deficits in prefrontal cortex function in medication-naive patients with schizophrenia. Archives of general psychiatry, 58:280-8.

Bassett, D.S., Bullmore, E.T., Meyer-Lindenberg, A., Apud, J.A., Weinberger, D.R., Coppola, R. (2009) Cognitive fitness of cost-efficient brain functional networks. Proceedings of the National Academy of Sciences of the United States of America, 106:11747-52.

Bearden, C.E., Freimer, N.B. (2006) Endophenotypes for psychiatric disorders: ready for primetime? Trends in genetics : TIG, 22:306-13.

Beckmann, C.F., DeLuca, M., Devlin, J.T., Smith, S.M. (2005) Investigations into resting-state connectivity using independent component analysis. Philosophical transactions of the Royal Society of London. Series B, Biological sciences, 360:1001-13.

Birn, R.M. (2012) The role of physiological noise in resting-state functional connectivity. NeuroImage, 62:864-870.

Biswal, B., Yetkin, F.Z., Haughton, V.M., Hyde, J.S. (1995) Functional connectivity in the motor cortex of resting human brain using echo-planar MRI. Magnetic resonance in medicine : official journal of the Society of Magnetic Resonance in Medicine / Society of Magnetic Resonance in Medicine, 34:537-41.

Blokland, G.A., McMahon, K.L., Thompson, P.M., Martin, N.G., de Zubicaray, G.I., Wright, M.J. (2011) Heritability of working memory brain activation. The Journal of neuroscience : the official journal of the Society for Neuroscience, 31:10882-90.

Bluhm, R.L., Miller, J., Lanius, R.A., Osuch, E.A., Boksman, K., Neufeld, R.W., Theberge, J., Schaefer, B., Williamson, P. (2007) Spontaneous low-frequency fluctuations in the BOLD signal in schizophrenic patients: anomalies in the default network. Schizophrenia bulletin, 33:1004-12.

Boos, H.B.M., Aleman, A., Cahn, W., Pol, H.H., Kahn, R.S. (2007) Brain volumes in relatives of patients with schizophrenia: a meta-analysis. Archives of general psychiatry, 64:297-304.

Bor, D., Duncan, J., Wiseman, R.J., Owen, A.M. (2003) Encoding strategies dissociate prefrontal activity from working memory demand. Neuron, 37:361-7.

Braskie, M.N., Jahanshad, N., Stein, J.L., Barysheva, M., McMahon, K.L., de Zubicaray, G.I., Martin, N.G., Wright, M.J., Ringman, J.M., Toga, A.W., Thompson, P.M. (2011) Common Alzheimer's disease risk variant within the CLU gene affects white matter microstructure in young adults. The Journal of neuroscience : the official journal of the Society for Neuroscience, 31:6764-70.

Breakspear, M., Terry, J.R., Friston, K.J. (2003) Modulation of excitatory synaptic coupling facilitates synchronization and complex dynamics in a biophysical model of neuronal dynamics. Network, 14:703-32.

Bressler, S.L., McIntosh, A.R. (2007) The role of neural context in large-scale neurocognitive network operations. Handbook of brain connectivity: Springer. p 403-419.

Bressler, S.L., Menon, V. (2010) Large-scale brain networks in cognition: emerging methods and principles. Trends in cognitive sciences, 14:277-90.

Brozoski, T.J., Brown, R.M., Rosvold, H.E., Goldman, P.S. (1979) Cognitive deficit caused by regional depletion of dopamine in prefrontal cortex of rhesus monkey. Science, 205:929-32.

Buckner, R.L., Sepulcre, J., Talukdar, T., Krienen, F.M., Liu, H., Hedden, T., Andrews-Hanna, J.R., Sperling, R.A., Johnson, K.A. (2009) Cortical hubs revealed by intrinsic functional connectivity: mapping, assessment of stability, and relation to Alzheimer's disease. The Journal of neuroscience : the official journal of the Society for Neuroscience, 29:1860-73.

Bullmore, E., Sporns, O. (2012) The economy of brain network organization. Nature reviews. Neuroscience, 13:336-49.

Buxton, R.B., Wong, E.C., Frank, L.R. (1998) Dynamics of blood flow and oxygenation changes during brain activation: the balloon model. Magnetic resonance in medicine : official journal of the Society of Magnetic Resonance in Medicine / Society of Magnetic Resonance in Medicine, 39:855-64.

Cabeza, R., Nyberg, L. (2000) Imaging cognition II: An empirical review of 275 PET and fMRI studies. Journal of cognitive neuroscience, 12:1-47.

Callicott, J.H., Egan, M.F., Mattay, V.S., Bertolino, A., Bone, A.D., Verchinksi, B., Weinberger, D.R. (2014) Abnormal fMRI response of the dorsolateral prefrontal cortex in cognitively intact siblings of patients with schizophrenia. American Journal of Psychiatry.

Callicott, J.H., Ramsey, N.F., Tallent, K., Bertolino, A., Knable, M.B., Coppola, R., Goldberg, T., van Gelderen, P., Mattay, V.S., Frank, J.A., Moonen, C.T., Weinberger, D.R. (1998) Functional magnetic resonance imaging brain mapping in psychiatry: methodological issues illustrated in a study of working memory in schizophrenia.

Neuropsychopharmacology : official publication of the American College of Neuropsychopharmacology, 18:186-96.
Cardno, A.G., Gottesman, I.I. (2000) Twin studies of schizophrenia: from bow‐and‐arrow concordances to star wars Mx and functional genomics. American journal of medical genetics, 97:12-17.
Carter, C., Robertson, L., Nordahl, T., Chaderjian, M., Kraft, L., O'Shora-Celaya, L. (1996) Spatial working memory deficits and their relationship to negative symptoms in unmedicated schizophrenia patients. Biological psychiatry, 40:930-2.
Carter, C.S., Perlstein, W., Ganguli, R., Brar, J., Mintun, M., Cohen, J.D. (1998) Functional hypofrontality and working memory dysfunction in schizophrenia. The American journal of psychiatry, 155:1285-7.
Castellanos, F.X., Zuo, X.-N., Williams, K., Bangaru, S., Kelly, C., Mennes, M., Fair, D., Biswal, B.B., Wright, M., Martin, N., de Zubicaray, G., McMahon, K., Hickie, I., Milham, M. (Genetic analyses of resting-state studies in adolescent twins: preliminary results). In; 2010; Barcelona, Spain.
Chafee, M.V., Goldman-Rakic, P.S. (1998) Matching patterns of activity in primate prefrontal area 8a and parietal area 7ip neurons during a spatial working memory task. Journal of neurophysiology, 79:2919-40.
Chai, X.J., Castanon, A.N., Ongur, D., Whitfield-Gabrieli, S. (2012) Anticorrelations in resting state networks without global signal regression. NeuroImage, 59:1420-8.
Chang, C., Glover, G.H. (2010) Time-frequency dynamics of resting-state brain connectivity measured with fMRI. NeuroImage, 50:81-98.
Chen, L.S., Rice, T.K., Thompson, P.A., Barch, D.M., Csernansky, J.G. (2009) Familial aggregation of clinical and neurocognitive features in sibling pairs with and without schizophrenia. Schizophr Res, 111:159-66.
Chiang, M.C., Barysheva, M., Shattuck, D.W., Lee, A.D., Madsen, S.K., Avedissian, C., Klunder, A.D., Toga, A.W., McMahon, K.L., de Zubicaray, G.I., Wright, M.J., Srivastava, A., Balov, N., Thompson, P.M. (2009) Genetics of brain fiber architecture and intellectual performance. The Journal of neuroscience : the official journal of the Society for Neuroscience, 29:2212-24.
Chiang, M.C., Barysheva, M., Toga, A.W., Medland, S.E., Hansell, N.K., James, M.R., McMahon, K.L., de Zubicaray, G.I., Martin, N.G., Wright, M.J., Thompson, P.M. (2011) BDNF gene effects on brain circuitry replicated in 455 twins. NeuroImage, 55:448-54.
Chun, M.M. (2011) Visual working memory as visual attention sustained internally over time. Neuropsychologia, 49:1407-9.
Compte, A., Brunel, N., Goldman-Rakic, P.S., Wang, X.J. (2000) Synaptic mechanisms and network dynamics underlying spatial working memory in a cortical network model. Cerebral cortex, 10:910-23.
Corbetta, M., Shulman, G.L., Miezin, F.M., Petersen, S.E. (1995) Superior parietal cortex activation during spatial attention shifts and visual feature conjunction. Science, 270:802-5.
Couvy-Duchesne, B., Blokland, G.A.M., Hickie, I.B., Thompson, P.M., Martin, N.G., de Zubicaray, G.I., McMahon, K.L., Wright, M.J. (2014) Heritability of head motion during resting state functional MRI in 462 healthy twins. NeuroImage, 102:424-434.
Cramer, A.O., Waldorp, L.J., van der Maas, H.L., Borsboom, D. (2010) Comorbidity: a network perspective. The Behavioral and brain sciences, 33:137-50; discussion 150-93.
Curtis, C.E., D'Esposito, M. (2003) Persistent activity in the prefrontal cortex during working memory. Trends in cognitive sciences, 7:415-423.
D'Esposito, M., Aguirre, G.K., Zarahn, E., Ballard, D., Shin, R.K., Lease, J. (1998) Functional MRI studies of spatial and nonspatial working memory. Brain research. Cognitive brain research, 7:1-13.

D'Esposito, M., Postle, B.R. (1999) The dependence of span and delayed-response performance on prefrontal cortex. Neuropsychologia, 37:1303-15.
Damoiseaux, J.S., Rombouts, S.A., Barkhof, F., Scheltens, P., Stam, C.J., Smith, S.M., Beckmann, C.F. (2006) Consistent resting-state networks across healthy subjects. Proceedings of the National Academy of Sciences of the United States of America, 103:13848-53.
Daunizeau, J., David, O., Stephan, K.E. (2011) Dynamic causal modelling: a critical review of the biophysical and statistical foundations. NeuroImage, 58:312-322.
Daunizeau, J., Friston, K.J., Kiebel, S.J. (2009) Variational Bayesian identification and prediction of stochastic nonlinear dynamic causal models. Physica D. Nonlinear phenomena, 238:2089-2118.
Daunizeau, J., Stephan, K.E., Friston, K.J. (2012) Stochastic dynamic causal modelling of fMRI data: should we care about neural noise? NeuroImage, 62:464-81.
de Geus, E.J. (2014) Molecular genetic psychophysiology: a perspective on the Minnesota contribution. Psychophysiology, 51:1203-4.
de Zubicaray, G.I., Chiang, M.C., McMahon, K.L., Shattuck, D.W., Toga, A.W., Martin, N.G., Wright, M.J., Thompson, P.M. (2008) Meeting the Challenges of Neuroimaging Genetics. Brain imaging and behavior, 2:258-263.
Deco, G., Jirsa, V.K., Robinson, P.A., Breakspear, M., Friston, K. (2008) The dynamic brain: from spiking neurons to neural masses and cortical fields. PLoS computational biology, 4:e1000092.
Deserno, L., Sterzer, P., Wustenberg, T., Heinz, A., Schlagenhauf, F. (2012) Reduced prefrontal-parietal effective connectivity and working memory deficits in schizophrenia. The Journal of neuroscience : the official journal of the Society for Neuroscience, 32:12-20.
DiCarlo, J.J., Zoccolan, D., Rust, N.C. (2012) How does the brain solve visual object recognition? Neuron, 73:415-434.
Dima, D., Jogia, J., Frangou, S. (2014) Dynamic causal modeling of load-dependent modulation of effective connectivity within the verbal working memory network. Human brain mapping, 35:3025-35.
Donohoe, G., Morris, D.W., Clarke, S., McGhee, K.A., Schwaiger, S., Nangle, J.M., Garavan, H., Robertson, I.H., Gill, M., Corvin, A. (2007) Variance in neurocognitive performance is associated with dysbindin-1 in schizophrenia: a preliminary study. Neuropsychologia, 45:454-8.
Edin, F., Klingberg, T., Johansson, P., McNab, F., Tegner, J., Compte, A. (2009) Mechanism for top-down control of working memory capacity. Proceedings of the National Academy of Sciences of the United States of America, 106:6802-7.
Ericcson, K.A., Chase, W.G., Faloon, S. (1980) Acquisition of a memory skill. Science, 208:1181-2.
Esslinger, C., Kirsch, P., Haddad, L., Mier, D., Sauer, C., Erk, S., Schnell, K., Arnold, C., Witt, S.H., Rietschel, M., Cichon, S., Walter, H., Meyer-Lindenberg, A. (2011) Cognitive state and connectivity effects of the genome-wide significant psychosis variant in ZNF804A. NeuroImage, 54:2514-23.
Esslinger, C., Walter, H., Kirsch, P., Erk, S., Schnell, K., Arnold, C., Haddad, L., Mier, D., Opitz von Boberfeld, C., Raab, K., Witt, S.H., Rietschel, M., Cichon, S., Meyer-Lindenberg, A. (2009) Neural mechanisms of a genome-wide supported psychosis variant. Science, 324:605.
Evans, D.M., Gillespie, N.A., Martin, N.G. (2002) Biometrical genetics. Biological psychology, 61:33-51.
Fair, D.A., Cohen, A.L., Power, J.D., Dosenbach, N.U., Church, J.A., Miezin, F.M., Schlaggar, B.L., Petersen, S.E. (2009) Functional brain networks develop from a "local to distributed" organization. PLoS computational biology, 5:e1000381.
Felleman, D.J., Van Essen, D.C. (1991) Distributed hierarchical processing in the primate cerebral cortex. Cerebral cortex, 1:1-47.

Filippini, N., MacIntosh, B.J., Hough, M.G., Goodwin, G.M., Frisoni, G.B., Smith, S.M., Matthews, P.M., Beckmann, C.F., Mackay, C.E. (2009) Distinct patterns of brain activity in young carriers of the APOE-epsilon4 allele. Proceedings of the National Academy of Sciences of the United States of America, 106:7209-14.

Fornito, A., Zalesky, A., Bassett, D.S., Meunier, D., Ellison-Wright, I., Yucel, M., Wood, S.J., Shaw, K., O'Connor, J., Nertney, D., Mowry, B.J., Pantelis, C., Bullmore, E.T. (2011) Genetic influences on cost-efficient organization of human cortical functional networks. The Journal of neuroscience : the official journal of the Society for Neuroscience, 31:3261-70.

Fornito, A., Zalesky, A., Pantelis, C., Bullmore, E.T. (2012) Schizophrenia, neuroimaging and connectomics. NeuroImage, 62:2296-314.

Fox, M.D., Raichle, M.E. (2007) Spontaneous fluctuations in brain activity observed with functional magnetic resonance imaging. Nature reviews. Neuroscience, 8:700-11.

Fox, M.D., Snyder, A.Z., Vincent, J.L., Corbetta, M., Van Essen, D.C., Raichle, M.E. (2005) The human brain is intrinsically organized into dynamic, anticorrelated functional networks. Proceedings of the National Academy of Sciences of the United States of America, 102:9673-8.

Fox, M.D., Snyder, A.Z., Zacks, J.M., Raichle, M.E. (2006) Coherent spontaneous activity accounts for trial-to-trial variability in human evoked brain responses. Nature neuroscience, 9:23-5.

Fox, M.D., Zhang, D., Snyder, A.Z., Raichle, M.E. (2009) The global signal and observed anticorrelated resting state brain networks. Journal of neurophysiology, 101:3270-83.

Friston, K. (2002a) Beyond phrenology: what can neuroimaging tell us about distributed circuitry? Annual review of neuroscience, 25:221-50.

Friston, K., Daunizeau, J., Stephan, K.E. (2013) Model selection and gobbledygook: Response to Lohmann et al. NeuroImage, 75:275-278.

Friston, K.J. (1994) Functional and effective connectivity in neuroimaging: A synthesis. Human brain mapping, 2:56-78.

Friston, K.J. (2002b) Bayesian estimation of dynamical systems: an application to fMRI. NeuroImage, 16:513-30.

Friston, K.J. (2011) Functional and effective connectivity: a review. Brain connectivity, 1:13-36.

Friston, K.J., Buechel, C., Fink, G.R., Morris, J., Rolls, E., Dolan, R.J. (1997) Psychophysiological and modulatory interactions in neuroimaging. NeuroImage, 6:218-229.

Friston, K.J., Frith, C.D. (1995) Schizophrenia: a disconnection syndrome? Clinical neuroscience, 3:89-97.

Friston, K.J., Harrison, L., Penny, W. (2003) Dynamic causal modelling. NeuroImage, 19:1273-302.

Funahashi, S., Bruce, C.J., Goldman-Rakic, P.S. (1989) Mnemonic coding of visual space in the monkey's dorsolateral prefrontal cortex. Journal of neurophysiology, 61:331-49.

Fuster, J.M., Alexander, G.E. (1971) Neuron activity related to short-term memory. Science, 173:652-4.

Garavan, H., Ross, T.J., Stein, E.A. (1999) Right hemispheric dominance of inhibitory control: an event-related functional MRI study. Proceedings of the National Academy of Sciences of the United States of America, 96:8301-6.

Gazzaley, A., Nobre, A.C. (2012) Top-down modulation: bridging selective attention and working memory. Trends in cognitive sciences, 16:129-35.

Glahn, D.C., Ragland, J.D., Abramoff, A., Barrett, J., Laird, A.R., Bearden, C.E., Velligan, D.I. (2005) Beyond hypofrontality: a quantitative meta-analysis of functional neuroimaging studies of working memory in schizophrenia. Human brain mapping, 25:60-9.

Glahn, D.C., Winkler, A.M., Kochunov, P., Almasy, L., Duggirala, R., Carless, M.A., Curran, J.C., Olvera, R.L., Laird, A.R., Smith, S.M., Beckmann, C.F., Fox, P.T., Blangero, J. (2010) Genetic control over the resting brain. Proceedings of the National Academy of Sciences of the United States of America, 107:1223-8.
Goldman-Rakic, P.S. (1995) Cellular basis of working memory. Neuron, 14:477-85.
Goldman-Rakic, P.S., Muly, E.C., 3rd, Williams, G.V. (2000) D(1) receptors in prefrontal cells and circuits. Brain research. Brain research reviews, 31:295-301.
Good, B.H., de Montjoye, Y.A., Clauset, A. (2010) Performance of modularity maximization in practical contexts. Physical review. E, Statistical, nonlinear, and soft matter physics, 81:046106.
Gottesman, II, Gould, T.D. (2003) The endophenotype concept in psychiatry: etymology and strategic intentions. The American journal of psychiatry, 160:636-45.
Greicius, M. (2008) Resting-state functional connectivity in neuropsychiatric disorders. Current opinion in neurology, 21:424-30.
Greicius, M.D., Flores, B.H., Menon, V., Glover, G.H., Solvason, H.B., Kenna, H., Reiss, A.L., Schatzberg, A.F. (2007) Resting-state functional connectivity in major depression: abnormally increased contributions from subgenual cingulate cortex and thalamus. Biological psychiatry, 62:429-37.
Greicius, M.D., Srivastava, G., Reiss, A.L., Menon, V. (2004) Default-mode network activity distinguishes Alzheimer's disease from healthy aging: evidence from functional MRI. Proceedings of the National Academy of Sciences of the United States of America, 101:4637-42.
Guastello, S.J., Koopmans, M., Pincus, D. (2009) Chaos and complexity in psychology. Cambridge, Cambridge University.
Haenisch, B., Herms, S., Mattheisen, M., Steffens, M., Breuer, R., Strohmaier, J., Degenhardt, F., Schmal, C., Lucae, S., Maier, W., Rietschel, M., Nothen, M.M., Cichon, S. (2013) Genome-wide association data provide further support for an association between 5-HTTLPR and major depressive disorder. Journal of affective disorders, 146:438-40.
Hahamy, A., Calhoun, V., Pearlson, G., Harel, M., Stern, N., Attar, F., Malach, R., Salomon, R. (2014) Save the Global: Global Signal Connectivity as a Tool for Studying Clinical Populations with Functional Magnetic Resonance Imaging. Brain connectivity, 4:395-403.
Hampson, M., Driesen, N., Roth, J.K., Gore, J.C., Constable, R.T. (2010) Functional connectivity between task-positive and task-negative brain areas and its relation to working memory performance. Magnetic resonance imaging, 28:1051-7.
Hampson, M., Driesen, N.R., Skudlarski, P., Gore, J.C., Constable, R.T. (2006) Brain connectivity related to working memory performance. The Journal of neuroscience : the official journal of the Society for Neuroscience, 26:13338-43.
Harding, I.H., Yücel, M., Harrison, B.J., Pantelis, C., Breakspear, M. (2014) Effective Connectivity within the Frontoparietal Control Network Differentiates Cognitive Control and Working Memory. NeuroImage.
Harrison, S.A., Tong, F. (2009) Decoding reveals the contents of visual working memory in early visual areas. Nature, 458:632-5.
Hartley, A.A., Speer, N.K. (2000) Locating and fractionating working memory using functional neuroimaging: storage, maintenance, and executive functions. Microscopy research and technique, 51:45-53.
Haykin, S. (1998) Neural Networks; A comprehensive foundation. Prentice Hall PTR.
He, Y., Wang, J., Wang, L., Chen, Z.J., Yan, C., Yang, H., Tang, H., Zhu, C., Gong, Q., Zang, Y., Evans, A.C. (2009) Uncovering intrinsic modular organization of spontaneous brain activity in humans. PloS one, 4:e5226.

Heinz, A., Braus, D.F., Smolka, M.N., Wrase, J., Puls, I., Hermann, D., Klein, S., Grusser, S.M., Flor, H., Schumann, G., Mann, K., Buchel, C. (2005) Amygdala-prefrontal coupling depends on a genetic variation of the serotonin transporter. Nature neuroscience, 8:20-1.
Honey, G.D., Fu, C.H., Kim, J., Brammer, M.J., Croudace, T.J., Suckling, J., Pich, E.M., Williams, S.C., Bullmore, E.T. (2002) Effects of verbal working memory load on corticocortical connectivity modeled by path analysis of functional magnetic resonance imaging data. NeuroImage, 17:573-82.
Hopfield, J.J. (1982) Neural networks and physical systems with emergent collective computational abilities. Proceedings of the National Academy of Sciences of the United States of America, 79:2554-8.
Hubel, D.H., Wiesel, T.N. (1962) Receptive fields, binocular interaction and functional architecture in the cat's visual cortex. The Journal of physiology, 160:106.
Iacono, W.G., Vaidyanathan, U., Vrieze, S.I., Malone, S.M. (2014) Knowns and unknowns for psychophysiological endophenotypes: integration and response to commentaries. Psychophysiology, 51:1339-47.
International Schizophrenia Consortium, Purcell, S.M., Wray, N.R., Stone, J.L., Visscher, P.M., O'Donovan, M.C., Sullivan, P.F., Sklar, P. (2009) Common polygenic variation contributes to risk of schizophrenia and bipolar disorder. Nature, 460:748-52.
Jentsch, J.D., Trantham-Davidson, H., Jairl, C., Tinsley, M., Cannon, T.D., Lavin, A. (2009) Dysbindin modulates prefrontal cortical glutamatergic circuits and working memory function in mice. Neuropsychopharmacology : official publication of the American College of Neuropsychopharmacology, 34:2601-8.
Jirsa, V.K. (2004) Connectivity and dynamics of neural information processing. Neuroinformatics, 2:183-204.
Jun, J.K., Miller, P., Hernandez, A., Zainos, A., Lemus, L., Brody, C.D., Romo, R. (2010) Heterogenous population coding of a short-term memory and decision task. The Journal of neuroscience : the official journal of the Society for Neuroscience, 30:916-29.
Karlsgodt, K.H., Bachman, P., Winkler, A.M., Bearden, C.E., Glahn, D.C. (2011) Genetic influence on the working memory circuitry: behavior, structure, function and extensions to illness. Behavioural brain research, 225:610-22.
Karlsgodt, K.H., Kochunov, P., Winkler, A.M., Laird, A.R., Almasy, L., Duggirala, R., Olvera, R.L., Fox, P.T., Blangero, J., Glahn, D.C. (2010) A multimodal assessment of the genetic control over working memory. The Journal of neuroscience : the official journal of the Society for Neuroscience, 30:8197-202.
Kelly, A.M., Uddin, L.Q., Biswal, B.B., Castellanos, F.X., Milham, M.P. (2008) Competition between functional brain networks mediates behavioral variability. NeuroImage, 39:527-37.
Kim, N.S., Ahn, W.K. (2002) Clinical psychologists' theory-based representations of mental disorders predict their diagnostic reasoning and memory. Journal of experimental psychology. General, 131:451-76.
Kubota, K., Niki, H. (1971) Prefrontal cortical unit activity and delayed alternation performance in monkeys. Journal of neurophysiology, 34:337-47.
Lachman, H.M., Papolos, D.F., Saito, T., Yu, Y.M., Szumlanski, C.L., Weinshilboum, R.M. (1996) Human catechol-O-methyltransferase pharmacogenetics: description of a functional polymorphism and its potential application to neuropsychiatric disorders. Pharmacogenetics, 6:243-50.
Lee, J., Park, S. (2005) Working memory impairments in schizophrenia: a meta-analysis. Journal of abnormal psychology, 114:599-611.
Li, B., Daunizeau, J., Stephan, K.E., Penny, W., Hu, D., Friston, K. (2011) Generalised filtering and stochastic DCM for fMRI. NeuroImage, 58:442-57.

Li, S.J., Li, Z., Wu, G., Zhang, M.J., Franczak, M., Antuono, P.G. (2002) Alzheimer Disease: evaluation of a functional MR imaging index as a marker. Radiology, 225:253-9.
Liu, Y., Liang, M., Zhou, Y., He, Y., Hao, Y., Song, M., Yu, C., Liu, H., Liu, Z., Jiang, T. (2008) Disrupted small-world networks in schizophrenia. Brain : a journal of neurology, 131:945-61.
Lohmann, G., Erfurth, K., Muller, K., Turner, R. (2012) Critical comments on dynamic causal modelling. NeuroImage, 59:2322-9.
Lynall, M.E., Bassett, D.S., Kerwin, R., McKenna, P.J., Kitzbichler, M., Muller, U., Bullmore, E. (2010) Functional connectivity and brain networks in schizophrenia. The Journal of neuroscience : the official journal of the Society for Neuroscience, 30:9477-87.
Ma, L., Steinberg, J.L., Hasan, K.M., Narayana, P.A., Kramer, L.A., Moeller, F.G. (2012) Working memory load modulation of parieto-frontal connections: evidence from dynamic causal modeling. Human brain mapping, 33:1850-67.
Machens, C.K., Romo, R., Brody, C.D. (2010) Functional, but not anatomical, separation of "what" and "when" in prefrontal cortex. The Journal of neuroscience : the official journal of the Society for Neuroscience, 30:350-60.
Mandeville, J.B., Marota, J.J., Ayata, C., Zaharchuk, G., Moskowitz, M.A., Rosen, B.R., Weisskoff, R.M. (1999) Evidence of a cerebrovascular postarteriole windkessel with delayed compliance. Journal of cerebral blood flow and metabolism : official journal of the International Society of Cerebral Blood Flow and Metabolism, 19:679-89.
Manoach, D.S. (2003) Prefrontal cortex dysfunction during working memory performance in schizophrenia: reconciling discrepant findings. Schizophrenia research, 60:285-298.
Markett, S.A., Montag, C., Reuter, M. (2010) The association between dopamine DRD2 polymorphisms and working memory capacity is modulated by a functional polymorphism on the nicotinic receptor gene CHRNA4. Journal of cognitive neuroscience, 22:1944-54.
Marrelec, G., Krainik, A., Duffau, H., Pelegrini-Issac, M., Lehericy, S., Doyon, J., Benali, H. (2006) Partial correlation for functional brain interactivity investigation in functional MRI. NeuroImage, 32:228-37.
Mason, M.F., Norton, M.I., Van Horn, J.D., Wegner, D.M., Grafton, S.T., Macrae, C.N. (2007) Wandering minds: the default network and stimulus-independent thought. Science, 315:393-5.
McClelland, J.L., Rogers, T.T. (2003) The parallel distributed processing approach to semantic cognition. Nature reviews. Neuroscience, 4:310-322.
McIntosh, A.R. (2000) Towards a network theory of cognition. Neural networks : the official journal of the International Neural Network Society, 13:861-70.
Mesulam, M.M. (1990) Large-scale neurocognitive networks and distributed processing for attention, language, and memory. Annals of neurology, 28:597-613.
Meunier, D., Lambiotte, R., Fornito, A., Ersche, K.D., Bullmore, E.T. (2009) Hierarchical modularity in human brain functional networks. Frontiers in neuroinformatics, 3:37.
Meyer-Lindenberg, A. (2009) Neural connectivity as an intermediate phenotype: brain networks under genetic control. Human brain mapping, 30:1938-46.
Meyer-Lindenberg, A. (2010) Intermediate or brainless phenotypes for psychiatric research? Psychological medicine, 40:1057-1062.
Meyer-Lindenberg, A., Poline, J.B., Kohn, P.D., Holt, J.L., Egan, M.F., Weinberger, D.R., Berman, K.F. (2001) Evidence for abnormal cortical functional connectivity during working memory in schizophrenia. The American journal of psychiatry, 158:1809-17.
Meyer-Lindenberg, A., Weinberger, D.R. (2006) Intermediate phenotypes and genetic mechanisms of psychiatric disorders. Nature reviews. Neuroscience, 7:818-27.
Meyer-Lindenberg, A.S., Olsen, R.K., Kohn, P.D., Brown, T., Egan, M.F., Weinberger, D.R., Berman, K.F. (2005) Regionally specific disturbance of dorsolateral prefrontal-

hippocampal functional connectivity in schizophrenia. Archives of general psychiatry, 62:379-86.
Micheloyannis, S., Pachou, E., Stam, C.J., Breakspear, M., Bitsios, P., Vourkas, M., Erimaki, S., Zervakis, M. (2006) Small-world networks and disturbed functional connectivity in schizophrenia. Schizophr Res, 87:60-6.
Miller, E.K. (2000) The prefrontal cortex and cognitive control. Nature reviews. Neuroscience, 1:59-65.
Mongillo, G., Barak, O., Tsodyks, M. (2008) Synaptic theory of working memory. Science, 319:1543-6.
Mountcastle, V.B., Edelman, G.M. (1979) An organizing principle for cerebral function: The unit module and the distributed system, Mountcastle VB, Edelman GM, The mindful brain, 1979, 7-50. MIT Press, Cambridge, MA.
Muller, N.G., Knight, R.T. (2006) The functional neuroanatomy of working memory: contributions of human brain lesion studies. Neuroscience, 139:51-8.
Muller, N.G., Machado, L., Knight, R.T. (2002) Contributions of subregions of the prefrontal cortex to working memory: evidence from brain lesions in humans. Journal of cognitive neuroscience, 14:673-86.
Munafo, M.R., Flint, J. (2014) The genetic architecture of psychophysiological phenotypes. Psychophysiology, 51:1331-2.
Murphy, K., Birn, R.M., Handwerker, D.A., Jones, T.B., Bandettini, P.A. (2009) The impact of global signal regression on resting state correlations: are anti-correlated networks introduced? NeuroImage, 44:893-905.
Neale, M., Cardon, L. (1992) Methodology for genetic studies of twins and families. Springer.
Newman, M.E. (2006) Modularity and community structure in networks. Proceedings of the National Academy of Sciences of the United States of America, 103:8577-82.
Nir, Y., Hasson, U., Levy, I., Yeshurun, Y., Malach, R. (2006) Widespread functional connectivity and fMRI fluctuations in human visual cortex in the absence of visual stimulation. NeuroImage, 30:1313-24.
O'Donovan, M.C., Craddock, N., Norton, N., Williams, H., Peirce, T., Moskvina, V., Nikolov, I., Hamshere, M., Carroll, L., Georgieva, L., Dwyer, S., Holmans, P., Marchini, J.L., Spencer, C.C., Howie, B., Leung, H.T., Hartmann, A.M., Moller, H.J., Morris, D.W., Shi, Y., Feng, G., Hoffmann, P., Propping, P., Vasilescu, C., Maier, W., Rietschel, M., Zammit, S., Schumacher, J., Quinn, E.M., Schulze, T.G., Williams, N.M., Giegling, I., Iwata, N., Ikeda, M., Darvasi, A., Shifman, S., He, L., Duan, J., Sanders, A.R., Levinson, D.F., Gejman, P.V., Cichon, S., Nothen, M.M., Gill, M., Corvin, A., Rujescu, D., Kirov, G., Owen, M.J., Buccola, N.G., Mowry, B.J., Freedman, R., Amin, F., Black, D.W., Silverman, J.M., Byerley, W.F., Cloninger, C.R., Molecular Genetics of Schizophrenia, C. (2008) Identification of loci associated with schizophrenia by genome-wide association and follow-up. Nature genetics, 40:1053-5.
Offen, S., Schluppeck, D., Heeger, D.J. (2009) The role of early visual cortex in visual short-term memory and visual attention. Vision research, 49:1352-62.
Ongur, D., Lundy, M., Greenhouse, I., Shinn, A.K., Menon, V., Cohen, B.M., Renshaw, P.F. (2010) Default mode network abnormalities in bipolar disorder and schizophrenia. Psychiatry research, 183:59-68.
Owen, A.M., McMillan, K.M., Laird, A.R., Bullmore, E. (2005) N-back working memory paradigm: a meta-analysis of normative functional neuroimaging studies. Human brain mapping, 25:46-59.
Owen, A.M., Morris, R.G., Sahakian, B.J., Polkey, C.E., Robbins, T.W. (1996) Double dissociations of memory and executive functions in working memory tasks following frontal lobe excisions, temporal lobe excisions or amygdalo-hippocampectomy in man. Brain : a journal of neurology, 119 (Pt 5):1597-615.

Park, S., Holzman, P.S. (1992) Schizophrenics show spatial working memory deficits. Archives of general psychiatry, 49:975-82.
Peper, J.S., Brouwer, R.M., Boomsma, D.I., Kahn, R.S., Hulshoff Pol, H.E. (2007) Genetic influences on human brain structure: a review of brain imaging studies in twins. Human brain mapping, 28:464-73.
Pessoa, L. (2008) On the relationship between emotion and cognition. Nature reviews. Neuroscience, 9:148-158.
Petrides, M., Milner, B. (1982) Deficits on subject-ordered tasks after frontal- and temporal-lobe lesions in man. Neuropsychologia, 20:249-62.
Pettersson-Yeo, W., Allen, P., Benetti, S., McGuire, P., Mechelli, A. (2011) Dysconnectivity in schizophrenia: where are we now? Neuroscience & Biobehavioral Reviews, 35:1110-1124.
Pezawas, L., Meyer-Lindenberg, A., Drabant, E.M., Verchinski, B.A., Munoz, K.E., Kolachana, B.S., Egan, M.F., Mattay, V.S., Hariri, A.R., Weinberger, D.R. (2005) 5-HTTLPR polymorphism impacts human cingulate-amygdala interactions: a genetic susceptibility mechanism for depression. Nature neuroscience, 8:828-34.
Pochon, J.B., Levy, R., Poline, J.B., Crozier, S., Lehericy, S., Pillon, B., Deweer, B., Le Bihan, D., Dubois, B. (2001) The role of dorsolateral prefrontal cortex in the preparation of forthcoming actions: an fMRI study. Cerebral cortex, 11:260-6.
Posthuma, D., Baare, W.F., Hulshoff Pol, H.E., Kahn, R.S., Boomsma, D.I., De Geus, E.J. (2003) Genetic correlations between brain volumes and the WAIS-III dimensions of verbal comprehension, working memory, perceptual organization, and processing speed. Twin research : the official journal of the International Society for Twin Studies, 6:131-9.
Postle, B.R. (2006) Working memory as an emergent property of the mind and brain. Neuroscience, 139:23-38.
Quintana, J., Fuster, J.M. (1999) From perception to action: temporal integrative functions of prefrontal and parietal neurons. Cerebral cortex, 9:213-21.
Raichle, M.E. (2006) Neuroscience. The brain's dark energy. Science, 314:1249-50.
Riggall, A.C., Postle, B.R. (2012) The relationship between working memory storage and elevated activity as measured with functional magnetic resonance imaging. The Journal of neuroscience : the official journal of the Society for Neuroscience, 32:12990-8.
Rommelse, N.N., Geurts, H.M., Franke, B., Buitelaar, J.K., Hartman, C.A. (2011) A review on cognitive and brain endophenotypes that may be common in autism spectrum disorder and attention-deficit/hyperactivity disorder and facilitate the search for pleiotropic genes. Neuroscience and biobehavioral reviews, 35:1363-96.
Romo, R., Brody, C.D., Hernandez, A., Lemus, L. (1999) Neuronal correlates of parametric working memory in the prefrontal cortex. Nature, 399:470-3.
Rowe, J.B., Toni, I., Josephs, O., Frackowiak, R.S., Passingham, R.E. (2000) The prefrontal cortex: response selection or maintenance within working memory? Science, 288:1656-60.
Rubinov, M., Sporns, O. (2010) Complex network measures of brain connectivity: uses and interpretations. NeuroImage, 52:1059-69.
Rubinov, M., Sporns, O. (2011) Weight-conserving characterization of complex functional brain networks. NeuroImage, 56:2068-79.
Saneyoshi, T., Fortin, D.A., Soderling, T.R. (2010) Regulation of spine and synapse formation by activity-dependent intracellular signaling pathways. Current opinion in neurobiology, 20:108-15.
Schizophrenia Working Group of the Psychiatric Genomics Consortium. (2014) Biological insights from 108 schizophrenia-associated genetic loci. Nature, 511:421-427.

Schlosser, R.G., Wagner, G., Sauer, H. (2006) Assessing the working memory network: studies with functional magnetic resonance imaging and structural equation modeling. Neuroscience, 139:91-103.
Schmittmann, V.D., Cramer, A.O.J., Waldorp, L.J., Epskamp, S., Kievit, R.A., Borsboom, D. (2013) Deconstructing the construct: A network perspective on psychological phenomena. New Ideas in Psychology, 31:43-53.
Schölvinck, M.L., Maier, A., Frank, Q.Y., Duyn, J.H., Leopold, D.A. (2010) Neural basis of global resting-state fMRI activity. Proceedings of the National Academy of Sciences, 107:10238-10243.
Schumacher, E.H., Elston, P.A., D'Esposito, M. (2003) Neural evidence for representation-specific response selection. Journal of cognitive neuroscience, 15:1111-21.
Seidman, L.J., Faraone, S.V., Goldstein, J.M., Goodman, J.M., Kremen, W.S., Toomey, R., Tourville, J., Kennedy, D., Makris, N., Caviness, V.S. (1999) Thalamic and amygdala–hippocampal volume reductions in first-degree relatives of patients with schizophrenia: an MRI-based morphometric analysis. Biological psychiatry, 46:941-954.
Shan, Z., Vinkhuyzen, A., Thompson, P., McMahon, K., Blokland, G., Zubicaray, G., Martin, N., Visscher, P., Wright, M., Reutens, D. (in preparation) Genes influence the amplitude and timing of brain hemodynamic responses.
Shulman, G.L., Fiez, J.A., Corbetta, M., Buckner, R.L., Miezin, F.M., Raichle, M.E., Petersen, S.E. (1997) Common Blood Flow Changes across Visual Tasks: II. Decreases in Cerebral Cortex. Journal of cognitive neuroscience, 9:648-63.
Sillito, A., Murphy, P. (1988) GABAergic Processes in the Central Visual System. In: Avoli, M., Reader, T., Dykes, R., Gloor, P., editors. Neurotransmitters and Cortical Function: Springer US. p 167-185.
Singer, W., Gray, C.M. (1995) Visual feature integration and the temporal correlation hypothesis. Annual review of neuroscience, 18:555-86.
Smit, D.J., Boersma, M., van Beijsterveldt, C.E., Posthuma, D., Boomsma, D.I., Stam, C.J., de Geus, E.J. (2010) Endophenotypes in a dynamically connected brain. Behavior genetics, 40:167-77.
Smit, D.J., Stam, C.J., Posthuma, D., Boomsma, D.I., de Geus, E.J. (2008) Heritability of "small-world" networks in the brain: a graph theoretical analysis of resting-state EEG functional connectivity. Human brain mapping, 29:1368-78.
Smith, S.M., Fox, P.T., Miller, K.L., Glahn, D.C., Fox, P.M., Mackay, C.E., Filippini, N., Watkins, K.E., Toro, R., Laird, A.R., Beckmann, C.F. (2009) Correspondence of the brain's functional architecture during activation and rest. Proceedings of the National Academy of Sciences of the United States of America, 106:13040-5.
Smith, S.M., Miller, K.L., Salimi-Khorshidi, G., Webster, M., Beckmann, C.F., Nichols, T.E., Ramsey, J.D., Woolrich, M.W. (2011) Network modelling methods for FMRI. NeuroImage, 54:875-91.
Sorg, C., Riedl, V., Muhlau, M., Calhoun, V.D., Eichele, T., Laer, L., Drzezga, A., Forstl, H., Kurz, A., Zimmer, C., Wohlschlager, A.M. (2007) Selective changes of resting-state networks in individuals at risk for Alzheimer's disease. Proceedings of the National Academy of Sciences of the United States of America, 104:18760-5.
Sreenivasan, K.K., Curtis, C.E., D'Esposito, M. (2014) Revisiting the role of persistent neural activity during working memory. Trends in cognitive sciences, 18:82-9.
Stam, C.J. (2004) Functional connectivity patterns of human magnetoencephalographic recordings: a 'small-world' network? Neuroscience letters, 355:25-8.
Stam, C.J., Jones, B.F., Nolte, G., Breakspear, M., Scheltens, P. (2007) Small-world networks and functional connectivity in Alzheimer's disease. Cerebral cortex, 17:92-9.

Staniloiu, A., Markowitsch, H.J. (2010) Looking at comorbidity through the glasses of neuroscientific memory research: A brain-network perspective. Behavioral and Brain Sciences, 33:170-171.

Stein, J.L., Medland, S.E., Vasquez, A.A., Hibar, D.P., Senstad, R.E., Winkler, A.M., Toro, R., Appel, K., Bartecek, R., Bergmann, O., Bernard, M., Brown, A.A., Cannon, D.M., Chakravarty, M.M., Christoforou, A., Domin, M., Grimm, O., Hollinshead, M., Holmes, A.J., Homuth, G., Hottenga, J.J., Langan, C., Lopez, L.M., Hansell, N.K., Hwang, K.S., Kim, S., Laje, G., Lee, P.H., Liu, X., Loth, E., Lourdusamy, A., Mattingsdal, M., Mohnke, S., Maniega, S.M., Nho, K., Nugent, A.C., O'Brien, C., Papmeyer, M., Putz, B., Ramasamy, A., Rasmussen, J., Rijpkema, M., Risacher, S.L., Roddey, J.C., Rose, E.J., Ryten, M., Shen, L., Sprooten, E., Strengman, E., Teumer, A., Trabzuni, D., Turner, J., van Eijk, K., van Erp, T.G., van Tol, M.J., Wittfeld, K., Wolf, C., Woudstra, S., Aleman, A., Alhusaini, S., Almasy, L., Binder, E.B., Brohawn, D.G., Cantor, R.M., Carless, M.A., Corvin, A., Czisch, M., Curran, J.E., Davies, G., de Almeida, M.A., Delanty, N., Depondt, C., Duggirala, R., Dyer, T.D., Erk, S., Fagerness, J., Fox, P.T., Freimer, N.B., Gill, M., Goring, H.H., Hagler, D.J., Hoehn, D., Holsboer, F., Hoogman, M., Hosten, N., Jahanshad, N., Johnson, M.P., Kasperaviciute, D., Kent, J.W., Jr., Kochunov, P., Lancaster, J.L., Lawrie, S.M., Liewald, D.C., Mandl, R., Matarin, M., Mattheisen, M., Meisenzahl, E., Melle, I., Moses, E.K., Muhleisen, T.W., Nauck, M., Nothen, M.M., Olvera, R.L., Pandolfo, M., Pike, G.B., Puls, R., Reinvang, I., Renteria, M.E., Rietschel, M., Roffman, J.L., Royle, N.A., Rujescu, D., Savitz, J., Schnack, H.G., Schnell, K., Seiferth, N., Smith, C., Steen, V.M., Valdes Hernandez, M.C., Van den Heuvel, M., van der Wee, N.J., Van Haren, N.E., Veltman, J.A., Volzke, H., Walker, R., Westlye, L.T., Whelan, C.D., Agartz, I., Boomsma, D.I., Cavalleri, G.L., Dale, A.M., Djurovic, S., Drevets, W.C., Hagoort, P., Hall, J., Heinz, A., Jack, C.R., Jr., Foroud, T.M., Le Hellard, S., Macciardi, F., Montgomery, G.W., Poline, J.B., Porteous, D.J., Sisodiya, S.M., Starr, J.M., Sussmann, J., Toga, A.W., Veltman, D.J., Walter, H., Weiner, M.W., Alzheimer's Disease Neuroimaging, I., Consortium, E., Consortium, I., Saguenay Youth Study, G., Bis, J.C., Ikram, M.A., Smith, A.V., Gudnason, V., Tzourio, C., Vernooij, M.W., Launer, L.J., DeCarli, C., Seshadri, S., Cohorts for, H., Aging Research in Genomic Epidemiology, C., Andreassen, O.A., Apostolova, L.G., Bastin, M.E., Blangero, J., Brunner, H.G., Buckner, R.L., Cichon, S., Coppola, G., de Zubicaray, G.I., Deary, I.J., Donohoe, G., de Geus, E.J., Espeseth, T., Fernandez, G., Glahn, D.C., Grabe, H.J., Hardy, J., Hulshoff Pol, H.E., Jenkinson, M., Kahn, R.S., McDonald, C., McIntosh, A.M., McMahon, F.J., McMahon, K.L., Meyer-Lindenberg, A., Morris, D.W., Muller-Myhsok, B., Nichols, T.E., Ophoff, R.A., Paus, T., Pausova, Z., Penninx, B.W., Potkin, S.G., Samann, P.G., Saykin, A.J., Schumann, G., Smoller, J.W., Wardlaw, J.M., Weale, M.E., Martin, N.G., Franke, B., Wright, M.J., Thompson, P.M., Enhancing Neuro Imaging Genetics through Meta-Analysis, C. (2012) Identification of common variants associated with human hippocampal and intracranial volumes. Nature genetics, 44:552-61.

Stelzel, C., Basten, U., Montag, C., Reuter, M., Fiebach, C.J. (2009) Effects of dopamine-related gene-gene interactions on working memory component processes. The European journal of neuroscience, 29:1056-63.

Stevens, A.A., Tappon, S.C., Garg, A., Fair, D.A. (2012) Functional brain network modularity captures inter- and intra-individual variation in working memory capacity. PloS one, 7:e30468.

Strike, L.T., Couvy-Duchesne, B., Hansell, N.K., Cuellar-Partida, G., Medland, S.E., Wright, M.J. (2015) Genetics and Brain Morphology. Neuropsychology review, 25:63-96.

Supekar, K., Menon, V., Rubin, D., Musen, M., Greicius, M.D. (2008) Network analysis of intrinsic functional brain connectivity in Alzheimer's disease. PLoS computational biology, 4:e1000100.

Tan, H.Y., Chen, Q., Sust, S., Buckholtz, J.W., Meyers, J.D., Egan, M.F., Mattay, V.S., Meyer-Lindenberg, A., Weinberger, D.R., Callicott, J.H. (2007) Epistasis between catechol-O-

methyltransferase and type II metabotropic glutamate receptor 3 genes on working memory brain function. Proceedings of the National Academy of Sciences of the United States of America, 104:12536-41.
Thompson, P.M., Cannon, T.D., Narr, K.L., van Erp, T., Poutanen, V.P., Huttunen, M., Lonnqvist, J., Standertskjold-Nordenstam, C.G., Kaprio, J., Khaledy, M., Dail, R., Zoumalan, C.I., Toga, A.W. (2001) Genetic influences on brain structure. Nature neuroscience, 4:1253-8.
Toulopoulou, T., Picchioni, M., Rijsdijk, F., Hua-Hall, M., Ettinger, U., Sham, P., Murray, R. (2007) Substantial genetic overlap between neurocognition and schizophrenia: genetic modeling in twin samples. Archives of general psychiatry, 64:1348-55.
Tsuang, M.T., Faraone, S.V. (1995) The case for heterogeneity in the etiology of schizophrenia. Schizophrenia Research, 17:161-175.
van den Heuvel, M.P., Sporns, O. (2011) Rich-club organization of the human connectome. The Journal of neuroscience : the official journal of the Society for Neuroscience, 31:15775-86.
van den Heuvel, M.P., Stam, C.J., Kahn, R.S., Hulshoff Pol, H.E. (2009) Efficiency of functional brain networks and intellectual performance. The Journal of neuroscience : the official journal of the Society for Neuroscience, 29:7619-24.
van den Heuvel, M.P., van Soelen, I.L., Stam, C.J., Kahn, R.S., Boomsma, D.I., Hulshoff Pol, H.E. (2013) Genetic control of functional brain network efficiency in children. European neuropsychopharmacology : the journal of the European College of Neuropsychopharmacology, 23:19-23.
Van Dijk, K.R., Sabuncu, M.R., Buckner, R.L. (2012) The influence of head motion on intrinsic functional connectivity MRI. NeuroImage, 59:431-8.
Van Dijk, K.R.A., Hedden, T., Venkataraman, A., Evans, K.C., Lazar, S.W., Buckner, R.L. (2010) Intrinsic functional connectivity as a tool for human connectomics: theory, properties, and optimization. Journal of neurophysiology, 103:297-321.
Van Geert, P. (2009) Nonlinear complex dynamical systems in developmental psychology.
Verweij, K.J.H., Mosing, M.A., Zietsch, B.P., Medland, S.E. (2012) Estimating heritability from twin studies. Statistical Human Genetics: Springer. p 151-170.
Wager, T.D., Smith, E.E. (2003) Neuroimaging studies of working memory: a meta-analysis. Cognitive, affective & behavioral neuroscience, 3:255-74.
Wallis, J.D., Anderson, K.C., Miller, E.K. (2001) Single neurons in prefrontal cortex encode abstract rules. Nature, 411:953-6.
Warden, M.R., Miller, E.K. (2010) Task-dependent changes in short-term memory in the prefrontal cortex. The Journal of neuroscience : the official journal of the Society for Neuroscience, 30:15801-10.
Watts, D.J., Strogatz, S.H. (1998) Collective dynamics of 'small-world' networks. Nature, 393:440-2.
Weissenbacher, A., Kasess, C., Gerstl, F., Lanzenberger, R., Moser, E., Windischberger, C. (2009) Correlations and anticorrelations in resting-state functional connectivity MRI: a quantitative comparison of preprocessing strategies. NeuroImage, 47:1408-1416.
Weissman, D.H., Roberts, K.C., Visscher, K.M., Woldorff, M.G. (2006) The neural bases of momentary lapses in attention. Nature neuroscience, 9:971-8.
Wexler, B.E., Stevens, A.A., Bowers, A.A., Sernyak, M.J., Goldman-Rakic, P.S. (1998) Word and tone working memory deficits in schizophrenia. Archives of general psychiatry, 55:1093-6.
Whitfield-Gabrieli, S., Thermenos, H.W., Milanovic, S., Tsuang, M.T., Faraone, S.V., McCarley, R.W., Shenton, M.E., Green, A.I., Nieto-Castanon, A., LaViolette, P., Wojcik, J., Gabrieli, J.D., Seidman, L.J. (2009) Hyperactivity and hyperconnectivity of the default network in schizophrenia and in first-degree relatives of persons with schizophrenia. Proceedings of the National Academy of Sciences of the United States of America, 106:1279-84.

Wiggins, J.L., Bedoyan, J.K., Peltier, S.J., Ashinoff, S., Carrasco, M., Weng, S.J., Welsh, R.C., Martin, D.M., Monk, C.S. (2012) The impact of serotonin transporter (5-HTTLPR) genotype on the development of resting-state functional connectivity in children and adolescents: a preliminary report. NeuroImage, 59:2760-70.
Wilson, F.A., Scalaidhe, S.P., Goldman-Rakic, P.S. (1993) Dissociation of object and spatial processing domains in primate prefrontal cortex. Science, 260:1955-8.
Wolf, M.E., Mangiavacchi, S., Sun, X. (2003) Mechanisms by which dopamine receptors may influence synaptic plasticity. Annals of the New York Academy of Sciences, 1003:241-9.
Woodward, T.S., Cairo, T.A., Ruff, C.C., Takane, Y., Hunter, M.A., Ngan, E.T. (2006) Functional connectivity reveals load dependent neural systems underlying encoding and maintenance in verbal working memory. Neuroscience, 139:317-25.
Wright, M.J., Martin, N.G. (2004) Brisbane Adolescent Twin Study: Outline of study methods and research projects. Australian Journal of Psychology, 56:65-78.
Xing, Y., Ledgeway, T., McGraw, P.V., Schluppeck, D. (2013) Decoding working memory of stimulus contrast in early visual cortex. The Journal of neuroscience : the official journal of the Society for Neuroscience, 33:10301-11.
Zanto, T.P., Rubens, M.T., Thangavel, A., Gazzaley, A. (2011) Causal role of the prefrontal cortex in top-down modulation of visual processing and working memory. Nature neuroscience, 14:656-61.
Zarahn, E., Aguirre, G.K., D'Esposito, M. (1997) Empirical analyses of BOLD fMRI statistics. NeuroImage, 5:179-197.
Zhou, D., Thompson, W.K., Siegle, G. (2009) MATLAB toolbox for functional connectivity. NeuroImage, 47:1590-607.
Zhou, Y., Liang, M., Tian, L., Wang, K., Hao, Y., Liu, H., Liu, Z., Jiang, T. (2007) Functional disintegration in paranoid schizophrenia using resting-state fMRI. Schizophr Res, 97:194-205.
Zimmermann, P., Bruckl, T., Nocon, A., Pfister, H., Lieb, R., Wittchen, H.U., Holsboer, F., Angst, J. (2009) Heterogeneity of DSM-IV major depressive disorder as a consequence of subthreshold bipolarity. Archives of general psychiatry, 66:1341-52.

7 Appendices

7.1 Information Sheet

GENETICS OF BRAIN STRUCTURE AND FUNCTION

(The Twin Imaging Study)

INFORMATION FOR PARTICIPANTS

1 Description and purpose of the study.
Humans show wide variation in the structure and function of their brains, and this is in part due to genetic variation. However, how genes exert their effects on the brain, and then map to behaviour remains a mystery. The aim of this study is to understand how, and to what extent, genes and the environment, and the complex interaction between them, influence brain structure and function, and ultimately behaviour. In doing so we hope to locate and characterise genes affecting complex behaviour that have relevance to human health and disease. The study uses a safe imaging method called magnetic resonance imaging, or MRI, in which high resolution pictures (images) of both brain structure, and brain activity during the performance of a task can be captured. DNA from blood samples donated previously by you in the Twin Moles or Twin MAPS study will be accessed to enable us to search for some of the specific genes influencing the structure and function of the human brain. If DNA is not available we will invite you to donate a small (40mls) blood sample for the purposes of this study. Detailed information about genetic analysis of samples donated by participants are given in the attached Human Genetics Research brochure.

The study is conducted by Dr. Margie Wright, Professor Nick Martin and colleagues from the Genetic Epidemiology Unit at the Queensland Institute of Medical Research and Dr. Greig de Zubicaray, Dr. Katie McMahon and colleagues from the Centre for Magnetic Resonance (CMR) at the University of Queensland.

2. Participation in the study involves an imaging and behavioural session.
The *imaging session* will take place in the MRI suite at the Wesley Hospital (Brisbane). A MRI scanner is a large magnet with a tunnel in the middle; the tunnel allows a person to lie on a padded table (narrow bed) and to slide into the centre of the magnet. To obtain a scan, it is essential that you remain still in the tunnel, within the magnet for up to 60 minutes. While you are in the scanner you will be presented with text and/or pictures on a screen, and asked to respond to some of these by pressing a button with your finger. You will be informed both about the nature of, and provided with practice on, the task before entering the scanner. While the imaging is underway, you will be in constant voice communication with the imaging staff through an intercom system.

The *cognitive session* will take place at the Wesley Hospital or at the Queensland Institute of Medical Research on the same or different day as the imaging session, whatever is the most convenient for the participant. This session comprises a series of standard tasks assessing cognitive function (e.g. memory).

3. Risks and discomforts that might be associated with this research.
MRI is a simple and safe procedure (for screened individuals). No X-rays or radiation are used to obtain images, the procedure depending on the magnetic properties of molecules within the brain. You will be interviewed and screened by a medical practitioner, just prior to entering the scanner room, to ascertain if you have any metal or shrapnel in your body, metal in your eye, or implanted electronic devices, such as a cardiac pacemaker, or other metal implants (e.g. cerebral aneurism clips). In addition, you will be checked for personal items that contain metal. Credit cards, which will be wiped by the field, and other personal items will be locked away during your visit.

While you are in the scanner there may be some potential discomforts. The tunnel may aggravate claustrophobia, and if so you will be removed from the tunnel immediately. On rare occasions, the magnet may cease to function, due to the loss of the magnetic field. If this occurs during the imaging procedure, you will be removed from the scanner.

If the MRI test indicates a potential abnormality we will inform you and advise that you contact your medical practitioner.

If you donate a blood sample, you may experience discomfort, bruising, and/or bleeding at the site of needle insertion. Occasionally, some people experience dizziness or feel faint.

4. The possible benefits to you and/ or society from this research.
Your participation will be of no direct benefit to you. However, society will benefit by the increased understanding of health behaviour that this study will bring.

5. This research is not intended for the purpose of diagnosing or treating any health problems.
This research is not intended for the purpose of diagnosing or treating any health problems you may have. Participation in this research study does not take the place of visits to a doctor or other health professionals.

6. Reimbursement for participation in this research study.
On completion of the testing you will receive Coles Myer vouchers to the value of $100 in appreciation of your time taken to participate in this study.

7. Participation is voluntary and you may choose not to participate in this research study.
You may withdraw your consent at any time, at any point in the study, without having to give a reason, and without consequence. If you choose to withdraw your consent you may request that your MRI pictures be destroyed. You will also be informed of any significant new findings developed during the course of participation in this research that may have a bearing on your willingness to continue in the study.

8. Confidentiality of your records and your identity.
The Institute will take all reasonable measures to protect the confidentiality of your records and your identity will not be revealed in any publication that may result from this study. All data collected during the study will be stored under code numbers, without names, in locked filing cabinets. Only staff directly involved with the conduct of the research, and who may need to contact you in the future, will have access to the master list linking names and code numbers, except under exceptional circumstances as required by law. Any data that are either communicated or released to other scientists will contain no

identifying information, only code numbers. Moreover, we will not share individual results with anyone participating in the study, to protect the confidentiality of everyone. The confidentiality of all study related records will be maintained in accordance with the National Health and Medical Research Council Guidelines.

9. Queensland Institute of Medical Research recognizes the importance of your contribution to research efforts intended to improve medical care.

The Institute makes every effort to minimise any health and safety risks to people participating in such research activities. The institute reserves the right to make all decisions concerning payment for all medical treatment for injuries solely and directly relating to your participation in a biomedical or behavioural project. If you believe you have been injured as a result of your participation in a research study, please contact the Chairperson of the Human Research Ethics Committee or the Principal Investigator (Dr. Margie Wright) as stated below.

10. Who to contact if you have any questions, concerns, or complaints, regarding this study.

If you have any questions or concerns, or if any problems arise, you may call the principal investigator, Dr Margie Wright, on 07-3362-0225, or the project coordinator (Alison MacKenzie) on 07-3362-0233 or free call: 1800-257-179. If you have any concerns or complaints regarding the conduct of this study, you may contact the Chairperson of the Queensland Institute of Medical Research Human Research Ethics Committee (QIMR-HREC) via the Secretary on Tel: 07-3362 0259. This study adheres to the Guidelines of the ethical review process of The Queensland Institute of Medical Research, The University of Queensland, and The Wesley Hospital.

7.2 Consent Form

GENETICS OF BRAIN STRUCTURE AND FUNCTION

(The Twin Imaging Study)

CONSENT FORM A

I agree to participate in The Twin Imaging Study and in doing so I acknowledge that:

1. I have read the attached *Participant Information Sheet* outlining the nature and purpose of the project and the extent of my involvement, and have had these details explained to me. I have had the opportunity to ask further questions and am satisfied that I understand.

2. I am aware that, although the project is directed to the expansion of knowledge generally, it may not result in any direct benefit to me.

3. I have been informed that I may withdraw from the project at my request at any time.

4. I have been advised that the Queensland Institute of Medical Research, University of Queensland and Wesley Hospital Research and Ethics Committees have given approval for this project to proceed.

5. I am aware that I may request further information about the project as it proceeds.

6. I understand that all study related records will be maintained in accordance with the National Health and Medical Research Council Guidelines and that, in the event of any results of the project being published, I will not be identified in any way.

YOUR NAME: _____ **(Please print clearly)**

YOUR SIGNATURE: _____ **DATE:** _____

NAME OF WITNESS: _____

WITNESS' SIGNATURE: _____ **DATE:** _____

Investigators: ***Dr Margie Wright and Professor Nick Martin, Queensland Institute of Medical Research, Dr Greig de Zubicaray and Dr Katie McMahon from the Centre for Magnetic Resonance (CMR) at the University of Queensland.***

7.3 Ethics Clearance

THE UNIVERSITY OF QUEENSLAND

Institutional Approval Form For Experiments On Humans Including Behavioural Research

Chief Investigator:	Dr Margaret Wright
Project Title:	Genetics Of Brain Structure And Function - 08/02/2007 - AMENDMENT
Supervisor:	None
Co-Investigator(s):	Dr Greig de Zubicaray, Dr Katie McMahon, Dr Paul Thompson, Professor Nick Martin
Department(s):	Queensland Institute of Medical Research
Project Number:	2004000185
Granting Agency/Degree:	National Institutes of Health (NICHD)
Duration:	31st December 2012

Comments:

Name of responsible Committee:-
Medical Research Ethics Committee
This project complies with the provisions contained in the *National Statement on Ethical Conduct in Research Involving Humans* and complies with the regulations governing experimentation on humans.

Name of Ethics Committee representative:-
Professor Bill Vicenzino
Chairperson
Medical Research Ethics Committee

Date: 14.02.2007 Signature: